

UC San Diego

UC San Diego Electronic Theses and Dissertations

Title

Predicting Post-Myocardial Infarction Matrix Responses

Permalink

<https://escholarship.org/uc/item/4mw9c7km>

Author

Whitehead, Alexander J

Publication Date

2022

Peer reviewed|Thesis/dissertation

UNIVERSITY OF CALIFORNIA SAN DIEGO

Predicting Post-Myocardial Infarction Matrix Responses

A dissertation submitted in partial satisfaction of the
requirements for the degree Doctor of Philosophy

in

Bioengineering

by

Alexander Jeffrey Whitehead

Committee in charge:

Professor Adam Engler, Chair
Professor Karen Christman
Professor Mohit Jain
Professor Kevin King
Professor Tatiana Kisseleva

2022

Copyright

Alexander Jeffrey Whitehead, 2022

All rights reserved.

The Dissertation of Alexander Jeffrey Whitehead is approved, and it is acceptable in quality and form for publication on microfilm and electronically.

University of California San Diego

2022

DEDICATION

To Mom, Dad, and Kiki

EPIGRAPH

“Yesterday’s price is not today’s price”

TABLE OF CONTENTS

Dissertation Approval Page	iii
Dedication.....	iv
Epigraph	v
Table of Contents.....	vi
List of Figures	ix
List of Tables	x
Acknowledgements.....	xi
Vita.....	xiv
Abstract of the Dissertation.....	xvi
Chapter 1: Physiology of post-MI Healing and Matrix Deposition	1
1.1 Clinical Observations, Risk Factors, and Generalized Standard of Care	2
1.2 Cellular Turnover	3
1.3 Known Post-MI Ligands and their Activating Pathways	4
1.4 Inflammation Initiation and Resolution	5
1.5 Fibroblast Form and Function	7
1.6 Extracellular Matrix Assembly and Structure	9
1.7 References	10
Chapter 2: Regenerative Crosstalk between Cardiac Cells and Macrophages...	14
2.1 Abstract.....	15
2.2 New and Noteworthy.....	16
2.3 Introduction	16
2.4 Methods	20

2.4.1	Bulk RNA-seq Processing	20
2.4.2	Single-Cell RNA-Seq Processing	20
2.4.3	Statistical Analysis	21
2.5	Results and Discussion.....	22
2.5.1	Chemokines, Cytokines, Suppressors, and Interferon Responses	28
2.5.2	Cellular Connectivity After Infarction	32
2.5.3	Cardiac Stress that are Enhanced in Non-regenerative Hearts.	36
2.5.4	Limitations of Analysis.....	38
2.5.5	Summary.....	40
2.6	Supplementary Figures.....	41
2.7	Supplementary Tables	45
2.8	Acknowledgements.....	47
2.9	References	47
Chapter 3:	Improved Epicardial Cardiac Fibroblast Generation from iPSCs.....	57
3.1	Abstract.....	58
3.2	Introduction	58
3.3	Methods and Materials.....	61
3.3.1	Ethical compliance and Cell lines.....	61
3.3.2	Differentiation Components and Methods.....	61
3.3.3	Cardiac Fibroblast Phenotyping	62
3.4	Protocol.....	69
3.5	Results and Discussion.....	77
3.6	Supplementary Figure.....	93

3.7	Acknowledgements.....	95
3.8	References	95
Chapter 4: Human Cardiac Fibroblast Stress Pathways and Matrix Production are Governed by lncRNA SNPs.....		100
4.1	Abstract.....	101
4.2	Non-standard Abbreviations and Acronyms.....	101
4.3	Introduction	102
4.4	Methods	104
4.5	Results.....	111
4.6	Discussion	120
4.7	Conclusions	122
4.8	Acknowledgements.....	122
4.9	Sources of Funding.....	123
4.10	Disclosures	123
4.11	References	123
4.12	Supplemental Table.....	128
Chapter 5: Concluding Remarks.....		130
5.1	Project Summary	131
5.2	Computational Modeling	131
5.3	iCF Culture and Limitations.....	132
5.4	9p21 Etiologies and Stress Response	133
5.5	Influence on Future Therapies	135
Appendix.....		136

LIST OF FIGURES

Figure 2.1: Transcriptomic analyses of infarct and sham bulk highlight changes in specific remodeling pathways.	23
Figure 2.2: MI induces the largest transcriptomic changes initially in younger mice but older mice maintain significant transcriptional differences.....	25
Figure 2.3: Model for cellular and molecular changes with age and infarction....	26
Figure 2.4. P8 cytokines recruit BMDMs deficient in growth proteins to an increasingly sensitive inflammatory microenvironment.	31
Supplemental Figure 2.1: Transcriptomic analyses of infarct and sham myocardia highlight prolonged remodeling in older hearts.	41
Supplemental Figure 2.2: Chemokine and cytokine signaling highlights generic and specific white blood cell recruitment.....	42
Supplemental Figure 2.3: Connectivity and growth, ECM, and hyaluronic acid signaling evolve with age and infarction.....	43
Supplemental Figure 2.4: Matricellular, hypoxic, and stretch responses are exaggerated with age, correlated with increased NF- κ B signaling.....	44
Figure 3.1. Comparison of CF differentiation protocols.....	79
Figure 3.2. Differentiation and characterization of PSC-derived CFs.....	82
Figure 3.3. Vimentin and PDGFR α expression are Hallmarks of Differentiated CFs.	86
Figure 3.4. ATAC sequencing of differentiation stages.	87
Supplemental Figure 3.1. Additional marker characterization for each protocol.	93
Figure 4.1: Inflammatory signatures drive differences in regenerative (non-scarring) and adult (scarring) hearts.	114
Figure 4.2: Computationally predicted post-MI agonists upregulate matrix and phosphorylate AP-1 and NF- κ B and AP-1 inhibition only partially rescues matrix production.	117
Figure 4.3. ANRIL is AP-1 inducible and silences GATA5 and Connexin 43.	119

LIST OF TABLES

Supplementary Table 2.1: Z-scores from Heatmap of selected genes and their ontologies.	45
Supplementary Table 2.2: Gene expression in TPM of Toll-Like Receptors in Fibroblasts.	46
Table 3.1. Materials Checklist.	76
Supplemental Table 4.1. Regions with predicted to have both AP-1 and GATA binding sites.	128

ACKNOWLEDGEMENTS

I would like to thank my PhD thesis advisor, Adam Engler for his guidance and support during my graduate career. He allowed me great intellectual freedom that bolstered my interests in bioengineering and adjacent fields. I also thank him, however, for reigning in my ideas from time to time and distilling my vision and scope. His instruction in writing, storytelling, and framing scientific arguments was central to my training, and something that will be foundational for the rest of my career. In addition, my committee members, Karen Christman, Mohit Jain, Kevin King, and Tatiana Kisseleva have been incredibly helpful. I appreciate their constructive feedback that guided me through the dissertation process.

I would also like to thank all the members of the Engler lab, especially Afsheen, Natalie, Gisselle, and Erin. It was a pleasure to work with them, learn from them, and experience their comradery.

Lastly, I am incredibly thankful for my family and friends. My parents supported me from across the country and lifted my spirits when they were low. I could always lean on Keerthana for reassurance, another critical viewpoint, and to keep things in perspective. My family's love continually motivated me to achieve to my greatest potential and put my best foot forward. I am also incredibly appreciative of the friends I have made during my time in San Diego - especially Afsheen and Chelsea, Matt, Oriq, Tom, and Garrett. They made southern California feel a bit more like home.

Chapter 2, in full, is a reprint of the material as it appears in the American Journal of Pathology, Heart and Circulatory Physiology 2021. Whitehead, Alexander J.; Engler, Adam J. American Physiological Society. The dissertation author is the primary investigator and author of this material.

Chapter 3, in full, a reprint of the material as it appears in the Journal of Molecular and Cellular Cardiology, 2022, Whitehead, Alexander J.; Hocker, James D.; Ren, Bing; Engler, Adam J. international Society for Heart Research. The dissertation author is the primary investigator and author of this material. Special thanks to our collaborators Jake Hocker and Bing Ren for their contributions with the ATAC-sequencing and advice when developing the analysis pipeline. The dissertation author is the primary investigator and author of this material.

Chapter 4, in full, is currently being prepared as a manuscript for submission and publication of the material. Whitehead, Alexander J.; Hocker, James D.; Ren, Bing; Engler, Adam J. I would again like to thank Jake and Bing for their sequencing contributions. The dissertation author is the primary investigator and author of this material.

Thank you to the UC San Diego Stem Cell and Genomics Core and Human Embryonic Stem Cell Core Facility, especially Cody Fine for his help with flow cytometry and Elsa Molina with microscopy.

Thank you to these funding sources: National Science Foundation Graduate Research Fellowship Program, Achievement Rewards for College

Scientists (ARCS) San Diego Chapter, and the National Institutes of Health (Grant RO1AG045428).

VITA

2017 Honors Bachelor of Science, Biomedical Engineering, Virginia Commonwealth University

2022 Doctor of Philosophy, Bioengineering, University of California San Diego

Field of Study

2017 – 2022 Regenerative Medicine

Publications

NJ Kirkland, **AJ Whitehead**, JD Hocker, P Beri, G Vogler, B Hum, B Ren, R Bodmer, AJ Engler. “Age-dependent Lamin remodeling induces cardiac dysfunction via dysregulation of cardiac transcriptional programs.” (in review)

AJ Whitehead, AJ Engler. Regenerative cross talk between cardiac cells and macrophages. *American Journal of Physiology – Heart and Circulatory Physiology*. 2021 Mar 26;320: H2211–H2221.

AJ Whitehead, JD Hocker, B Ren, AJ Engler. Improved epicardial cardiac fibroblast generation from iPSCs. *Journal of Molecular and Cellular Cardiology*, 2022. 164, 58-58

JO Abaricia*, **AJ Whitehead***, S Kandalam, AH Shah, KM Hotchkiss, L Morandini, R Olivares-Navarette. “E-cigarette Aerosol Mixtures Inhibit Biomaterial-Induced Osseointegrative Cell Phenotypes” *Materiala*. 2021. <https://doi.org/10.1016/j.mtla.2021.101241> * Contributed equally

S Ruoss, ST Ball, SN Dorn, JN Parekh, **AJ Whitehead**, AJ Engler, S Ward. “Acetabular bone marrow aspiration during total hip arthroplasty” *Journal of the American Academy of Orthopedic Surgeons*. 2021.

SL Hyzy, A Cheng, DJ Cohen, G Yatzkaier, **AJ Whitehead**, RM Clohessy, RA Gittens, BD Boyan, Z Schwartz. “Novel Hydrophilic Nanostructured Microtexture on Direct Metal Laser Sintered Ti-6Al-4V Surfaces Enhances Osteoblast Response in Vitro and Osseointegration in a Rabbit Model” *Journal of Biomedical Materials Research Part A*. 2016. 104(8):2086-2098.

DJ Cohen, A Cheng, A Kahn, M Aviram, **AJ Whitehead**, SL Hyzy, RM Clohessy, BD Boyan, Zvi Schwartz. “Novel Osteogenic Ti-6Al-4V Device for Restoration of

Dental Function in Patients with Large Bone Deficiencies: Design, Development and Implementation” Nature Scientific Reports. 2016. 6:20493

Book Chapter

AJ Whitehead, N Kirkland, AJ Engler. “Atomic Force Microscopy for Live-Cell and Hydrogel Measurement” in *Myofibroblasts: Fundamentals, Laboratory Methods and Anti-Fibrotic Drug Discovery*, Series: Methods. Mol. Biol., Hinz, B. and Lagares, D., Editors. 2021, Springer Nature. Vol: 2299, pg. 217-226.

Podcast

Macrophage Regulation of Matrix Remodeling. *AJP Heart and Circulatory Physiology Podcast*. 2021.

Honors and Awards

2019-2022 Achievement Rewards for College Scientists (ARCS) Fellowship
2018 National Science Foundation Graduate Research Fellowship
2017 *Magna Cum Laude*, Biomedical Engineering, Virginia Commonwealth University
2017 2nd Place Young Investigator Award, International Association of Dental Research
2014 Outstanding Poster for Undergraduate Research, Virginia Commonwealth University
2013 Provost Scholarship, Virginia Commonwealth University

ABSTRACT OF THE DISSERTATION

Predicting Post-Myocardial Infarction Matrix Responses

by

Alexander Jeffrey Whitehead

Doctor of Philosophy in Bioengineering

University of California San Diego, 2022

Professor Adam Engler, Chair

After myocardial infarction (MI), the matrix response largely dictates how long you will live. Most heart failure after MI occurs a few months thereafter, aligning with the time fibroblasts require to deposit a scar. This dissertation focuses on how neonatal mammals can regenerate their hearts after MI and how we can

interrogate these molecular hypotheses *in-vitro*. Chapter 1 provides an overview of the infarction cascade, known cellular and biomolecular contributions to inflammation, and the composition and structure of the extracellular matrix. Chapter 2 discusses how neonatal and adult cardiac healing differ. RNA-seq datasets were mined to provide insight to key pathways, receptors, and ligands that uniquely contribute to adult scar formation. Chapter 3 establishes an induced pluripotent stem cell (iPSC) to cardiac fibroblast (CF) differentiation through the epicardial lineage. Marker expression, matrix assembly, stress response, and chromatin architecture relative to other contemporary protocols and primary cells are characterized. Chapter 4 tests the central informatic hypotheses generated in chapter 2, particularly with respect to sterile inflammatory ligands (TGF- β , low molecular weight hyaluronic acid, and angiotensin II). It also investigates how these stress responses manifest in patients with single nucleotide polymorphisms (SNPs) in a long noncoding RNA (lncRNA) that worsen cardiovascular outcomes clinically. Chapter 5 is an extended discussion of the cumulative results, significance, and potential future approaches to cardiac fibrosis modeling. The discoveries herein demonstrate a novel method of reductionist fibrotic modeling *in-vitro*, highlight central fibrotic pathways, and suggest therapeutic targets.

Chapter 1: Physiology of post-MI Healing and Matrix Deposition

1.1 Clinical Observations, Risk Factors, and Generalized Standard of Care

Coronary heart disease (including myocardial infarction) is the number one cause of death globally, accounting for an approximate 18.6 million fatalities. Many risk factors for cardiovascular disease have been identified, including smoking, physical inactivity, poor nutrition and obesity, diabetes, and genetics. While many of these risk factors are preventable, the overall healthcare burden of heart attacks is still enormous, accounting for approximately \$12.1 billion treatment expenses in the United States alone¹.

Though the standard of care has drastically improved over the past few decades (particularly with improved engineering approaches to percutaneous coronary interventions [PCI] and angiography), much of the healing after myocardial infarction (MI) is reliant on the natural healing processes of the body; the drugs prescribed after MI focus on prevention of additional occlusions and blood pressure management rather than guiding the immune system to better repair the damaged tissue. After admission, patients are given anti-coagulants and anti-platelet drugs, nitrates to enlarge blood vessels, and beta blockers to prevent secondary MI². Following thrombolysis, PCI, or bypass surgery, patients are often prescribed a regime of statins to lower blood cholesterol, additional antiplatelet drugs, and angiotensin converting enzyme (ACE) inhibitors to prevent ventricular remodeling³. Except for the ACE inhibitors, these therapies stabilize the patient and prevent short-term recurrent infarction, doing nothing to direct the sterile immune response, fibrosis, and cardiomyocyte viability; this highlights an area in

desperate need for innovation to provide better patient care and improve healthspan and lifespan.

1.2 Cellular Turnover

Following the blockade of an artery, the heart tissue fails to establish nutrient transport, generating a hypoxic environment that damages and kills resident cells. Most importantly, cardiomyocytes, which generate the contractile force of the heart pump, fail to contract and ultimately necrose, leaving a dead infarct zone^{4,5}. Sensing of dead cells in the peri-infarct region by a variety of innate pattern recognition receptors on cells such as fibroblasts, neutrophils, macrophages, and other resident leukocytes initiates an inflammatory cascade to patch the damage⁶⁻⁸. Many chemokines are secreted in a temporally dependent fashion to attract several waves of immune cells to the damaged region and begin the process dead cell clearance and scar formation⁹⁻¹¹. This process is critical, as the depletion of many chemokines or their cognate cell types can result in the abrogation of the healing cascade and cause cardiac rupture as the hole left by the dead cells remains unfilled¹²⁻¹⁵. Conversely, however, if this healing response is exaggerated, too much scar tissue is deposited, generating a stiff region of the ventricular wall that can no longer contract¹⁶. In the long term this mechanical dysregulation results in poor ejection fraction, thinning of the ventricular wall, and dilation of the heart chamber¹⁷. Taken together, this presents a Goldilocks scenario in which the healing cascade must be activated to a happy medium, patching the

necrosed region while still allowing mechanical function. Cellular composition of the heart and their corresponding knockout's effect on infarct healing will be discussed in greater detail in chapter 2.

1.3 Known Post-MI Ligands and their Activating Pathways

Once the infarction event occurs, stress causes resident cardiac cells to necrose and apoptose and neutrophils to degranulate. Platelets from the blood along with the neutrophils generate large amounts of TGF- β 1 locally, and cardiac fibroblasts release matrix metalloproteinases to digest the debris¹³. Endothelial cells quickly release TNF- α and cardiomyocytes and fibroblasts secrete IL-1 β and chemokine gradients in response to damage signals sensed via extracellular toll-like receptors (TLRs)¹⁸. Circulating TNF- α and IL-1 β then spur IL-6 and acute phase protein responses in the liver that help activate platelets and red blood cells to secrete thrombin and generate a fibrin scaffold around the site of injury¹⁸. In addition to activating the clotting cascade, thrombin has also been demonstrated to cleave other proteins, including osteopontin, a pro-fibrotic matricellular protein, into a shorter isoform that provides better adhesion of leukocytes to the site of injury^{19,20}. This, plus the upregulation of fibroblast-derived fibronectin, allows for attachment of leukocytes recruited by chemokines and additional secretion of pro-fibrotic factors over the first few days after injury. These events also initiate the renin-angiotensin-aldosterone system, which, in concert with stretched cells secreting atrial natriuretic peptide, causes fluid retention and vasoconstriction^{3,21}.

While this helps prevent blood loss in the short term, this can also prolong ischemia in the infarct site, and therefore ACE inhibitors are commonly prescribed in response to MI. This cocktail of inflammation of the heart initiates a pro-inflammatory cascade involving many central signaling pathways, though central stress pathways such as AP-1 and NF- κ B appear to be driving many of these changes. An overview of the critical post-MI ligands and pathways is provided in chapter 2, and in-vitro validation of AP-1 and NF- κ B contributions to matrix formation are discussed in chapter 4.

1.4 Inflammation Initiation and Resolution

In the 1980's several observations relating to how the body clears different types of pathogens (bacteria, parasites, fungi, and viruses) led to the postulation of Th1 and Th2 responses in T cells, describing intracellular vs extracellular (antibody-mediated) responses, respectively²². A decade later, regulatory T cells which dampen immunological responses were discovered, and a decade later still, Th17 cells were added to the dichotomy as contributors to autoimmunity and later as anti-fungal and antiviral responses²³. These classifications were built around T lymphocyte phenotypes in response to several stimuli and were then thought to shape the phenotypes of other plastic leukocytes in the microenvironment, such as macrophages and innate lymphoid cells. Over time, the M1/M2 (corresponding to Th1/Th2 cytokines) paradigm began to expand into many more subtypes as researchers tried to force the transposition of T cell classifications onto

macrophages. The invention of single-cell sequencing technologies and the discovery of heterogeneous macrophage phenotypes in-vivo and ex-vivo, combined with contradictory and poorly defined macrophage dichotomies, suggests these classifications may not be representative for each cell type^{15,24}. In contrast, innate lymphoid cells (ILCs), which were discovered less than a decade ago, seem to better fit the helper T classifications, though it remains to be seen if this will remain true in another decade²⁵. While these labels can be helpful in pathogenic models, many of these programs may differ in the context of sterile injury.

Regarding post-MI sterile injury, much of the immunological focus is shifted to innate populations and regulatory T cells. Several groups have demonstrated the importance of macrophage subsets in producing either helpful or hurtful responses after MI, and these subsets are better defined by ontology-based marker expression rather than M1/M2. For example, the macrophage compartments in many organs can be classified based on yolk-sac, CCR2^{hi}, and CCR2^{low} expression, with CXCR4 better defining CCR2^{low} populations in the heart^{15,25}. The latter two populations are derived from definitive hematopoiesis and are knockout studies have demonstrated their detrimental effect on heart repair (see chapter 2). These reductive studies highlight the importance of the innate system coordinating the adaptive (specifically Treg) responses after injury and ultimately abrogating the pro-fibrotic programs²⁶. Dysregulation of these processes can then result in either prolonged inflammation that results in autoimmune and

degenerative phenotypes, or pro-fibrotic/pro-tumor environments that skew towards matrix deposition. While both the anabolic and catabolic stages of inflammation are required for a healthy healing process, thus clearing and repopulating the damaged area, the cues that instruct the advancement from one phase to the next remain elusive. Broadly speaking, regulatory T cells are thought to quench inflammation as demonstrated by their abrogation of Th1 responses and Treg KO experiments yielding autoimmune degenerative tissue milieus^{27,28}. Quickly quenching a pro-inflammatory environment via Tregs, however, does not yield the same result as a tissue that was never insulted at all²⁶; Similarly, artificially inducing a Th2 response does not offset Th1 effects²⁹. That is to say that Th1 and Th2 do not exist on a single axis, and Tregs do not center the inflammatory microenvironment to a central neutral state. For this reason, therapeutic approaches should consider inhibiting initiation of inflammatory polarization rather than bolstering the “opposite” inflammatory axis.

1.5 Fibroblast Form and Function

The heart is composed of four chambers that contract to pump blood, septa that carry electrical signals with each heartbeat and separate the pulmonary from systemic circulation, and valves that allow pressure gradient formation between atria and ventricles. The developmental origins of fibroblasts define which anatomical location they populate, with second heart field progenitor cells infiltrating the atria, septa, and valves, and epicardial-derived cells residing in the

ventricular walls^{30,31}. Single-cell ATAC and RNA sequencing experiments have demonstrated that the chromatin organization of cardiac fibroblasts, regardless of location, are almost identical³². Their transcriptional programs, however, differ in meaningful ways, suggesting that their topology provides cues to inform function³². This priming becomes important when considering a cell's propensity to differentiate or activate into a myofibroblast, a type of contractile, proliferating, and matrix-secreting fibroblast – the culprit in scar formation. Though the transition from fibroblast to myofibroblast is sometimes described as a type of differentiation, these states are not stable, and cells can activate in the presence of inflammatory agonists and return to quiescence after prolonged withdrawal from agonists. Activation markers such as alpha smooth muscle actin (ACTA2) and fibroblast activation protein (FAP) provide useful markers for pro-fibrotic regions and often serve as a surrogate for measuring fibrosis^{33,34}. For in-vitro assays, using surrogate markers may prove helpful as collagen can take several weeks to become assembled without exogenous stabilizers of bone morphogenic protein 1 (BMP1), which helps to cleave procollagen into collagen for assembly³⁵. For this reason, many groups chose to measure collagen 1 and 3 production by mRNA transcription rather than at the protein level. In 3D culture, however, BMP1 is stabilized and thus collagen is more easily quantified in a short-term assay. While collagen 1 is most commonly associated with scar composition, other matrix components such as fibronectin, matricellular proteins, and proteoglycans, and proteoglycans are critical to the structure and integrity of the heart ECM³⁶.

1.6 Extracellular Matrix Assembly and Structure

After the clot is formed in the site of injury, it is gradually degraded and replaced by an immature scar, which is then further remodeled in both structure and composition. Initially, large amounts of serum-derived fibronectin and fibrin are incorporated into the scar, which are then replaced by fibroblast-derived isoforms, fibrillar collagens, matricellular proteins, and glycosaminoglycans¹⁷. Additional matrix crosslinking enzymes such as lysyl oxidases then bind collagen fibers together and further increase tensile strength³⁷. A healthy heart can be thought of as having several layers of muscle (stacking from the luminal surface to the pericardial space), each with its own alignment, thus allowing for the unique upward and twisting motion of heart contraction¹⁷. Scar fibers, however, will remodel over time to align along the axis of greatest strain (generally the outermost radial plane), providing stability against the greatest stresses, but also preventing effective contraction. The collagen-rich scar then thins and stiffens over time, which is modeled by the Law of LaPlace, dictating that an increasingly thin-walled sphere must increase in rigidity to accommodate a constant load. The noncompliant scar then increases wall stresses, further mechanically stimulating fibroblasts to secrete and assemble more matrix, establishing a positive fibrotic feedback loop³⁸. For this reason, attempts at regenerating cardiac tissue account for the organization in addition to composition of the tissue to prevent naturally occurring fibrotic pitfalls.

1.7 References

1. Heart Association, A. 2021 Heart Disease and Stroke Statistics Update Fact Sheet At-a-Glance.
2. Overview of the acute management of ST-elevation myocardial infarction - UpToDate. <https://www.uptodate.com/contents/overview-of-the-acute-management-of-st-elevation-myocardial-infarction>.
3. Palardy, M., Ducharme, A. & O'Meara, E. Inhibiting the Renin-Angiotensin System with ACE Inhibitors or ARBs After MI. *Current Heart Failure Reports* **4**, 190–197 (2007).
4. Collart, M. A., Baeuerle, P. & Vassalli, P. Regulation of tumor necrosis factor alpha transcription in macrophages: involvement of four kappa B-like motifs and of constitutive and inducible forms of NF-kappa B. *Molecular and Cellular Biology* **10**, 1498–1506 (1990).
5. Kapadia, S. R. *et al.* Hemodynamic Regulation of Tumor Necrosis Factor- Gene and Protein Expression in Adult Feline Myocardium. *Circulation Research* **81**, 187–195 (1997).
6. Erridge, C. Endogenous ligands of TLR2 and TLR4: agonists or assistants? *Journal of Leukocyte Biology* **87**, 989–999 (2010).
7. Previtiera, M. L. & Sengupta, A. Substrate stiffness regulates proinflammatory mediator production through TLR4 activity in macrophages. *PLoS ONE* **10**, (2015).
8. Elsaid Marwa Qadri, A., Almadani, S. & Jay, G. D. Expression of Proinflammatory Cytokines of Human Macrophages and Downstream Role of CD44 in Regulating TLR2 Activation. (2019) doi:10.4049/jimmunol.1700713.
9. Sierra-Filardi, E. *et al.* CCL2 Shapes Macrophage Polarization by GM-CSF and M-CSF: Identification of CCL2/CCR2-Dependent Gene Expression Profile. *The Journal of Immunology* **192**, 3858–3867 (2014).
10. Döring, Y., Pawig, L., Weber, C. & Noels, H. The CXCL12/CXCR4 chemokine ligand/receptor axis in cardiovascular disease. *Frontiers in Physiology* **5 JUN**, 212 (2014).
11. Kew, R. R., Penzo, M., Habel, D. M. & Marcu, K. B. The IKK α -Dependent NF- κ B p52/RelB Noncanonical Pathway Is Essential To Sustain a CXCL12 Autocrine Loop in Cells Migrating in Response to HMGB1. *The Journal of Immunology* **188**, 2380–2386 (2012).

12. Horckmans, M. *et al.* Neutrophils orchestrate post-myocardial infarction healing by polarizing macrophages towards a reparative phenotype. *European Heart Journal* **38**, 187–197 (2017).
13. Ma, Y. *et al.* Temporal neutrophil polarization following myocardial infarction. *Cardiovascular Research* **110**, 51–61 (2016).
14. Wang, L. *et al.* Inhibition of toll-like receptor 2 reduces cardiac fibrosis by attenuating macrophage-mediated inflammation. *Cardiovascular Research* **101**, 383–392 (2014).
15. Dick, S. A. *et al.* Self-renewing resident cardiac macrophages limit adverse remodeling following myocardial infarction. *Nature Immunology* **20**, 29–39 (2019).
16. Schafer, S. *et al.* IL-11 is a crucial determinant of cardiovascular fibrosis. *Nature* **552**, 110–115 (2017).
17. Richardson, W. J., Clarke, S. A., Alexander Quinn, T. & Holmes, J. W. Physiological implications of myocardial scar structure. *Compr Physiol* **5**, 1877–1909 (2015).
18. Murphy, K. & Weaver, C. *Janeway's Immunobiology*. (Garland Science/Taylor & Francis Group, LLC, 2016).
19. Schulze, E. B., Chambers, A. F., Tuck, A. B. & Allan, A. L. The thrombin cleavage domain of osteopontin is important for mediating growth and adhesive properties of human breast cancer cells. *Cancer Research* **66**, (2006).
20. Grassinger, J. *et al.* Thrombin-cleaved osteopontin regulates hemopoietic stem and progenitor cell functions through interactions with $\alpha 9\beta 1$ and $\alpha 4\beta 1$ integrins. *Blood* **114**, 49–59 (2009).
21. Moubarak, M. *et al.* Effects of atrial natriuretic peptide on rat ventricular fibroblasts during differentiation into myofibroblasts. *Physiological Research* **64**, 495–503 (2015).
22. Mosmann, T. R. & Coffman, R. L. Two types of mouse helper T-cell clone. Implications for immune regulation. *Immunology Today* **8**, 223–227 (1987).
23. Sakaguchi, S., Sakaguchi, N., Asano, M., Itoh, M. & Toda, M. Immunologic self-tolerance maintained by activated T cells expressing IL-2 receptor alpha-chains (CD25). Breakdown of a single mechanism of self-tolerance causes various autoimmune diseases. *The Journal of Immunology* **155**, (1995).

24. Dick, S. A. *et al.* Three tissue resident macrophage subsets coexist across organs with conserved origins and life cycles. *Science Immunology* **7**, (2022).
25. Spits, H. *et al.* *Innate lymphoid cells — a proposal for uniform nomenclature.* *Nature Reviews Immunology* vol. 13 www.nature.com/reviews/immunol (2013).
26. Jung, M. *et al.* IL-10 improves cardiac remodeling after myocardial infarction by stimulating M2 macrophage polarization and fibroblast activation. *Basic Research in Cardiology* **112**, 33 (2017).
27. Dejaco, C., Duftner, C., Grubeck-Loebenstien, B. & Schirmer, M. Imbalance of regulatory T cells in human autoimmune diseases. *Immunology* **117**, 289 (2006).
28. Tai, Y., Sakamoto, K., Takano, A., Haga, K. & Harada, Y. Dysregulation of humoral immunity in Foxp3 conditional-knockout mice. *Biochemical and Biophysical Research Communications* **513**, 787–793 (2019).
29. Shintani, Y. *et al.* IL-4 as a Repurposed Biological Drug for Myocardial Infarction through Augmentation of Reparative Cardiac Macrophages: Proof-of-Concept Data in Mice. *Scientific Reports* **7**, (2017).
30. Ivey, M. J. & Tallquist, M. D. Defining the Cardiac Fibroblast: A New Hope. doi:10.1253/circj.CJ-16-1003.
31. Souders, C. A., Bowers, S. L. K. & Baudino, T. A. Cardiac Fibroblast, The Renaissance Cell. *Circulation Research* **105**, 1164–1176 (2009).
32. Hocker, J. D. *et al.* Cardiac cell type-specific gene regulatory programs and disease risk association. *Science Advances* **7**, eabf1444 (2021).
33. Tillmanns, J. *et al.* Fibroblast activation protein alpha expression identifies activated fibroblasts after myocardial infarction. *Journal of Molecular and Cellular Cardiology* **87**, 194–203 (2015).
34. van Putten, S., Shafieyan, Y. & Hinz, B. Mechanical control of cardiac myofibroblasts. *Journal of Molecular and Cellular Cardiology* vol. 93 133–142 (2016).
35. Puerta Cavanzo, N., Bigaeva, E., Boersema, M., Olinga, P. & Bank, R. A. Macromolecular Crowding as a Tool to Screen Anti-fibrotic Drugs: The Scar-in-a-Jar System Revisited. *Frontiers in Medicine* **7**, 1092 (2021).
36. Lindsey, M. L., Jung, M., Hall, M. E. & DeLeon-Pennell, K. Y. Expert Review of Proteomics Proteomic analysis of the cardiac extracellular matrix: clinical

research applications Proteomic analysis of the cardiac extracellular matrix: clinical research applications. (2018) doi:10.1080/14789450.2018.1421947.

37. López, B. *et al.* Role of lysyl oxidase in myocardial fibrosis: from basic science to clinical aspects López B, González A, Hermida N, Valencia F, de Teresa E, Díez J. Role of lysyl oxidase in myocardial fibrosis: from basic science to clinical aspects. *Am J Physiol Heart Circ Physiol* **299**, 1–9 (2010).

38. Herum, K. M., Choppe, J., Kumar, A., Engler, A. J. & McCulloch, A. D. Mechanical regulation of cardiac fibroblast profibrotic phenotypes. *Mol Biol Cell* **28**, 1871–1882 (2017).

Chapter 2: Regenerative Crosstalk between Cardiac Cells and Macrophages

2.1 Abstract

Aside from the first week postnatal, murine heart regeneration is restricted and responses to damage follow classic fibrotic remodeling. Recent transcriptomic analyses have suggested that significant crosstalk with the sterile immune response could maintain a more embryonic-like signaling network that promotes acute, transient responses. However with age, this response—likely mediated by neonatal yolk sac macrophages—then transitions to classical macrophage-mediated, cardiac fibroblast (CF)-based remodeling of the extracellular matrix (ECM) after myocardial infarction (MI). The molecular mechanisms that govern the change with age and drive fibrosis via inflammation are poorly understood. Using multiple RNA-seq datasets, we attempt to resolve the relative contributions of CFs and macrophages in the bulk healing response of regenerative (postnatal day 1) and non-regenerative hearts (postnatal day 8+). We performed an analysis of bulk RNA-seq datasets from myocardium and cardiac fibroblasts as well as a single-cell RNA-seq dataset from cardiac macrophages. MI-specific pathway differences revealed that non-regenerative hearts generated more ECM and had larger matricellular responses correlating with inflammation, produced greater chemotactic gradients to recruit macrophages, and expressed receptors for danger-associated molecular patterns at higher levels than neonates. These changes could result in elevated stress response pathways compared to neonates, converging at NF- κ B and AP-1 signaling. Pro-fibrotic gene programs, which greatly diverge on day 3 post-MI, lay the foundation for chronic fibrosis, and thus postnatal

hearts older than 7 days typically exhibit significantly less regeneration. Our analyses suggest that the macrophage ontogenetic shift in the heart postnatally could result in detrimental stress signaling that suppresses regeneration.

2.2 New and Noteworthy

Members Immediately post-natal mammalian hearts are able to regenerate after infarction, but the cells, pathways, and molecules that regulate this behavior are unclear. By comparing RNA-seq datasets from regenerative mouse hearts and older, non-regenerative hearts, we are able to identify biological processes that are hallmarks of regeneration. We find that sterile inflammatory processes are upregulated in non-regenerative hearts, initiating pro-fibrotic gene programs 3 days after myocardial infarction that can cause myocardial disease.

2.3 Introduction

The heart wall is often mistakenly viewed as being enriched in contractile cells, but cardiomyocytes only compose about 25% of the myocardium; endothelial cells (~60%) and cardiac fibroblasts (~15%) make up the majority of the tissue along with other smaller cell populations¹. During myocardial infarction (MI), coronary artery occlusion results in ischemic injury to cardiac tissue, which recruits several white blood cell populations². The resulting sterile inflammatory cascade begins with neutrophils, mast cells, and macrophages sensing damage-associated molecular patterns (DAMPs) or hypoxia^{3,4}. Responding cells pick up molecular

cues from the microenvironment which then dictate their inflammatory status^{5,6}. Once educated, these cells are able to directly or indirectly steer tissue resorption, growth, and extracellular matrix (ECM) deposition, as well as recruit regulatory T-lymphocytes to quench the inflammatory process⁷. What naturally results from excessive matrix production is a non-contractile, rigid scar that dramatically reduces heart ejection fraction.

While the steps in this process are well known, contributions by individual resident myocardial cell types, the specific molecular pathways they utilize, and how they change with age are not completely clear. For example, epicardially-derived cardiac fibroblasts (CFs) are the primary ECM producers in the heart and secrete a wide variety of scaffolding proteins for parenchymal cells⁸. They also sense and respond to many structural and secreted cues, e.g. pro-inflammatory signals to increase their contractility and ECM assembly⁹ as they become “myofibroblasts.” In addition to traditional cues such as TGF- β , fibroblasts can be activated via Toll-Like Receptors (TLRs), such as TLR2 and TLR4¹⁰. Both receptors are promiscuous and bind to many DAMPS including lipopolysaccharide (LPS), low molecular weight hyaluronic acid (LMW HA), the chromatin binding protein HMGB1, and others¹¹. The end-result of this signaling is increased collagen I, collagen III, and fibronectin synthesis, matrix cross-linking, and secretion of ECM binding proteins¹²⁻¹⁷ that create a stiff scar and can induce myofibroblast trans-differentiation¹⁸. Scar formation is also balanced by ECM degradation rate; fibroblast-secreted matrix metalloproteinases, metalloproteinases, calpain,

cathepsins, and caspases enzymatically digest and help recycle matrix¹⁹, while tissue inhibitors of metalloproteases (TIMPs) skew the equilibrium toward matrix deposition. Chronically, age-associated heart stiffening is both a symptom as well as an agonist of disease²⁰.

Alongside resident CFs, macrophages are also present early in heart development and arise from yolk sac (YS) progenitors that migrate between developing organs before differentiating into tissue-specific, resident macrophages^{21,22}. Later in development, definitive hematopoiesis generates marrow-derived monocytes²³ which are also recruited to the myocardium and then become macrophages. YS and bone marrow-derived macrophages (BMDMs) appear functionally distinct in many organs, including responding differently to pathological cues^{24,25}; for example, LYVE1 and TIMD4 are restricted to the YS-lineage⁴ and facilitate hyaluronan binding²⁶ and phagocytosis²⁷, respectively, to help “cloak” pro-inflammatory signals²⁸. In contrast, more BMDMs are recruited after infarction⁴ via well documented chemokine cascades, e.g. CCL2-CCR2, that create acute inflammation²⁹ detrimental to the repair process³⁰. Yet once these BMDMs have integrated with the destination tissue, they become transcriptionally similar to cardiac YS macrophages⁴ but without the regenerative capacity. Thus, YS macrophages may be the only pro-regenerative subpopulation in the heart.

Differences in developmental lineage, as well as tissue priming and response to pathogens can lead to a diverse set of macrophage phenotypes. While many groups have relied on the M1/M2 dichotomy that was introduced in the late 1990s

to describe macrophages impacted by a Th1 or Th2 response³¹, this system fails to encompass the plurality of characteristics that macrophages exhibit³². Therefore, additional discussion of macrophage phenotype and marker expression will be primarily described by functional attributes for the remainder of this study.

The complex signaling networks introduced above imply that matrix expression and healing are not simply composed of “on” or “off” cues. Identifying clusters of genes that are coordinated by conserved regulatory mechanisms and are involved in CF-macrophage crosstalk may more easily identify mechanism(s) and reveal better targets for therapy. Thus, we analyzed immediately postnatal (P1) and 1+ week old (P8) RNA-seq datasets from bulk ventricular tissue³³ (GSE123868), sorted cardiac fibroblasts³⁴ (GSE49906), and single-cell macrophages⁴ (GSE119355) with the goal of elucidating age and MI-dependent programmatic changes. While the bulk ventricular dataset contains all experimental groups (postnatal day 1 and 8 and MI/sham), it lacks the cellular resolution to understand macrophage and cardiac fibroblast signaling differences. Therefore, we employ the latter two datasets to attribute tissue-level changes to either cell type. Together the literature and our analyses suggest that the window of opportunity for successful regeneration, likely mediated by CF crosstalk with YS macrophages rather than with BMDMs, is restricted to 3 days post-MI.

2.4 Methods

2.4.1 Bulk RNA-seq Processing

Sequencing files were obtained from the GEO database under accessions GSE123868, GSE49906, and GSE119355. Bulk FASTQ files were aligned to the mm10 genome using STAR with the following settings: `--readFilesCommand zcat --genomeLoad LoadAndRemove --outFilterType BySJout --outFilterMultimapNmax 10 --alignSJoverhangMin 8 --alignSJDBoverhangMin 1 --outFilterMismatchNmax 4 --alignIntronMin 20 --alignIntronMax 1000000 --alignMatesGapMax 100000`. BAM files were sorted and indexed using samtools. Raw and transcripts per kilobase million (TPM) normalized tag directories were generated using HOMER command `makeTagDirectory` and `analyzeRepeats` scripts. Statistical significance for Giudice et al.⁴⁸ and Wang et al.³³ raw counts was determined using EdgeR³⁵ and DESEQ2³⁶ in the `getDiffExpression` HOMER script, respectively based on replicate numbers (no replicates justified EdgeR, replicate of 3 justified DESEQ2). Biological process and molecular function gene ontologies were generated using Panther³⁷ over-representation with a Bonferroni test. Graphs of TPM-normalized values were generated using R and `ggplot` and `heatmap` packages. PCA plots were generated using Clustvis³⁸.

2.4.2 Single-Cell RNA-Seq Processing

Single-cell macrophage data⁴ was read into the Seurat³⁹ package of R (Version 3.1) using provided matrix and TSV files. Data was filtered by selecting

only cells with 1000 to 5800 features (referring to unique genes), where those features were detected in at least 3 cells. Cells with >18% mitochondrial reads were removed from analysis due to indicating apoptosis. Default log normalization was performed across separate Seurat objects for control, infarcted, and combined datasets. Differential gene expression was determined using default FindVariableFeatures parameters, and then the data was scaled to regress mitochondrial counts. Dimensionality of each dataset was determined using Elbow and JackStraw Plots for each Seurat object. A chemokine-receptor specific Seurat object was subset from the original combined object, selecting only cells with expression of CCR2 >1, CXCR4 >1, and Timd4 >0.5, encompassing 60% of the original cells. Values were experimentally determined based on yielding a significant sample size and specific marker expression of the cells that best binned into the three categories while minimizing noise. This object was used to generate Spp1 and Ccl24 plots from Figure 2.1.

2.4.3 Statistical Analysis

Statistical significance was determined using default parameters of HOMER's DESEQ2 for bulk myocardium and EdgeR for cardiac fibroblast datasets, respectively. For DESEQ2 (version 1.22.1), samples were grouped by age, timepoint, and infarction status, with each permutation representing a treatment in the design matrix. Counts were generated using the DESEQDataSetFromMatrix command and compared using a Wald test and

corrected using the Benjamini-Hochberg procedure. P values, \log_2 fold change, and adjusted p values were generated for each gene and filtered manually using R, selecting only genes with an adjusted p-value of 0.05, minimum fold change of +/- 2 and minimum 32 tags in one dataset per gene. For EdgeR (version 3.26.0), counts were read in using DGEList while library sizes and normalization factors were calculated from Tag Directory sizes. Reads were counted using DGEList, with each sample constituting a treatment in the design matrix. Common dispersion was estimated at 0.05 as recommended. P-values were generated using an Exact Test and corrected using the Benjamini-Hochberg method. As before, only genes with an adjusted p-value of 0.05, minimum fold change of +/- 2 and minimum 32 tags in one dataset per gene. For single-cell data, FindMarkers was used to identify gene landmarks of clusters. Summarily, a $\log(\text{variance})$ and $\log(\text{mean})$ relationship was determined using local polynomial regression and variance was calculated using standardized values after clipping to a maximum. Statistical significance was calculated by only comparing positive markers with a minimum \log_2 fold change of 0.25 and minimum percentage positive of 0.25 using a Wilcox test.

2.5 Results and Discussion

Statistical The onset of a myocardial infarction produces many biological, chemical, and physical signals that activate the microenvironment: ECM degradation, excessive wall stretch, necrosing cells that release damage-

associated molecular patterns (DAMPs) and disrupt cell-cell communication, and hypoxia. These signals result in an increase in ECM deposition, upregulation of cell adhesion molecules, an increase in DAMP sensitivity, chemokine production, and reduction of cytokine suppressors. Each of these signals may impact cell types antagonistically or synergistically, so analyses here focus on key myocardial cell

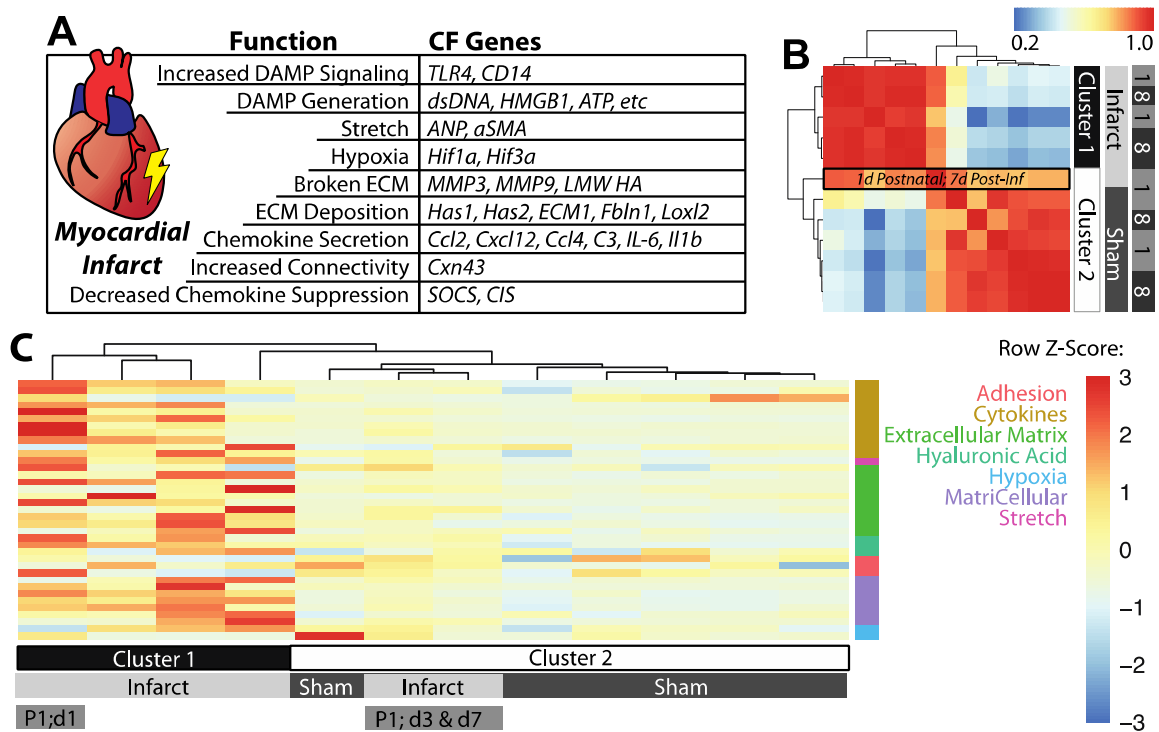


Figure 2.1: Transcriptomic analyses of infarct and sham bulk highlight changes in specific remodeling pathways.

(A) Table of gene groupings and corresponding genes that literature suggest are differentially expressed with myocardial infarction. (B) Heatmap of bulk RNA-seq data (averaged across three mice per group) showing hierarchical clustering of myocardia based on infarction. The only MI group that clustered with sham controls is indicated in the black box and is the 1d postnatal MI group after 7 days of healing. (C) Heatmap of the TPM Z-scores of the 37 genes, with rows grouped by functional process and columns clustered using K-means. Cluster 1 denotes all the infarct groups from day-8 postnatal mice (independent of days post-infarct) and the first timepoint after infarction for day-1 mice. Days 3 and 7 post-infarct groups of postnatal day-1 infarcted hearts clustered with sham samples, indicating their return to baseline in as little as 3 days.

types and the genes that regulate their behavior. More specifically, we analyzed gene transcription in critical functional categories mentioned above and found 37 that were statistically significant and differentially regulated with age and infarction in the bulk ventricular dataset (**Fig. 2.1A**).

Hierarchical clustering of these genes in infarcted and sham myocardia from postnatal day-1 and -8 (P1/P8) hearts showed clustering based on injury and not postnatal age, except for the P1 samples one week after infarction (**Fig. 2.1B**) - at this time point, prior analyses indicated functional recovery of the tissue³³. Since the clustering of our 37 genes mirror that of the whole transcriptome (i.e., Figure 2.1B in reference 33), these genes are likely to play a key role in regeneration, or at least be representative of processes that drive global transcriptional changes. K-means clustering of the per-gene heatmap revealed activation of a distinct transcriptional program in P1 hearts immediately after infarction, in which every process except hypoxia was upregulated (**Fig. 2.1C, Table S2.1**). To further highlight these genes and their functional groupings, we examined their change in expression over time post-injury. We found that regenerative hearts resembled sham more quickly after infarction (i.e., there were fewer differentially expressed genes); extracellular matrix genes largely returned to baseline after 7 days (**Fig. 2.2A**). In contrast, hearts infarcted at day-8 upregulated ECM and matricellular genes through day 7 (**Fig. S2.1**) and had prolonged differential expression of cytokine genes. These data indicate that the acute response to MI of postnatal

day-8 hearts activates gene programs associated with chronic fibrosis and are detectable as early as 3-7 days post-infarction.

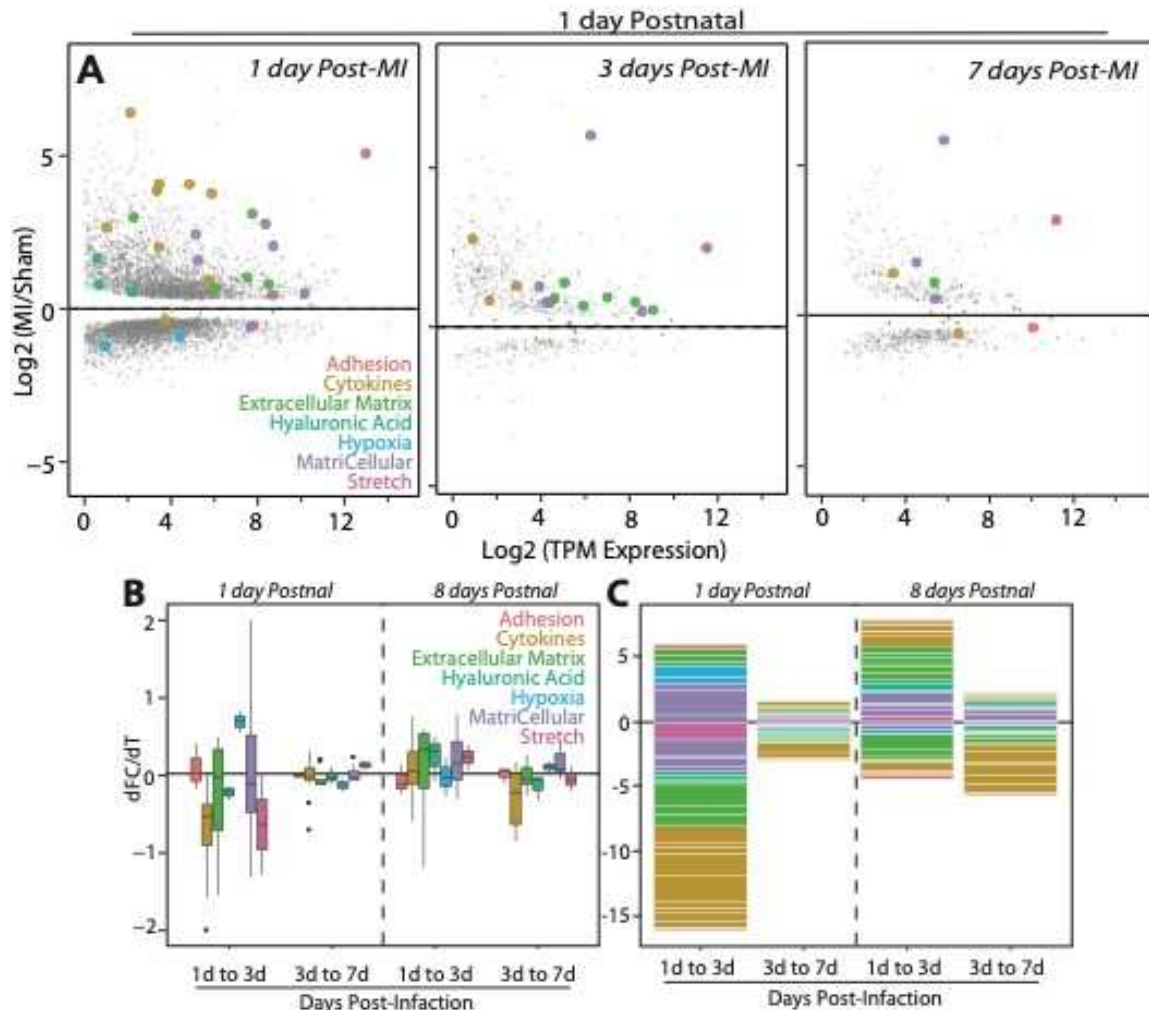


Figure 2.2: MI induces the largest transcriptomic changes initially in younger mice but older mice maintain significant transcriptional differences.

(A) MA plots show the relationship between the MI/Sham gene ratio (i.e., fold change) and the transcript per million reads for murine myocardia infarcted 1-day postnatal and chased for up to 7 days post-MI as indicated in each panel. Gene functional groupings listed are annotated in the figure by color and with large data points for visualization (when individual gene is statistically significant by Wald test with Benjamini-Hochberg correction; $q < 0.05$). Gray data points are coded by size for significance but are not the 37 literature-identified genes used in the rest of the analysis. (B) Box-and-whisker plot indicate the changes, broken down by category, in gene ratio (MI/sham) between transcriptome sampled over time as indicated at bottom. Data for mice infarcted 1 day and 8 days postnatal are separated by a dashed line. (C) Stacked bar plot annotates the log₂ of the fold change for genes of the indicated ontologies/functions (genes with ratios less than one result in a negative number).

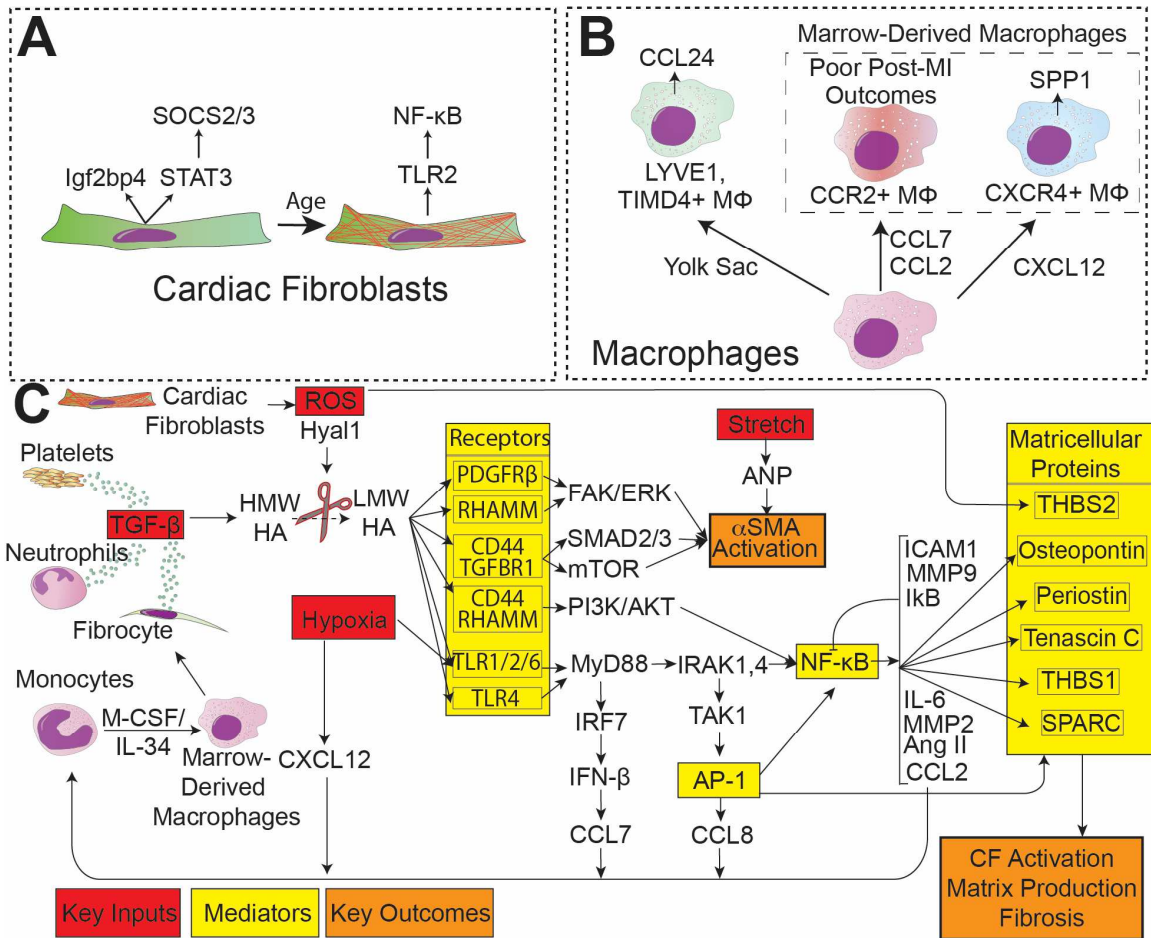


Figure 2.3: Model for cellular and molecular changes with age and infarction.

(A) Age related transcriptional differences in fibroblasts. As fibroblasts progress through development, they upregulate TLR2 expression and downregulate STAT3 and Igf2bp3. **(B)** Macrophage composition of the heart shifts from CCL24-producing YS lineage cells to two ontogenies of BMDMs: CXCR4+ and CCR2+. **(C)** Proposed molecular mechanism for non-regenerative cardiac fibroblasts. MI in postnatal day 8 hearts generate inflammatory ligands (red) to a greater extent than postnatal day 1 hearts, which are sensed to a greater extent by TLR2, and ultimately result in NF-κB and AP-1 activation (yellow). Lastly, the signal propagation results in excess matricellular protein and ECM deposition (orange). Signaling from receptors and continuing to the right is believed to occur in fibroblasts.

Expression differences over time indicate differential gene program acceleration/deceleration between timepoints; ECM, matricellular, cytokine, and HA signaling processes were among the most volatile after infarction, but day-1

hearts largely stabilized three days after infarction as their fold-change differences are markedly reduced at day 7. In contrast, processes such as hypoxia, stretch, and adhesion and growth underwent modest fold-change differences, but remained persistent in their expression over time (**Fig. 2.2B-C**). These data are suggestive of two key changes in cardiac fibroblasts and macrophages that result from these transcriptional differences: namely that inflammatory cascades^{29,40} cause cardiac fibroblasts to activate and resemble contractile myofibroblasts⁹ (**Fig. 2.3A**) and that macrophages transition to a BMDM origin through activation of CCL2/7 and CXCL12 (**Fig. 2.3B**). To better understand how post-MI processes are affected by aging, we created a signaling model from our RNA-seq meta-analysis and fibroblast literature; in this model in Figure 2.3C, we map important inputs (red), which our meta-analysis shows are most differentially expressed, intermediaries (yellow), and resulting outcomes that are linked to poor patient prognosis (orange). The summary outcome is that non-regenerative day 8 hearts exaggerate hypoxic response, chemoattraction, and DAMP generation and sensitivity while losing embryonic-restricted growth signals through macrophages and fibroblasts. The culmination of these processes results in increased NF- κ B and AP-1 signaling (yellow noted in **Fig. 2.3C**) that spurs matricellular and extracellular matrix protein production. Compositional differences between day-1 and -8 hearts activate divergent responses which either return to baseline or activate the processes highlighted here that ultimately become pathogenic. Each

post-MI process in this model is explained in greater detail below, with background provided before analysis in each category.

2.5.1 Chemokines, Cytokines, Suppressors, and Interferon Responses

Chemokines—a chemotactic subset of cytokines—are responsible for immune recruitment to the site of injury, and many of these proteins are expressed in response to infarction. When cross-referenced with a whole-heart dataset³³, several chemokines are differentially expressed between regenerative and nonregenerative hearts initially but decrease by day 3, e.g. Cxcl2 and Ccl3/4 (**Fig. S2.2A**). In the context of the regenerative phenotype, Ccl3 binds Ccr1, which is expressed on YS macrophages, as well as some interferon-responsive and recruited macrophages that are unique to injury. Ccl3/4 also bind to Ccr5⁴¹, which is expressed across all populations (**Fig. S2.2C**); these ligands likely serve as generic macrophage recruitment ligands. Cxcl2 recruits neutrophils by binding to Cxcr2 in the bone marrow, though neutrophils can also be recruited by Ccr2 and Ccr5⁴¹. This demonstrates that a wide variety of neutrophils and macrophages are recruited by regenerative hearts 24 hours post-infarct and that their contribution to healing is less likely ontogenically-based (since Ccl3/4 and Cxcl2 are promiscuous and do not recruit specific subsets) but rather dictated by the microenvironment.

In contrast to non-specific and lowly-expressed chemokines, Ccl2/7 have similar levels at day 1 but peak at day 3 in nonregenerative P8 hearts, while the expression is quenched in regenerative postnatal regenerative day-1 hearts (Fig.

2.4A, Fig. S2.2A). In the context of the signaling network, Ccl7 is secreted by IFN- β stimulated monocytes and B cells to attract classical monocytes and neutrophils, which scavenge dead cells^{2,36,37}. IFN- β is secreted by non-regenerative cardiac fibroblasts at steady-state after myocardial remodeling (**Fig. S2.2B**) as well as by macrophages that have phagocytosed dead cardiomyocytes². Blockade of either Ccl7 or IFN- β signaling increases fractional shortening, decreases infarct size, and improves survival after MI^{2,43}. Similarities between Ccl2/7 and common receptor targets suggests redundancy in recruiting Ccr2⁺ monocytes. As a third expression pattern, we found that the second highest expressed chemokine, Cxcl12, is uniquely upregulated at day 7 in nonregenerative hearts (**Fig. 2.4A**); This ligand binds the receptor CXCR4 and could explain the appearance of this third subset of macrophages prior to harvest on post-natal day 11. Chemokine signatures of non-regenerative (postnatal day-8) hearts, e.g. Cxcl12 and Ccl2/7, are expressed orders of magnitude higher than less specific chemokines, and this very clearly differentiates ontogenies of macrophages post-MI. These observations reinforce the concept that subset-specific chemokines likely ascribe function, while less specific chemokines broadly recruit cells that are informed by local environmental cues to reinforce regeneration.

While understanding white blood cell recruitment helps describe phenotype at the time of injury, cellular effects are achieved primarily through their *in-situ* phenotype during the remodeling process. Classical cytokines associated with wound healing and fibrosis include IL-1 β , TNF α , IL-6, and TGF- β , though only the

latter two cytokines were differently expressed between regenerative and non-regenerative hearts (i.e., upregulated for non-regenerative hearts). IL-1 β , IL-6, and TNF α are all regulated by NF- κ B and less classically STAT3 and AP-1^{44–46}. In macrophages, NF- κ B is also stimulates secretion of Ccl2⁴⁷, which attracts pathogenic CCR2+ monocytes and is upregulated in day-8 hearts three days post-MI (**Fig. 2.4A**). Along with CCR2+ macrophages, the microenvironment is populated with inflammatory proteins linked to poor prognoses. For instance, when fibroblasts bind TGF- β , they become activated, triggering the secretion of IL-6⁴⁸ on day 3 post-infarction in older hearts and correlating with the TGF- β spike (**Fig. S2.2B**). These spikes cause hypertrophy and decrease cardiomyocyte contractility⁴⁹, suggesting that signaling immediately after infarction ultimately leads to the divergent chronic outcomes, i.e. regeneration or pathogenic remodeling as outlined in Fig. 2.3C. This signaling is often transcribed via JAK/STAT pathways, which encode SOCS genes as a negative feedback mechanism to prevent cytokines storms. STAT3 is typically inhibited by SOCS2 and SOCS3, the latter of which results in a downregulation of IL-6⁵⁰. We found that STAT3 is upregulated on day 1 by regenerative hearts, but quickly returns to baseline, correlating with the observed transcription of IL-6. Though SOCS3 is widely expressed across macrophage populations and in steady-state adult cardiac fibroblasts (**Fig. S2.2C-D**), SOCS2 was not highly expressed in either macrophage or fibroblast datasets, suggesting that the primary source of the protein is another cardiac cell type. In summary, STAT3 signaling occurs earlier in

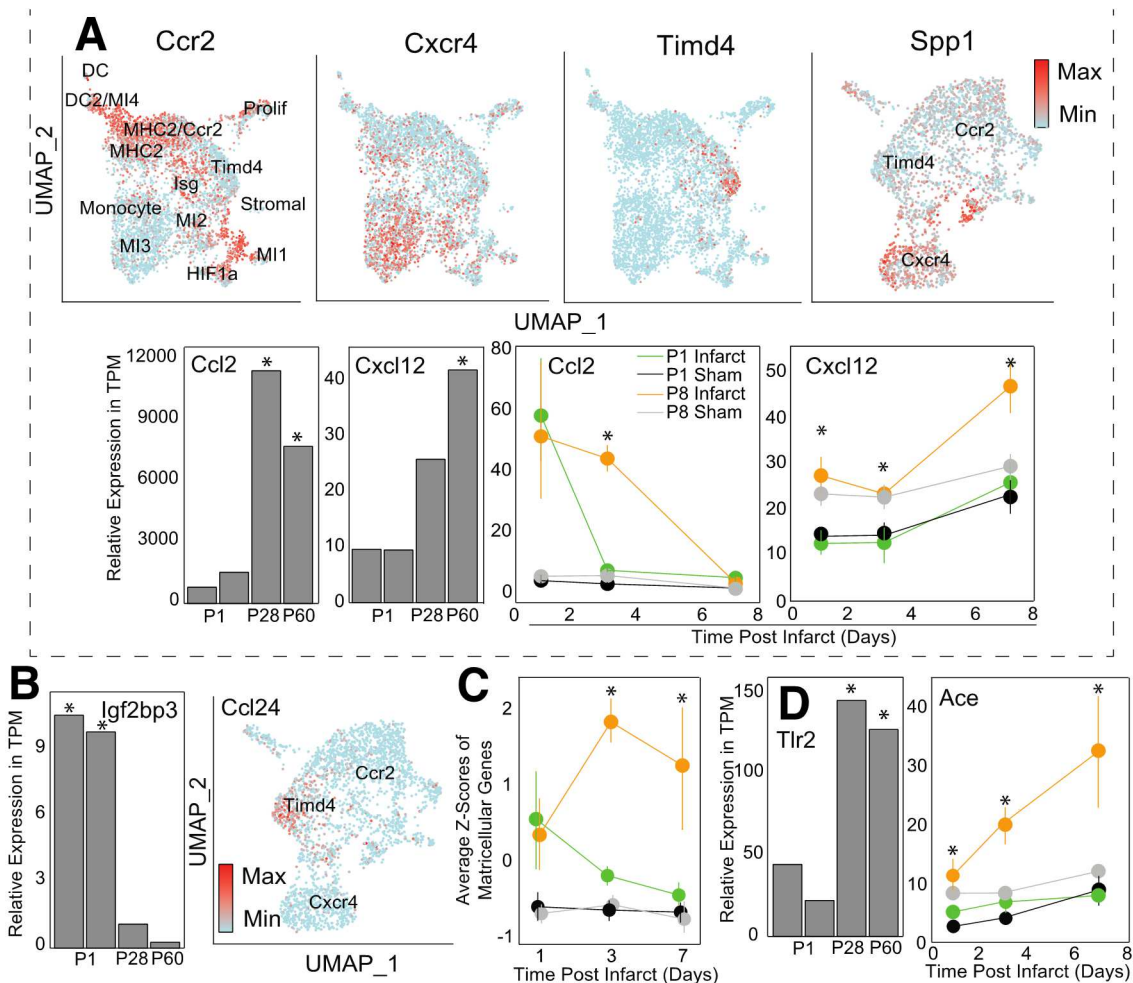


Figure 2.4. P8 cytokines recruit BMDMs deficient in growth proteins to an increasingly sensitive inflammatory microenvironment.

(A) Post-MI Macrophages were clustered according to original⁴ study's markers. Macrophages either express high levels of CCR2 (classical monocytes), CXCR4 (late-phase monocytes) or Timd4 (YS macrophages). Spp1 graph was generated by examining a subset of cells based on expression of previous three genes and then re-clustering and demonstrates high Spp1 expression by Cxcr4+ macrophages. Bar graphs are from fibroblast dataset, line graphs are from bulk tissue, and UMAPs are from single-cell macrophages. (B) Growth factors identified from original bulk analysis identified in neonatal CF and Mac populations, respectively. Ccl24 was from same Seurat object that generated Spp1 plot. (C) Average Z-Scores of matricellular genes demonstrating similar trends between genes by group and timepoint. Individual genes and functional groupings are listed in Supplemental Table 2.1. (D) TLR2 expression in fibroblasts on postnatal days 1, 28 and 60³⁴ is plotted here. Significance is indicated as $p < 0.05$ as determined by Exact Test with Benjamini-Hochberg correction. Conversely, ACE expression is plotted from the bulk heart dataset³³, with significance determined by Wald Test with Benjamini-Hochberg correction, $p < 0.05$.

day-1 hearts, leading to an earlier resolution of TGF- β and IL-6 production versus day-8 hearts. The delayed cytokine signaling in these day-8 hearts is then more likely to affect a greater number of leukocytes and amplify inflammatory processes.

Along with cytokine diffusion, regenerative hearts produced a number of growth factors. Igfbp3, which enhances IGF-2 translation, was originally³³ associated with day-1 hearts and we were able to identify neonatal CFs as a cellular source (**Fig. 2.4B, Fig. S2.3A**). IGF-2 has been shown to induce cardiomyocyte proliferation and aid in heart regeneration³³. An additional neonatal-restricted growth factor was identified as CCL24, which also induces cardiomyocyte cell cycle reentry³³. When referenced with the macrophage single-cell dataset, YS macrophages were found to be the primary transcribers of this protein (**Fig. 2.4B**). Thus, we have identified the cellular contributions of both neonatal growth factors, though it is possible that YS macrophages are required for the CF production of CCL24.

2.5.2 Cellular Connectivity After Infarction

Cytokines may diffuse over significant distance, but for cardiac cells, additional cell-cell communication is possible through inter-cellular structures such as gap junctions, i.e. homotypic gated intercellular connections. In the heart, the primary gap junctions—connexin 43 and 45—propagate not only ion currents between cells, but also DAMPS and secondary messengers⁵¹. In response to infarction, day-1 regenerative mouse hearts increased connexin expression after

3 days, while day-8 hearts downregulated production of these junctions (**Fig. S2.3A**). An increase in intercellular permeability may help disperse DAMPS around the infarct area and reduce local concentrations; this in turn lowers the concentration of danger signals received by individual cells and reduces their inflammatory response. Moreover, DAMP dispersion allows a greater number of cells to bind and degrade the ligands, reducing the duration of danger signals.

For extra-cellular adhesions, no significant differential changes were observed between regenerative and non-regenerative hearts for common leukocyte adhesion molecules in the bulk dataset, but non-regenerative heart fibroblasts expressed more adhesion molecules (**Fig. S2.3A**). In addition to having a higher affinity for leukocytes, fibroblasts from non-regenerative hearts become larger, suggesting that these day-8 hearts are “stickier” to white blood cells⁵² and thus more effective in inducing inflammation versus regenerative hearts. Once adhered to the myocardium, platelets and neutrophils secrete TGF- β and PDGF into the infarct zone⁵³, binding to TGF β R and activating fibroblasts to produce the long isoforms of the large glycosaminoglycan called hyaluronic acid (HA) via HAS1 and HAS2⁵⁴. HA is then cleaved in non-regenerative hearts into lower molecular weights, which are then able to bind many receptors and initiate detrimental functions as highlighted in the schematic in Fig. 2.3C. For example, high molecular weight HA sterically hinders Toll-Like Receptor (TLR) signaling and induces IL-4 producing macrophages in-vitro⁵⁵. In contrast, low molecular weight HA is able to bind many receptors, e.g. CD44, receptor for HA-mediated motility (RHAMM),

TLR2, TLR4, and PDGFR- β , some of which complex together^{56,57}, resulting in SMAD2/3, FAK/ERK, and p38 and PI3K/AKT signaling. Since HA is able to bind many receptors with diverging downstream signaling, preventing this pro-inflammatory signaling by limiting low molecular weight HA production is likely the best approach. Hypertrophied hearts contain greater concentration of HA, especially lower molecular weight oligomers⁵⁸; HA degradation from high to low molecular weight is typically mediated by hyaluronidases⁵⁹, hence HYAL1 transcript was elevated in non-regenerative mice⁷ (**Fig. S2.3B**). This HA size conversion has also been a therapeutic target; when RHAMM, but not CD44 or TLR2/4, was blocked by a peptide receptor mimic, macrophage influx was prevented and TGF- β production decreased⁵⁶, preventing dermal scar formation in rats. Conversely, NF- κ B is a central regulator of RHAMM that activates CCL2 production in a variety of cell types^{47,60} and this cytokine is overexpressed by non-regenerative hearts on day 3 (**Fig. 2.4A**). Thus, we conclude that HA conversion is a critical node in converting hearts into a non-regenerative mode and is mediated by upstream signals from inflammatory cells, e.g. platelets and neutrophils.

Beyond HA, several other matrix constituents undergo significant remodeling; matrix naturally turns over slowly with time in a tightly regulated process. However in non-regenerative hearts, expression of several matrix components, e.g. *Fbln1*, *Col1a2*, *, and *Col3a1*, is noticeably increased. *Loxl2*, a gene in the family of collagen crosslinking enzymes, is also highly expressed in non-regenerative hearts, which along with matrix overproduction could suggest*

why infarct scars are hard⁶¹. Components that process and remodel matrix, primary matrix metalloproteases (MMPs) 2, 3, 9, and 14^{62–65}, are also differentially expressed over time between P1 and P8 mice. Similarly, the duration of high TIMP1 expression, the inhibitor of MMPs, was longer for non-regenerative P8 mice (**Fig. S2.3C**), suggesting that MMP activity may be inhibited in non-regenerative hearts to enable further accumulation of matrix. This additional matrix (including low molecular weight HA) present in the infarct could become an extracellular adhesion substrate for myofibroblast trans-differentiation¹⁸ and disease progression.

In addition to proteins that form the ECM network, many other smaller matricellular proteins modify the properties of this network, e.g. Ccn3, periostin, osteopontin, and tenascin C among many others; these matricellular proteins are critical in the balance between healing and fibrosis. Of all the gene genes analyzed in these datasets, matricellular proteins show the most striking differences between regenerative and non-regenerative hearts (**Fig. 2.4C, S2.4A**). These proteins are secreted by fibroblasts as well as activate them⁶⁶, forming a positive feedback loop, though they each have unique functions; for example, thrombospondin-1 cleaves the latent form of TGF- β to activate it, while osteopontin and periostin increase fibroblast activation in response to TGF- β ^{67–69}. Osteopontin (e.g. *Spp1*) was primarily detected in CXCR4+ recruited macrophages, and in negligible amounts by Timd4+ macrophages, suggesting that the later wave of recruited macrophages could contribute to fibrosis. TnC is

overexpressed in non-regenerative hearts (**Fig. S2.4A**) and together with TGF- β , induces the production of each other in fibroblasts, along with collagen 1 and smooth muscle actin⁷⁰. Another upregulated protein, SPARC (i.e. osteonectin) helps process and assemble collagen fibrils⁷¹ and propagates mechanotransductive signals. SPARC knockout increases cardiac rupture risk after MI as well as decreases SMAD2/3 signaling⁷². Finally, Thrombospondins (*Thbs1* and *Thbs2*) are calcium-binding glycoproteins that bind collagens, fibrinogen, and integrins⁷³. *Thbs1* is inducible via angiotensin II, whereas *Thbs2* is regulated through reactive oxygen species^{74,75}. Both stimulate TGF- β signaling through NF- κ B⁷⁶ but Thrombospondin 1 also binds to TLR4, further propagating damage-associated signaling. Taken together, these extracellular matrix proteins are necessary to prevent cardiac rupture, but upregulation is associated with poor outcomes via increased cardiac fibroblast activation and secretion and assembly of fibronectin, fibulin, and several collagens.

2.5.3 Cardiac Stress that are Enhanced in Non-regenerative Hearts

Working in concert with the emergence of many biological inflammatory signals after MI, the establishment of an acute hypoxic microenvironment is equally important in spurring fibroblast activation and matrix deposition. Responses to hypoxia were more severe in non-regenerative mice, resulting in peak expression of HIF1 α , positive regulation of hypoxic response, and a decrease in HIF3 α , negative regulation of hypoxic response⁷⁷ (**Fig. S2.4B**). Hif1 α regulates NF- κ B

signaling⁷⁸, which binds the periostin promoter during fibrosis¹⁶, and induces BMDM recruitment through CXCL12⁷⁹ further causing activation. Thus, hypoxia is able to activate cardiac fibroblasts to divide and secrete matrix⁸⁰.

Another hypoxia-related impact of MI is stretch response. When cardiomyocytes in the infarct region are deprived of oxygen, they stop contracting, while peri-infarct myocytes continue to beat. This creates a region of high tension around the infarct, spurring atrial-natriuretic peptide (ANP, whose gene is *Nppa*) production and the activation of fibroblasts¹⁸. While Herum et. al, were able to decouple the biological effects of stretch and stiffening on cardiac fibroblasts, biological activation of fibroblasts is usually accompanied by an increase in matrix production¹⁵. Interestingly, an increase in *Acta2* expression (which encodes smooth muscle actin, a marker of fibroblast to myofibroblast conversion), is not accompanied by a spike in collagen 1 mRNA production in P1 mice (**Fig. S2.4C**). An increase in *Acta2* expression suggests that P1 hearts are more sensitive to stretch stimuli, and this is corroborated by an increase in ANP transcription. ANP has been shown to inhibit fibroblast proliferation and matrix deposition⁸¹, and the P1 spike in ANP correlates with decreased collagen production. This trend is not conserved in non-regenerative P8 hearts, suggesting that additional signaling overrides ANP-associated matrix suppression.

When cells apoptose or necrose such as with excessive stretch, they release their intracellular content into the interstitium where they can then be

sensed by membrane-bound TLRs. Sensing of nuclei acids, histones, and other nuclear components by TLRs 2 and 4 result in NF- κ B induced CXCL12-mediated monocyte recruitment to the heart⁷⁹ and an inflammatory response. TLRs 2 and 4 are the primary TLRs expressed on cardiac fibroblasts, though *only TLR2* expression increases from postnatal day-1 to day-60 mice (**Fig. 2.4D, Table S2.2**)^{33,34}. TLR2 heterodimerizes with TLRs 1 and 6, and can recognize the chromatin binding protein HMBG1, hyaluronan, heparin sulfate, fibrinogen, and angiotensin II^{56,57}. These native proteins are generated by cell lysis, through the clotting cascade, or in the case of angiotensin II, through the renin-angiotensin-aldosterone system which is engaged by MI-induced hypotension. This causes systemic release of angiotensin I after conversion to its active form via angiotensin converting enzyme (ACE). Angiotensin can then bind to TLR2, induce downstream NK- κ B activation, macrophage recruitment, and ultimately fibrosis¹⁰. ACE expression is upregulated in non-regenerative day-8 hearts after MI, but not regenerative day-1 samples (**Fig. 2.4D**), suggesting that ACE or Ang2 inhibitors may help reduce mortality via TLR inhibition; thus, this treatment strategy is modeled after neonatal-like healing response.

2.5.4 Limitations of Analysis

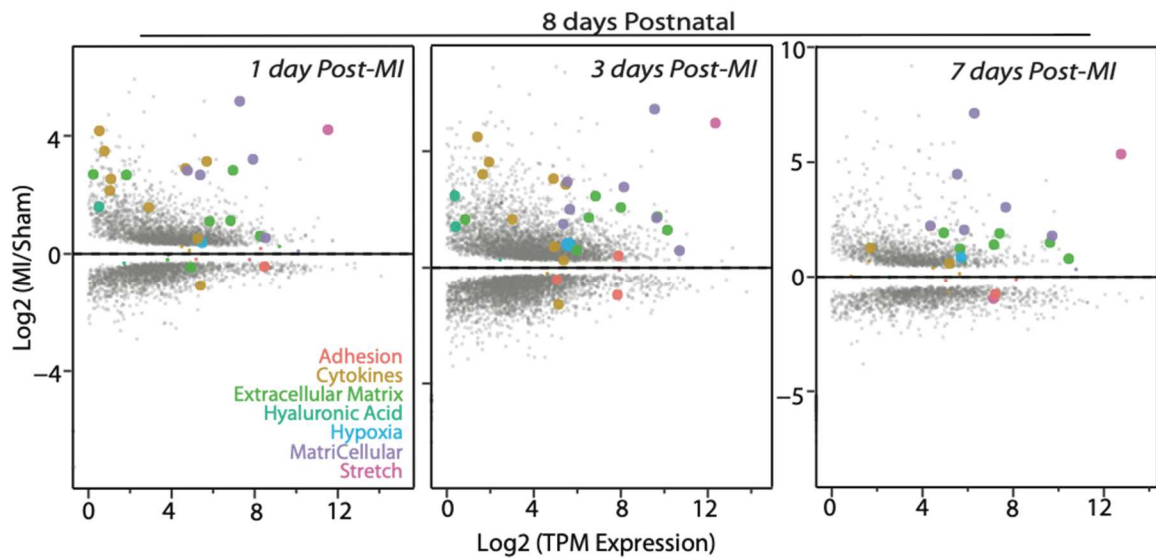
The observations in this analysis are based on mRNA expression across several cardiac populations in mice^{4,33,34}. It is important to note that while next generation RNA sequencing has provided an in-depth tool for mRNA

quantification, it has several limitations. Particularly in single-cell analysis, low level transcripts are difficult to detect at current sequencing depths, making it more difficult to separate true and false negatives. For that reason, this analysis focused on positive data or population differences in non-zero comparisons of differentially expressed genes. Moreover, mRNA does not necessarily scale to protein production and especially not to biological function or protein half-life; they also do not account for the effects of any post translational modifications. Therefore, the conclusions from these studies were compared against existing protein-level or *in-vivo* studies examining the function of the resultant proteins. Finally, this analysis is based on datasets with limited time course. Significant follow-up could strengthen the conclusions drawn here. Conversely other attempts at longitudinal assessment exist but are restricted to older heart⁸², further motivating the need for longer observations post-MI of postnatal day 1 regenerative hearts. The strengths of this approach include many instances of compounding evidence across several datasets, researchers, and models of mice. Common regulation of MI-response pathways bodes well for evolutionarily preserved mechanisms that are likely similar in humans. While additional studies will need to be conducted to compare human and mouse differences in stress-responses, we hope that this study helps to parcel critical pathways and compare them against a regenerative positive control model for subsequent analyses in other platforms.

2.5.5 Summary

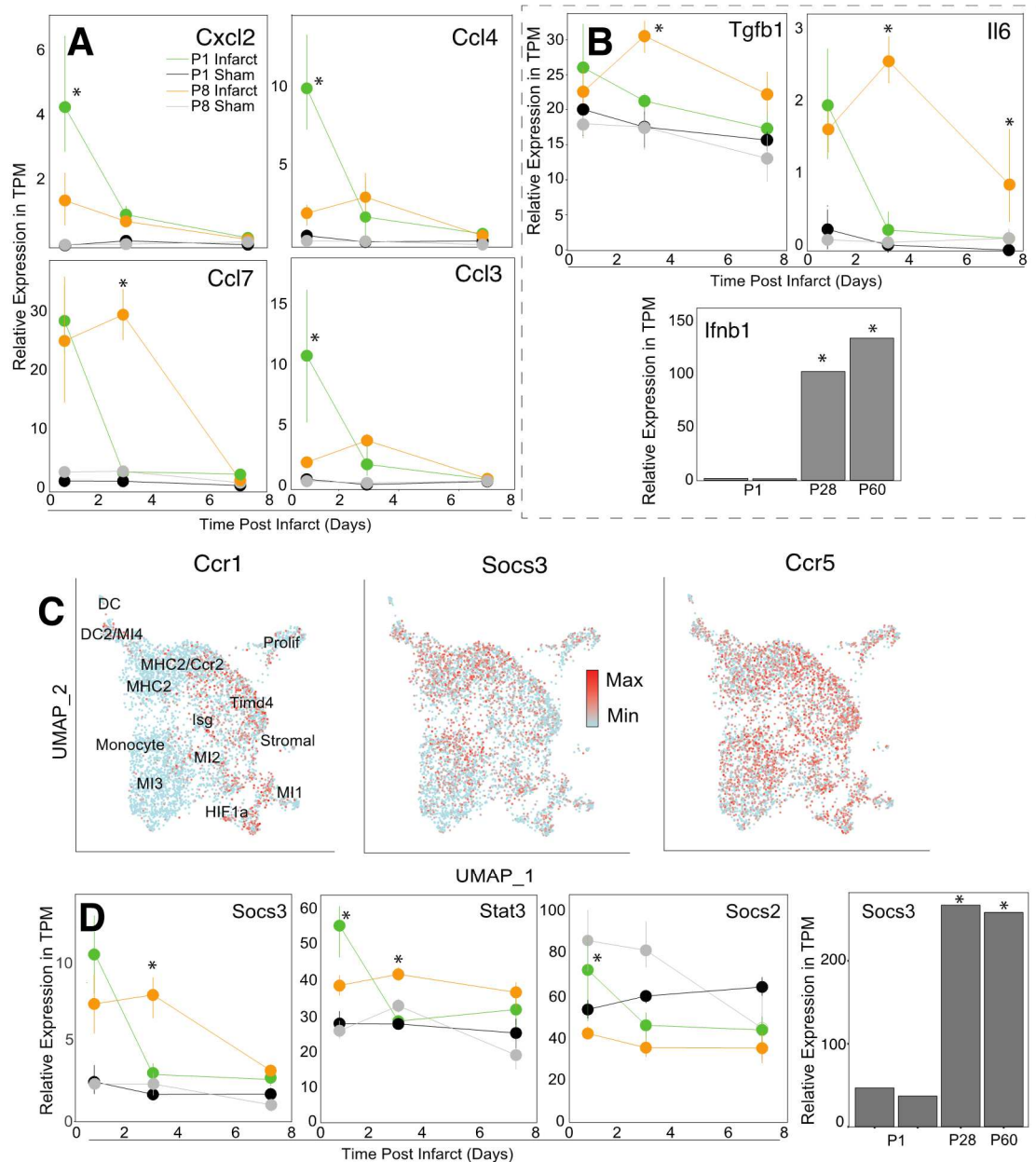
Differential regulation of non-regenerative vs. regenerative hearts seems restricted to key pathways: NF- κ B, AP-1, hypoxia, stretch, and STAT3. On day 3, many proteins are upregulated by NF- κ B, including but not limited to TnC, Ccl2, Ang2, thrombospondins, HAS, and MMP2/9. While NF- κ B is likely induced immediately after infarction in both regenerative and non-regenerative hearts, only regenerative hearts quench the signaling cascade (**Fig. S2.4D**). This could be due to stronger NF- κ B induction in non-regenerative hearts via greater TLR2 and 4 expression and ligand availability, particularly low molecular weight HA. Moreover, NF- κ B induction and the macrophage recruitment steadily increases TGF- β and IL-6 post-infarction. Combined with the sudden emergence of synergistic pro-fibrotic extracellular matrix proteins and increased TGF- β sensitivity, fibroblasts are more likely to be activated and secrete an overabundance of matrix, resulting in a myocardial scar as outlined in Figure 2.3C. In contrast, regenerative hearts have an acute induction of STAT3 signaling on day 1, which activates SOCS3 as a negative feedback regulator, reducing TLR sensitivity, inhibiting IL-6, and likely reducing the induction of NF- κ B. While many of the detrimental effects of non-regenerative P8 signaling can be attributed to NF- κ B, improper dosing could be fatal. Instead, our analysis suggests that pharmacological inhibition of TLR/TGF β R/RHAMM ligands such as low molecular weight HA, Angiotensin II, stretch signaling, and monocyte recruitment could provide more promise for clinical translation.

2.6 Supplementary Figures



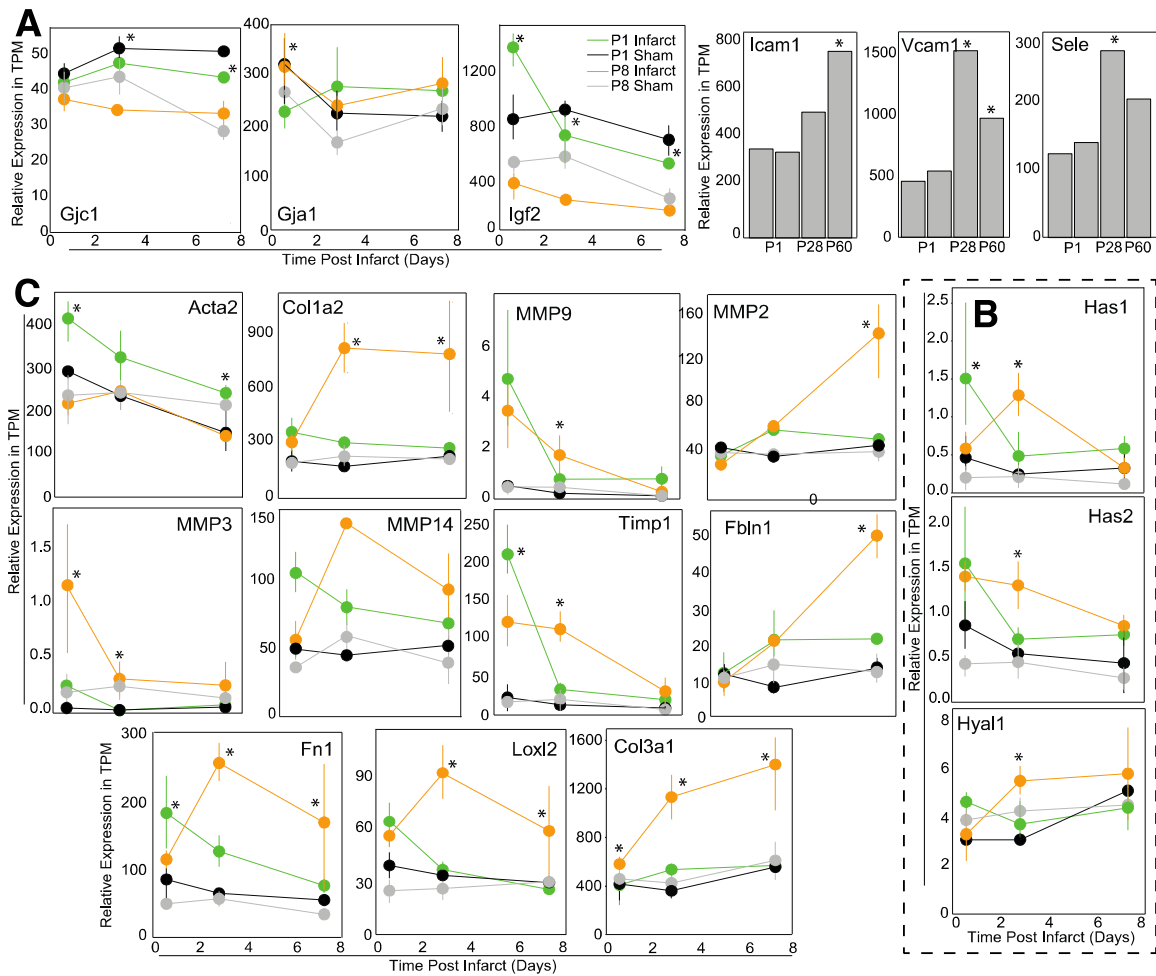
Supplemental Figure 2.1: Transcriptomic analyses of infarct and sham myocardia highlight prolonged remodeling in older hearts.

MA plots show the relationship between the MI/Sham gene ratio and the transcript per million reads for murine myocardia infarcted 8-day postnatal and chased for up to 7 days post-MI as indicated in each panel. Functional gene groupings listed are annotated in the figure by color and with large data points for visualization (when data is statistically significant; $p < 0.05$). Gray data points are coded by size for significance but do not correspond to a classification used in this analysis



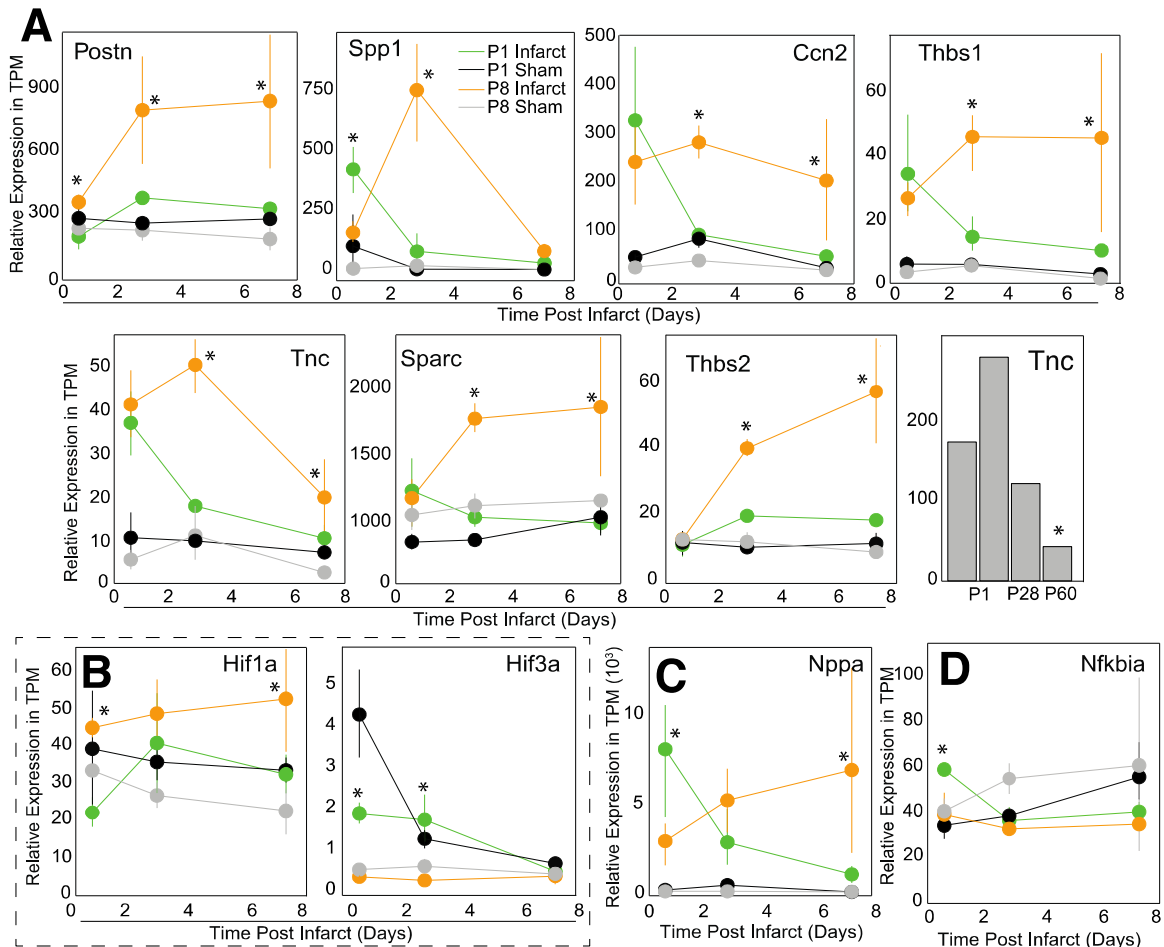
Supplemental Figure 2.2: Chemokine and cytokine signaling highlights generic and specific white blood cell recruitment.

(A) Gene plots of differentially regulated cytokines (e.g., Ccl3/4/7 and Cxcl2). Ligands are promiscuous and lowly expressed relative to Ccl2 and Cxcl12. (B) Pro-inflammatory cytokine expression is uniquely elevated 3 days after infarction in non-regenerative day-8 hearts, while interferon beta (Ifnb1; an IL-6 and TGF- β agonist), is upregulated in postnatal day-28 or older cardiac fibroblasts. (C) Macrophage Ccr1 and Ccr5 are expressed across several subpopulations, suggesting their role as a general recruitment receptor. SOCS gene expression was uniform across macrophage clusters, though bulk signaling (D) indicates early STAT3/SOCS2/SOCS3 signaling as a facet of regenerative hearts. Socs3 was found to be upregulated in adult cardiac fibroblasts as determined by Exact test with Benjamini-Hochberg correction.



Supplemental Figure 2.3: Connectivity and growth, ECM, and hyaluronic acid signaling evolve with age and infarction.

(A) Gap junction (Gjc1 and Gja1) and IGF2 gene plots from bulk sequencing (left) and adhesion molecules from fibroblasts (right). Fibroblasts expressed greater adhesion molecules at steady state (Icam1, Vcam1, and Sele), and in bulk, older hearts produce less IGF2. (B) Hyaluronic acid signaling genes from bulk myocardium are plotted (Has1, Has2, and Hyal1) and required for synthesis and truncation of HMW HA, yielding LMW HA is upregulated in post-natal day 8 hearts after infarction. (C) ECM gene signatures of post-natal day 8 infarcted hearts. ECM deposition and crosslinking are likely the result of upregulated expression through day 7 via lysyl oxidase 2 (Lox2), fibulin (Fbln1), and collagen (Col1a2, Col3a1).



Supplemental Figure 2.4: Matricellular, hypoxic, and stretch responses are exaggerated with age, correlated with increased NF- κ B signaling.

(A) In bulk³³, matricellular gene expression is upregulated in post-natal day 8 infarcted hearts, beginning on day 3 (e.g., *Spp1*, *Tnc*), and extending through day 7 in most cases (e.g., *Postn*, *Ccn2*, *Thbs1/2*, *Sparc*). Specifically in cardiac fibroblasts³⁴, Tenascin C (*Tnc*) is downregulated with age. (B) Hypoxic response, positively regulated by *Hif1 α* and negatively by *Hif3 α* , is increased in post-natal day 8 infarcted hearts. (C) Atrial natriuretic peptide (*Nppa*) is elevated in post-natal day 8 infarcted hearts in response to stretch signaling, while post-natal day 1 infarcted hearts undergo a more acute elevation. (D) NF- κ B inhibitor alpha is upregulated 1 day after infarction in regenerative hearts, preempting the day 3 NF- κ B signaling that is observed in post-natal day 8 hearts.

2.7 Supplementary Tables

Supplementary Table 2.1: Z-scores from Heatmap of selected genes and their ontologies.

Z-Scores were calculated by subtracting the average gene expression of each sample from the overall gene mean and dividing by the standard deviation. These are the underlying values used in Fig. 2.1C.

Gene	Group	P1_D1_MI	P1_D1_S	P1_D3_MI	P1_D3_S	P1_D7_MI	P1_D7_S	P8_D1_MI	P8_D1_S	P8_D3_MI	P8_D3_S	P8_D7_MI	P8_D7_S
Soes3	Cytokine	2.22	-0.46	-0.25	-0.72	-0.36	-0.72	1.16	-0.51	1.35	-0.52	-0.23	-0.95
Stat3	Cytokine	2.40	-0.49	-0.41	-0.50	-0.07	-0.77	0.61	-0.72	0.94	0.02	0.41	-1.43
Soes2	Cytokine	0.97	-0.10	-0.54	0.27	-0.67	0.51	-0.76	1.76	-1.15	1.49	-1.16	-0.62
Ccl7	Cytokine	1.71	-0.60	-0.47	-0.60	-0.51	-0.66	1.43	-0.46	1.81	-0.45	-0.58	-0.62
Ccl4	Cytokine	3.00	-0.38	0.05	-0.52	-0.33	-0.50	0.14	-0.49	0.50	-0.50	-0.38	-0.58
Il6	Cytokine	1.46	-0.45	-0.46	-0.69	-0.59	-0.77	1.08	-0.64	2.13	-0.68	0.23	-0.62
Ccl3	Cytokine	2.97	-0.41	0.00	-0.56	-0.41	-0.47	0.06	-0.47	0.65	-0.52	-0.39	-0.46
Cxcl2	Cytokine	2.96	-0.56	0.23	-0.44	-0.36	-0.54	0.58	-0.53	0.05	-0.52	-0.41	-0.46
Ccl2	Cytokine	1.96	-0.55	-0.39	-0.60	-0.51	-0.65	1.64	-0.48	1.31	-0.47	-0.59	-0.67
Cxcl1 2	Cytokine	-1.10	-0.89	-1.08	-0.87	0.31	-0.03	0.45	0.03	0.03	-0.05	2.52	0.67
Tgfb1	Cytokine	1.24	-0.01	0.24	-0.54	-0.59	-0.93	0.51	-0.46	2.17	-0.56	0.43	-1.50
Nppa	Stretch	1.98	-0.74	0.18	-0.65	-0.44	-0.78	0.20	-0.77	0.99	-0.77	1.58	-0.77
Acta2	Stretch	2.30	0.62	1.07	-0.15	-0.06	-1.33	-0.39	-0.14	-0.01	-0.05	-1.42	-0.44
Col1a 2	ECM	0.10	-0.63	-0.16	-0.75	-0.29	-0.50	-0.16	-0.67	2.15	-0.51	2.00	-0.57
Mmp9	ECM	2.43	-0.42	-0.25	-0.62	-0.25	-0.69	1.59	-0.46	0.40	-0.46	-0.58	-0.69
Mmp2	ECM	-0.50	-0.28	0.24	-0.54	-0.02	-0.22	-0.75	-0.43	0.34	-0.47	3.01	-0.40
Mmp3	ECM	0.06	-0.59	-0.66	-0.66	-0.51	-0.57	3.00	-0.14	0.26	0.04	0.07	-0.31
Timp1	ECM	2.52	-0.46	-0.29	-0.61	-0.50	-0.67	1.11	-0.54	0.96	-0.49	-0.33	-0.70
Fbln1	ECM	-0.45	-0.48	0.36	-0.79	0.39	-0.31	-0.68	-0.57	0.29	-0.24	2.91	-0.42
Fn1	ECM	1.16	-0.31	0.32	-0.62	-0.43	-0.76	0.12	-0.84	2.24	-0.73	0.93	-1.07
Lox12	ECM	1.04	-0.19	-0.30	-0.47	-0.84	-0.66	0.64	-0.88	2.36	-0.83	0.77	-0.64
Col3a 1	ECM	-0.68	-0.65	-0.27	-0.83	-0.17	-0.21	-0.13	-0.50	1.61	-0.61	2.46	-0.02
Has1	HA	2.25	-0.15	-0.10	-0.65	0.13	-0.47	0.13	-0.75	1.74	-0.73	-0.46	-0.95
Has2	HA	1.81	0.15	-0.20	-0.60	-0.08	-0.86	1.43	-0.88	1.20	-0.83	0.12	-1.26
Hyal1	HA	0.40	-1.32	-0.62	-1.32	0.14	0.91	-1.07	-0.42	1.36	-0.01	1.69	0.27
Gjc1	Adhesion	0.09	0.43	0.86	1.43	0.28	1.31	-0.56	-0.14	-0.99	0.29	-1.13	-1.87
Gja1	Adhesion	-0.58	1.54	0.55	-0.66	0.36	-0.79	1.40	0.31	-0.35	-2.00	0.65	-0.44
Igf2	Adhesion	2.27	0.72	0.36	0.92	-0.25	0.27	-0.67	-0.22	-1.03	-0.10	-1.27	-1.01
Postn	MatriCellular	-0.76	-0.37	0.07	-0.47	-0.16	-0.38	-0.02	-0.59	1.96	-0.63	2.16	-0.82
Spp1	MatriCellular	1.25	-0.16	-0.26	-0.59	-0.48	-0.60	0.09	-0.58	2.71	-0.53	-0.25	-0.60
Ccn2	MatriCellular	1.85	-0.65	-0.24	-0.32	-0.64	-0.85	1.09	-0.84	1.45	-0.71	0.75	-0.89
Thbs1	MatriCellular	1.05	-0.65	-0.12	-0.66	-0.38	-0.84	0.58	-0.80	1.72	-0.68	1.71	-0.92
Tnc	MatriCellular	1.19	-0.52	-0.04	-0.57	-0.51	-0.74	1.44	-0.84	2.03	-0.48	0.07	-1.03
Sparc	MatriCellular	0.17	-1.03	-0.45	-0.99	-0.59	-0.45	0.00	-0.40	1.86	-0.18	2.13	-0.06
Thbs2	MatriCellular	-0.53	-0.47	0.06	-0.57	-0.03	-0.50	-0.41	-0.43	1.45	-0.48	2.60	-0.68
Hif1a	Hypoxia	-1.44	0.33	0.48	-0.03	-0.39	-0.26	0.91	-0.27	1.30	-0.96	1.71	-1.38
Hif3a	Hypoxia	0.71	2.78	0.59	0.17	-0.50	-0.34	-0.63	-0.48	-0.70	-0.41	-0.61	-0.57

Supplementary Table 2.2: Gene expression in TPM of Toll-Like Receptors in Fibroblasts.

Sample³⁴ names are listed as days postnatal, with two replicates for post-natal day 1. TLR2 and TLR4 are the highest expressed receptors, with TLR2 steadily increasing with age.

Gene	PN1_2	PN1_3	PN28	PN60
Tlr1	240.03	156.92	1275.29	409.63
Tlr2	13656.05	6694.62	45536.47	40946.32
Tlr3	1071.45	877.63	3200.45	937.7
Tlr4	15851.01	17563.13	8303.09	8988.04
Tlr5	153.27	99.58	35.44	94.65
Tlr6	506.57	576.87	591.97	464.45
Tlr7	630.92	266.56	2730.76	1512.83
Tlr8	107.48	59.85	333.92	222.4
Tlr9	247.26	129.76	1549.31	2015.56
Tlr11	0	0	0	0
Tlr13	1297.5	623.64	447.72	563.24
Tlr12	13.5	2.01	1	2.07
Tlr13	1297.5	623.64	447.72	563.24

2.8 Acknowledgements

Chapter 2, in full, is a reprint of the material as it appears in the American Journal of Pathology, Heart and Circulatory Physiology 2021. Whitehead, Alexander J.; Engler, Adam J. American Physiological Society. The dissertation author is the primary investigator and author of this material.

Thank you to these funding sources: National Science Foundation Graduate Research Fellowship Program, Achievement Rewards for College Scientists (ARCS) San Diego Chapter, and the National Institutes of Health (Grant RO1AG045428)

2.9 References

1. Perbellini F, Watson SA, Bardi I, Terracciano CM. Heterocellularity and Cellular Cross-Talk in the Cardiovascular System. *Frontiers in Cardiovascular Medicine*. 2018;5.
2. King KR, Aguirre AD, Ye YX, Sun Y, Roh JD, Ng RP, Kohler RH, Arlauckas SP, Yoshiko V, Savo A, Sadreyev RI, Kelly M, Fitzgibbons TP, Fitzgerald KA, Mitchison T, et al. IRF3 and type I interferons fuel a fatal response to myocardial infarction. *Nature Medicine*. 2017;23(12):1481–1487.
3. Prabhu SD, Frangogiannis NG. The biological basis for cardiac repair after myocardial infarction. *Circulation Research*. 2016;119(1):91–112.
4. Dick SA, Macklin JA, Nejat S, Momen A, Clemente-Casares X, Althagafi MG, Chen J, Kantores C, Hosseinzadeh S, Aronoff L, Wong A, Zaman R, Barbu I, Besla R, Lavine KJ, et al. Self-renewing resident cardiac macrophages limit adverse remodeling following myocardial infarction. *Nature Immunology*. 2019;20(1):29–39.
5. Ma Y, Mouton AJ, Lindsey ML. Cardiac macrophage biology in the steady-state heart, the aging heart, and following myocardial infarction. *Translational Research*. 2018;191:15–28.

6. Ma Y, Yabluchanskiy A, Iyer RP, Cannon PL, Flynn ER, Jung M, Henry J, Cates CA, Deleon-Pennell KY, Lindsey ML. Temporal neutrophil polarization following myocardial infarction. *Cardiovascular Research*. 2016;110(1):51–61.
7. Wang Y, Dembowsky K, Chevalier E, Stüve P, Korf-Klingebiel M, Lochner M, Napp LC, Frank H, Brinkmann E, Kanwischer A, Bauersachs J, Gyöngyösi M, Sparwasser T, Wollert KC. C-X-C Motif Chemokine Receptor 4 Blockade Promotes Tissue Repair after Myocardial Infarction by Enhancing Regulatory T Cell Mobilization and Immune-Regulatory Function. *Circulation*. 2019;139(15):1798–1812.
8. Fang M, Xiang FL, Braitsch CM, Yutzey KE. Epicardium-derived fibroblasts in heart development and disease. *Journal of Molecular and Cellular Cardiology*. 2016;91:23–27.
9. Moore-Morris T, Guimarães-Camboa N, Banerjee I, Zambon AC, Kisseleva T, Velayoudon A, Stallcup WB, Gu Y, Dalton ND, Cedenilla M, Gomez-Amaro R, Zhou B, Brenner DA, Peterson KL, Chen J, et al. Resident fibroblast lineages mediate pressure overload-induced cardiac fibrosis. *Journal of Clinical Investigation*. 2014;124(7):2921–2934.
10. Wang L, Li YL, Zhang CC, Cui W, Wang X, Xia Y, Du J, Li HH. Inhibition of toll-like receptor 2 reduces cardiac fibrosis by attenuating macrophage-mediated inflammation. *Cardiovascular Research*. 2014;101(3):383–392.
11. Erridge C. Endogenous ligands of TLR2 and TLR4: agonists or assistants? *Journal of Leukocyte Biology*. 2010;87(6):989–999.
12. Wang KX, Denhardt DT. Osteopontin: Role in immune regulation and stress responses. *Cytokine and Growth Factor Reviews*. 2008;19(5–6):333–345.
13. Li L, Fan D, Wang C, Wang JY, Cui XB, Wu D, Zhou Y, Wu LL. Angiotensin II increases periostin expression via Ras/p38 MAPK/CREB and ERK1/2/TGF- β 1 pathways in cardiac fibroblasts. *Cardiovascular Research*. 2011;91(1):80–89.
14. Huebener P, Abou-Khamis T, Zymek P, Bujak M, Ying X, Chatila K, Haudek S, Thakker G, Frangogiannis NG. CD44 Is Critically Involved in Infarct Healing by Regulating the Inflammatory and Fibrotic Response. *The Journal of Immunology*. 2008;180(4):2625–2633.
15. Hao J, Ju H, Zhao S, Junaid A, Scammell-La Fleur T, Dixon IMC. Elevation of expression of Smads 2, 3, and 4, decorin and TGF- β in the chronic phase

- of myocardial infarct scar healing. *Journal of Molecular and Cellular Cardiology*. 1999;31(3):667–678.
16. Prakoura N, Kavvadas P, Kormann R, Dussaule JC, Chadjichristos CE, Chatziantoniou C. NFandkappa;B-induced periostin activates integrin- β 3 signaling to promote renal injury in GN. *Journal of the American Society of Nephrology*. 2017;28(5):1475–1490.
 17. Ghatak S, Misra S, Norris RA, Moreno-Rodriguez RA, Hoffman S, Levine RA, Hascall VC, Markwald RR. Periostin induces intracellular cross-talk between kinases and hyaluronan in atrioventricular valvulogenesis. *Journal of Biological Chemistry*. 2014;289(12):8545–8561.
 18. Herum KM, Choppe J, Kumar A, Engler AJ, McCulloch AD. Mechanical regulation of cardiac fibroblast profibrotic phenotypes. *Molecular biology of the cell*. 2017;28(14):1871–1882.
 19. Müller AL, Dhalla NS. Role of various proteases in cardiac remodeling and progression of heart failure. *Heart Failure Reviews*. 2012;17(3):395–409.
 20. Ho CY, López B, Coelho-Filho OR, Lakdawala NK, Cirino AL, Jarolim P, Kwong R, González A, Colan SD, Seidman JG, Díez J, Seidman CE. Myocardial fibrosis as an early manifestation of hypertrophic cardiomyopathy. *New England Journal of Medicine*. 2010;363(6):552–563.
 21. Epelman S, Lavine KJ, Randolph GJ. Origin and Functions of Tissue Macrophages. *Immunity*. 2014;41(1):21–35.
 22. Takata K, Kozaki T, Lee CZW, Thion MS, Otsuka M, Lim S, Utami KH, Fidan K, Park DS, Malleret B, Chakarov S, See P, Low D, Low G, Garcia-Miralles M, et al. Induced-Pluripotent-Stem-Cell-Derived Primitive Macrophages Provide a Platform for Modeling Tissue-Resident Macrophage Differentiation and Function. *Immunity*. 2017;47(1):183-198.e6.
 23. Lin WY, Xu D, Austin CD, Caplazi P, Senger K, Sun Y, Jeet S, Young J, Delarosa D, Suto E, Huang Z, Zhang J, Yan D, Corzo C, Barck K, et al. Function of CSF1 and IL34 in Macrophage Homeostasis, Inflammation, and Cancer. *Frontiers in Immunology*. 2019;10:2019.
 24. El Khoury J, Toft M, Hickman SE, Means TK, Terada K, Geula C, Luster AD. Ccr2 deficiency impairs microglial accumulation and accelerates progression of Alzheimer-like disease. *Nature Medicine*. 2007;13(4):432–438.

25. Zigmond E, Samia-Grinberg S, Pasmanik-Chor M, Brazowski E, Shibolet O, Halpern Z, Varol C. Infiltrating Monocyte-Derived Macrophages and Resident Kupffer Cells Display Different Ontogeny and Functions in Acute Liver Injury. *The Journal of Immunology*. 2014;193(1):344–353.
26. Lawrence W, Banerji S, Day AJ, Bhattacharjee S, Jackson DG. Binding of hyaluronan to the native lymphatic vessel endothelial receptor LYVE-1 is critically dependent on receptor clustering and hyaluronan organization. *Journal of Biological Chemistry*. 2016;291(15):8014–8030.
27. Miyanishi M, Tada K, Koike M, Uchiyama Y, Kitamura T, Nagata S. Identification of Tim4 as a phosphatidylserine receptor. *Nature*. 2007;450(7168):435–439.
28. Uderhardt S, Martins AJ, Tsang JS, Lämmermann T, Germain RN. Resident Macrophages Cloak Tissue Microlesions to Prevent Neutrophil-Driven Inflammatory Damage. *Cell*. 2019;177(3):541-555.e17.
29. Narasimhan PB, Marcovecchio P, Hamers AAJ, Hedrick CC. Nonclassical Monocytes in Health and Disease. *Annual Review of Immunology*. 2019;37(1):439–456.
30. Bajpai G, Bredemeyer A, Li W, Zaitsev K, Koenig AL, Lokshina I, Mohan J, Ivey B, Hsiao HM, Weinheimer C, Kovacs A, Epelman S, Artyomov M, Kreisel D, Lavine KJ. Tissue Resident CCR2- and CCR2+ Cardiac Macrophages Differentially Orchestrate Monocyte Recruitment and Fate Specification Following Myocardial Injury. *Circulation Research*. 2019;124(2):263–278.
31. Stein M, Keshav S, Harris N, Gordon S. Interleukin 4 potently enhances murine macrophage mannose receptor activity: A marker of alternative immunologic macrophage activation. *Journal of Experimental Medicine*. 1992;176(1):287–292.
32. Nahrendorf M, Swirski FK. Abandoning M1/M2 for a Network Model of Macrophage Function. *Circulation research*. 2016;119(3):414–7.
33. Wang Z, Cui M, Shah AM, Ye W, Tan W, Min YL, Botten GA, Shelton JM, Liu N, Bassel-Duby R, Olson EN. Mechanistic basis of neonatal heart regeneration revealed by transcriptome and histone modification profiling. *Proceedings of the National Academy of Sciences of the United States of America*. 2019;116(37):18455–18465.
34. Giudice J, Xia Z, Wang ET, Scavuzzo MA, Ward AJ, Kalsotra A, Wang W,

- Wehrens XHT, Burge CB, Li W, Cooper TA. Alternative splicing regulates vesicular trafficking genes in cardiomyocytes during postnatal heart development. *Nature Communications*. 2014;5.
35. Robinson MD, McCarthy DJ, Smyth GK. edgeR: A Bioconductor package for differential expression analysis of digital gene expression data. *Bioinformatics*. 2009;26(1):139–140.
 36. Love MI, Huber W, Anders S. Moderated estimation of fold change and dispersion for RNA-seq data with DESeq2. *Genome Biology*. 2014;15(12):550.
 37. Thomas PD, Campbell MJ, Kejariwal A, Mi H, Karlak B, Daverman R, Diemer K, Muruganujan A, Narechania A. PANTHER: A library of protein families and subfamilies indexed by function. *Genome Research*. 2003;13(9):2129–2141.
 38. Metsalu T, Vilo J. ClustVis: A web tool for visualizing clustering of multivariate data using Principal Component Analysis and heatmap. *Nucleic Acids Research*. 2015;43(W1):W566–W570.
 39. Stuart T, Butler A, Hoffman P, Hafemeister C, Papalexi E, Mauck WM, Hao Y, Stoeckius M, Smibert P, Satija R. Comprehensive Integration of Single-Cell Data. *Cell*. 2019;177(7):1888-1902.e21.
 40. Willenborg S, Lucas T, Van Loo G, Knipper JA, Krieg T, Haase I, Brachvogel B, Hammerschmidt M, Nagy A, Ferrara N, Pasparakis M, Eming SA. CCR2 recruits an inflammatory macrophage subpopulation critical for angiogenesis in tissue repair. *Blood*. 2012;120(3):613–625.
 41. Ley K, Laudanna C, Cybulsky MI, Nourshargh S. Getting to the site of inflammation: The leukocyte adhesion cascade updated. *Nature Reviews Immunology*. 2007;7(9):678–689.
 42. Swirski FK, Nahrendorf M. Cardioimmunology: the immune system in cardiac homeostasis and disease. *Nature Reviews Immunology*. 2018;18(12):733–744.
 43. Zougari Y, Ait-Oufella H, Bonnin P, Simon T, Sage AP, Guérin C, Vilar J, Caligiuri G, Tsiantoulas D, Laurans L, Dumeau E, Kotti S, Bruneval P, Charo IF, Binder CJ, et al. B lymphocytes trigger monocyte mobilization and impair heart function after acute myocardial infarction. *Nature Medicine*. 2013;19(10):1273–1280.

44. Meléndez GC, McLarty JL, Levick SP, Du Y, Janicki JS, Brower GL. Interleukin 6 mediates myocardial fibrosis, concentric hypertrophy, and diastolic dysfunction in rats. *Hypertension*. 2010;56(2):225–231.
45. Haghikia A, Ricke-Hoch M, Stapel B, Gorst I, Hilfiker-Kleiner D. STAT3, a key regulator of cell-to-cell communication in the heart. *Cardiovascular Research*. 2014;102(2):281–289.
46. Gordon JW, Shaw JA, Kirshenbaum LA. Multiple facets of NF- κ B in the heart: to be or not to NF- κ B. *Circulation research*. 2011;108(9):1122–32.
47. Ueda A, Okuda K, Ohno S, Shirai A, Igarashi T, Matsunaga K, Fukushima J, Kawamoto S, Ishigatsubo Y, Okubo T. NF-kappa B and Sp1 regulate transcription of the human monocyte chemoattractant protein-1 gene. *Journal of immunology (Baltimore, Md. : 1950)*. 1994;153(5):2052–63.
48. Eickelberg O, Pansky A, Mussmann R, Bihl M, Tamm M, Hildebrand P, Perruchoud AP, Roth M. Transforming growth factor- β 1 induces interleukin-6 expression via activating protein-1 consisting of JunD homodimers in primary human lung fibroblasts. *Journal of Biological Chemistry*. 1999;274(18):12933–12938.
49. Hirota H, Yoshida K, Kishimoto T, Taga T. Continuous activation of gp130, a signal-transducing receptor component for interleukin 6-related cytokines, causes myocardial hypertrophy in mice. *Proceedings of the National Academy of Sciences of the United States of America*. 1995;92(11):4862–4866.
50. Croker BA, Krebs DL, Zhang JG, Wormald S, Willson TA, Stanley EG, Robb L, Greenhalgh CJ, Förster I, Clausen BE, Nicola NA, Metcalf D, Hilton DJ, Roberts AW, Alexander WS. SOCS3 negatively regulates IL-6 signaling in vivo. *Nature Immunology*. 2003;4(6):540–545.
51. Wang P, Yang H, Chen W, Ochani M, Qiang X, Al-Abed Y, Zhu S, D'Angelo J, Wang S, He M, Wang H, Tracey KJ, Ma G, Bao G, Li W. Connexin 43 Hemichannel as a Novel Mediator of Sterile and Infectious Inflammatory Diseases. *Scientific Reports*. 2018;8(1):166.
52. Jonsson MKB, Hartman RJG, Ackers-Johnson M, Tan WLW, Lim B, van Veen TAB, Foo RS. A Transcriptomic and Epigenomic Comparison of Fetal and Adult Human Cardiac Fibroblasts Reveals Novel Key Transcription Factors in Adult Cardiac Fibroblasts. *JACC: Basic to Translational Science*. 2016;1(7):590–602.

53. Frangogiannis NG. The role of transforming growth factor (TGF)- β in the infarcted myocardium. *Journal of Thoracic Disease*. 2017;9(Suppl 1):S52–S63.
54. Stuhlmeier KM, Pollaschek C. Differential Effect of Transforming Growth Factor β (TGF- β) on the Genes Encoding Hyaluronan Synthases and Utilization of the p38 MAPK Pathway in TGF- β -induced Hyaluronan Synthase 1 Activation. *Journal of Biological Chemistry*. 2004;279(10):8753–8760.
55. Rayahin JE, Buhrman JS, Zhang Y, Koh TJ, Gemeinhart RA. High and Low Molecular Weight Hyaluronic Acid Differentially Influence Macrophage Activation. *ACS Biomaterials Science and Engineering*. 2015;1(7):481–493.
56. Tolg C, Hamilton SR, Zalinska E, McCulloch L, Amin R, Akentieva N, Winnik F, Savani R, Bagli DJ, Luyt LG, Cowman MK, McCarthy JB, Turley EA. A RHAMM mimetic peptide blocks hyaluronan signaling and reduces inflammation and fibrogenesis in excisional skin wounds. *American Journal of Pathology*. 2012;181(4):1250–1270.
57. Porsch H, Mehić M, Olofsson B, Heldin P, Heldin CH. Platelet-derived growth factor β -receptor, transforming growth factor β type I receptor, and CD44 protein modulate each other's signaling and stability. *Journal of Biological Chemistry*. 2014;289(28):19747–19757.
58. Lorén C, Dahl C, Do L, Almaas V, Geiran O, Mörner S, Hellman U. Low Molecular Mass Myocardial Hyaluronan in Human Hypertrophic Cardiomyopathy. *Cells*. 2019;8(2):97.
59. Fallacara A, Baldini E, Manfredini S, Vertuani S. Hyaluronic acid in the third millennium. *Polymers*. 2018;10(7).
60. Collart MA, Baeuerle P, Vassalli P. Regulation of tumor necrosis factor alpha transcription in macrophages: involvement of four kappa B-like motifs and of constitutive and inducible forms of NF-kappa B. *Molecular and Cellular Biology*. 1990;10(4):1498–1506.
61. Berry MF, Engler AJ, Woo YJ, Pirolli TJ, Bish LT, Jayasankar V, Morine KJ, Gardner TJ, Discher DE, Sweeney HL. Mesenchymal stem cell injection after myocardial infarction improves myocardial compliance. *American Journal of Physiology - Heart and Circulatory Physiology*. 2006;290(6):2196–2203.
62. Kaplan RC, Smith NL, Zucker S, Heckbert SR, Rice K, Psaty BM. Matrix

- metalloproteinase-3 (MMP3) and MMP9 genes and risk of myocardial infarction, ischemic stroke, and hemorrhagic stroke. *Atherosclerosis*. 2008;201(1):130–137.
63. Squire IB, Evans J, Ng LL, Loftus IM, Thompson MM. Plasma MMP-9 and MMP-2 following acute myocardial infarction in man: Correlation with echocardiographic and neurohumoral parameters of left ventricular dysfunction. *Journal of Cardiac Failure*. 2004;10(4):328–333.
 64. Donnini S, Morbidelli L, Taraboletti G, Ziche M. ERK1-2 and p38 MAPK regulate MMP/TIMP balance and function in response to thrombospondin-1 fragments in the microvascular endothelium. *Life Sciences*. 2004;74(24):2975–2985.
 65. Vanhoutte D, Schellings M, Pinto Y, Heymans S. Relevance of matrix metalloproteinases and their inhibitors after myocardial infarction: A temporal and spatial window. *Cardiovascular Research*. 2006;69(3):604–613.
 66. Hinz B, Phan SH, Thannickal VJ, Prunotto M, Desmouliere A, Varga J, De Wever O, Mareel M, Gabbiani G. Recent developments in myofibroblast biology: Paradigms for connective tissue remodeling. *American Journal of Pathology*. 2012;180(4):1340–1355.
 67. Murphy-Ullrich JE, Schultz-Cherry S, Höök M. Transforming growth factor- β complexes with thrombospondin. *Molecular Biology of the Cell*. 1992;3(2):181–188.
 68. Lenga Y, Koh A, Perera AS, McCulloch CA, Sodek J, Zohar R. Osteopontin expression is required for myofibroblast differentiation. *Circulation research*. 2008;102(3):319–27.
 69. Ashley SL, Wilke CA, Kim KK, Moore BB. Periostin regulates fibrocyte function to promote myofibroblast differentiation and lung fibrosis. *Mucosal Immunology*, 2017;10(2):341-351.
 70. Bhattacharyya S, Wang W, Morales-Nebreda L, Feng G, Wu M, Zhou X, Lafyatis R, Lee J, Hinchcliff M, Feghali-Bostwick C, Lakota K, Budinger GRS, Raparia K, Tamaki Z, Varga J. Tenascin-C drives persistence of organ fibrosis. *Nature Communications*. 2016;7(1):1–14.
 71. Harris BS, Zhang Y, Card L, Rivera LB, Brekken RA, Bradshaw AD. SPARC regulates collagen interaction with cardiac fibroblast cell surfaces. *American Journal of Physiology - Heart and Circulatory Physiology*. 2011;301(3):H841.

72. Schellings MWM, Vanhoutte D, Swinnen M, Cleutjens JP, Debets J, Van Leeuwen REW, D'Hooge J, Van Werf F De, Carmeliet P, Pinto YM, Sage EH, Heymans S. Absence of SPARC results in increased cardiac rupture and dysfunction after acute myocardial infarction. *Journal of Experimental Medicine*. 2009;206(1):113–123.
73. Adams JC, Lawler J. The thrombospondins. *Cold Spring Harbor Perspectives in Biology*. 2011;3(10):1–29.
74. Zhou Y, Poczatek MH, Berecek KH, Murphy-Ullrich JE. Thrombospondin 1 mediates angiotensin II induction of TGF- β activation by cardiac and renal cells under both high and low glucose conditions. *Biochemical and Biophysical Research Communications*. 2006;339(2):633–641.
75. Lopes N, Gregg D, Vasudevan S, Hassanain H, Goldschmidt-Clermont P, Kovacic H. Thrombospondin 2 Regulates Cell Proliferation Induced by Rac1 Redox-Dependent Signaling. *Molecular and Cellular Biology*. 2003;23(15):5401–5408.
76. Pahl HL. Activators and target genes of Rel/NF- κ B transcription factors. *Oncogene*. 1999;18(49):6853–6866.
77. Serocki M, Bartoszewska S, Janaszak-Jasiecka A, Ochocka RJ, Collawn JF, Bartoszewski R. miRNAs regulate the HIF switch during hypoxia: a novel therapeutic target. *Angiogenesis*. 2018;21(2):183–202.
78. D'Ignazio L, Bandarra D, Rocha S. NF- κ B and HIF crosstalk in immune responses. *FEBS Journal*. 2016;283(3):413–424.
79. Kew RR, Penzo M, Habel DM, Marcu KB. The IKK α -Dependent NF- κ B p52/RelB Noncanonical Pathway Is Essential To Sustain a CXCL12 Autocrine Loop in Cells Migrating in Response to HMGB1. *The Journal of Immunology*. 2012;188(5):2380–2386.
80. Pillai MS, Sapna S, Shivakumar K. P38 MAPK regulates G1-S transition in hypoxic cardiac fibroblasts. *International Journal of Biochemistry and Cell Biology*. 2011;43(6):919–927.
81. Moubarak M, Magaud C, Saliba Y, Chatelier A, Bois P, Faivre JF, Farès N. Effects of atrial natriuretic peptide on rat ventricular fibroblasts during differentiation into myofibroblasts. *Physiological Research*. 2015;64(4):495–503.
82. Deleon-Pennell KY, Iyer RP, Ma Y, Yabluchanskiy A, Zamilpa R, Chiao YA,

Cannon PL, Kaplan A, Cates CA, Flynn ER, Halade G V., de Castro Brás LE, Lindsey ML. The mouse heart attack research tool 1.0 database. *American Journal of Physiology - Heart and Circulatory Physiology*. 2018;315(3):H522–H530.

Chapter 3: Improved Epicardial Cardiac Fibroblast Generation from iPSCs

3.1 Abstract

Since the initial isolation of human embryonic stem cells and subsequent discovery of reprogramming methods for somatic cells, thousands of protocols have been developed to create each of the hundreds of cell types found in vivo with significant focus on disease-prone systems, e.g., cardiovascular. Robust protocols exist for many of these cell types, except for cardiac fibroblasts (CF). Very recently, several competing methods have been developed to generate these cells through a developmentally conserved epicardial pathway. Such methods generate epicardial cells, but here we report that prolonged exposure to growth factors such as bFGF induces fibroblast spindle-like morphology and similar chromatin architecture to primary CFs. Media conditions for growth and assays are provided, as well as suggestions for seeding densities and timepoints for protein harvest of extracellular matrix. We demonstrate marker expression and matrix competency of resultant cells as shown next to primary human cardiac fibroblasts. These methods provide additional guidance to the original protocol and result in an increasingly stable phenotype.

3.2 Introduction

Fibrotic diseases are thought to account for 45% of US mortality and include conditions such as heart failure, where the myocardium gradually builds up scar tissue over time and ultimately inhibits mechanical function¹. Fibroblasts are thought to be at the center of fibrosis, as they secrete the extracellular matrix

(ECM) proteins that are crosslinked into a scar. While several molecules and physical signals have been identified as being pro-fibrotic (i.e. stiffness, stretch, TGF- β , IL-4, IL-10, etc), the stimuli that activate these pro-fibrotic gene programs are not fully understood²⁻⁴; animal models help to understand tissue-level processes such as leukocyte infiltration and gross ECM remodeling, but lack the resolution of a reductionist system. Therefore, in-vitro models have been developed to better understand the cellular crosstalk that occurs between cardiac populations in the context of their microenvironment. While primary cells allow for the use of a human system, they rapidly activate in normal culture conditions⁵. Thus, any human primary fibroblast study is likely to require several patient samples of varying backgrounds, which can confound independent variables being tested, in addition to incurring large costs.

Recently, several groups have worked to overcome these limitations by using pluripotent stem cell-based systems, in which a continuous supply of cardiac fibroblasts can be produced from one donor's stem cells. Over the last decade, large strides have been made in the production of epicardial cells, which are precursors to the fibroblasts lining the coronary arteries (among other cell types), reducing the amount of growth factors and time required to generate these cells⁶⁻¹⁰. To further differentiate epicardial cells, several groups have proposed using bFGF with different media to accomplish a fibroblast fate^{10,11}. A similar bFGF treatment has also been shown to differentiate cardiac progenitor cells directly into fibroblasts by way of second heart field progenitors – a method most likely to

accurately model atrial and aortal fibroblasts¹². However, the left ventricular wall is primarily populated by epicardial fibroblasts that progress through the cardiac progenitor stage, and therefore a Gsk3/Wnt/Gsk3 inhibiting (GiWiGi) protocol is most likely to recapitulate native physiology of ventricular fibrosis in conditions such as heart failure and myocardial infarction^{9,13}. Here we focus on the epicardial lineage, particularly as it relates to using cardiac fibroblasts (CFs) for in-vitro disease modeling of the impacts of left ventricular fibrosis.

Two epicardial-derived protocols have recently been published, both yielding cardiac fibroblasts 18 days from initial GSK3 inhibition with CHIR9902^{10,11}. While largely similar though epicardial cell generation, protocols diverge in their approaches to generate CFs with basic fibroblast growth factor (bFGF). A protocol from Bao *et al.* relies on a serum-free media with low doses of bFGF (10 ng/mL) over 6 days⁹, while a protocol from Zhang *et al.* opts for a proprietary serum-containing medium (i.e., Promocell Cardiac Fibroblast Growth Medium 3) with bFGF and human insulin, which is then supplemented with additional bFGF¹⁰ and TGF- β inhibitor (**Fig. 3.1A**). While neither is serum-free, the protocol from Bao *et al.* is substantially more chemically defined (but 20% serum-containing media to neutralize Accutase after passaging) and employs more efficient use of growth factors.

In differentiating CFs from patient-specific iPSCs using the protocols from Bao *et al.* and Wu *et al.*, we were unable to obtain proper morphologic phenotype (**Fig. 3.1B**). However, several modifications to the protocol produced a proper

phenotype that yielded a similar chromatin architecture to primary CFs. Specifically, we found that: (1) extending the bFGF treatment of epicardial cells from 6 days to 20 days and (2) adjusting culture and assay mediums improved CF differentiation. While this protocol is longer in duration than the aforementioned methods, it presents a low-serum approach that reliably yields fibroblasts that can be grown for at least 15 passages.

3.3 Methods and Materials

3.3.1 Ethical compliance and Cell lines

The authors have complied with all ethical regulations via a study approved by UCSD (IRB #141315) for all patient-derived iPSCs, which were derived originally by the Scripps Research Institute (IRB #11-5676). Full characterization of these lines is available elsewhere⁸³. The authors commercially acquired H9 human embryonic stem cells (ESCs) from WiCell (Madison, WI). Primary cells were obtained from CellBiologics (Cat. H-6049, Chicago, IL) for use in ATAC sequencing and Promocell (Cat. C-12375, Heidelberg, DE) for immunofluorescence and western blot.

3.3.2 Differentiation Components and Methods

H9 ESCs and patient-derived iPSCs were maintained in their pluripotent state using mTeSR1 and by passaging with Versene and cell scrapers prior to differentiation. All materials required for differentiation are noted in **Table 3.1**. Cells

were differentiated into epicardial cells according to the protocol from Bao *et al.* but with notable exceptions outlined below. In the progenitor stage, changes include the use of 5-6 μM of CHIR99021 on day 0, 2.5 μM of IWP2 on day 3, and 3 μM of CHIR99021 on days 7 and 8 (**Fig. 3.2A**). Representative transcription factor expression was confirmed by immunofluorescence and morphology resembled reported images (**Fig. 3.2B**). Differentiation of epicardial cells into fibroblasts was achieved by 20 days of 10 ng/mL bFGF treatment in LaSR basal medium (Advanced DMEM/F12, 2.5 mM GlutaMAX and 60 $\mu\text{g}/\text{mL}$ ascorbic acid)¹⁵. Differentiations using Zhang-Kamp and Bao protocols were performed according to their publications^{9,12}. To test the Zhang-Wu method, epicardial cells generated from Bao protocol were treated with 10ng/mL of bFGF (R&D Systems, Cat. 233-FB, Minneapolis, MN) and A83-01 (Tocris, Cat. 2939, Minneapolis, MN) for six days.

3.3.3 Cardiac Fibroblast Phenotyping

3.3.3.1 Immunofluorescence

Expansion and maintenance of CFs with Fibroblast Growth Medium 3 (Promocell, Heidelberg, DE) and 0.25% Trypsin allowed for expansion through at least 16 passages. CFs of passage 8 or below were cultured in either Fibroblast Growth Medium 3 or RPMI1640 + 10% FBS and 250 μM of ascorbic acid for 3 days and stained for αSMA (ab32575, Abcam, 1:500) as an activation marker, TE-7 (NBP2-50082, Novus Bio, 1:100) and PDGFR α (AF-307-NA, RnD Systems,

1:250), to confirm identity, and fibronectin EDA (NBP1-51723, Novus Bio, 1:200) to confirm matrix competency. WT1 (R&D Systems, Cat. AF5729, Minneapolis, MN) and vimentin (Cell Signaling Technology, Cat. 5741, Danvers, MA) were used as epicardial and post-epithelial to mesenchymal transition markers. TCF21 (PA5-53031, ThermoFisher, 1:100) was used to confirm epicardial lineage and requisite CF transcription factor expression. Samples were blocked in 10% donkey serum, 0.3M glycine, and 1% bovine serum albumin for 1 hour, permeabilized in blocking buffer with 0.1% Triton X-100 for 20 minutes, stained with primary antibodies for 2 hours, and then incubated with secondary antibodies (A21202, A10042, and A21447, Invitrogen) for another two hours. Nuclei were stained with DAPI for 15 minutes at 1:10,000 dilution in DI water, and three washes were performed between each incubation for 5 minutes each.

3.3.3.2 *Western Blot*

To identify proteins by western blot, samples were lysed using mRIPA buffer, collected using cell scrapers, and vortexed every 5 minutes for 30 minutes total. Afterward, samples were centrifuged at 23,000 g for 15 minutes and the supernatant was transferred to a new tube. Protein concentrations were calculated using a bicinchoninic acid assay (23225, ThermoFisher Scientific), and after denaturing at 95 ° Celsius for 5 minutes, 10 µg of protein in 30 µL of RIPA buffer was loaded per lane on a 4-12% Bis-Tris Plus Gel (NW04122BOX, Thermo Fisher) in reducing conditions. Gels were run at 140V for 55 minutes and transferred using

an iBlot nitrocellulose transfer membrane (IB301001, Thermo Fisher). Membranes were blocked using Azure Blot blocking buffer (AC2190, Azure Biosystems) for 1 hour, incubated with primary antibodies (Collagen 1: 14695-1-AP, Proteintech, 1:100, GAPDH: ab8245, Abcam, 1:500, Fibronectin-EDA, NBP1-51723, Novus Bio, 1:2500, Beta Actin, ab-8226, Abcam, 1:500) overnight at 4° Celsius, secondary antibodies (A11374 and A10038, Invitrogen) for 1 hour, and imaged using a LI-COR Odyssey (LI-COR, Lincoln, NE).

3.3.3.3 *qPCR*

RNA was isolated after washing cells with 1X PBS twice, using Trizol (15596026, ThermoFisher). After 5 minutes of incubation, cells were scraped, transferred to 1.5 mL Eppendorf tubes, and 0.2 mL of molecular-grade chloroform was added. Tubes were shaken and let equilibrate for 3 minutes, after which tubes were centrifuged for 30 minutes at 4 degrees Celsius and 3700 RCF. Aqueous phases were transferred to new tubes and 0.5 mL of isopropanol was added. Tubes were inverted and let sit for 10 minutes. Tubes were centrifuged again using the same parameters as before, but for 20 minutes. The supernatant was removed and 1 mL of cold 75% molecular grade ethanol in DEPC water was added and vortexed. Tubes were then centrifuged at 3700 RCF for 12 minutes, decanted, and allowed to air dry. RNA was then resuspended in DEPC water and purified using the RNeasy Mini Kit (74104, Qiagen). RNA concentration was measured by Nanodrop (ND-2000, ThermoFisher), and 1µg of RNA was used per reverse

transcription reaction using Superscript IV and oligo(dT) (18091050, ThermoFisher). cDNA was stored at -20 Celsius prior to amplification. 10uL reactions were performed using 5 ng of cDNA, 1 μM forward and reverse primers in DEPC water, and 5 μL of Sybr Green (4309155, ThermoFisher). Each primer pair was optimized for melt temperature, and efficiency was validated to be between 80-120%. GAPDH primers (ran at 61 Celsius) were as follows: F- TCGACAGTCAGCCGCATCTTC, R- ACCAAATCCGTTGACTCCGAC, and ACTA2 (ran at 64 Celsius) was: F- AGCCAAGCACTGTCAGGAAT and R- CACCATCACCCCCTGATGTC. Expression was calculated using $2^{-\Delta\Delta CT}$ method using GAPDH as the housekeeping gene.

3.3.3.4 *Flow Cytometry*

Cells were passaged using Accutase (07922, Stem Cell Technologies), counted using a hemocytometer, resuspended in FACS buffer (1X PBS + 2% BSA w/v), and 100k cells were added to each well of a 96-well round bottom plate (3799, Corning). Cells were heated at 67 degrees Celsius for 4 minutes as a dead control and added to the plate. Cells were washed with PBS, centrifuged at 1200 RCF for 1 minutes, and wrist-flicked to remove supernatant. 100μL of 1:10,000 Tonbo Ghost Dye Red 780 (13-0865-T100, Tonbo Biosciences) in PBS was added to each well as a viability stain and incubated in the dark on ice for 20 minutes. Antibody solutions (PDGFRα: AF-307-NA, RnD Systems, cTNT: 130-119-674, Miltenyl Biotech, Nanog: PA5-46891, ThermoFisher, αSMA: IC1420A, RnD

Systems) were diluted in FACS buffer according to saturation points determined in previous experiments and kept on ice in the dark. Cells were then washed thrice with 150 μ L of FACS buffer, centrifuging, wrist-flicking, and triturating with each rinse. 50 μ L of each surface antibody was then added to appropriate wells and incubated in the dark on ice for 60 minutes. Three more rinses were then performed, and the cells were fixed and permeabilized using Cytofix/Cytoperm (554714, BD Biosciences) in a fume hood in the dark. Following three more rinses, intracellular antibodies and BV421 (705-675-147, Jackson Labs) (the secondary antibody used for PDGFR α), were added and incubated in the dark for 1 hour. Compensation beads (01-2222-41, ThermoScientific) for each antibody were added with 30 minutes of incubation time left. After three more rinses, cells were transferred to FACS tubes and analyzed using an LSRFortessa X-20 Analyzer (BD Biosciences) and FlowJo (BD Biosciences). Forward and side scatter gates were drawn for each sample type and gates were drawn above unstained control samples.

3.3.3.5 Assay for Transposase-Accessible Chromatin (ATAC) Sequencing

ATAC-sequencing was performed on patient-derived iPSC clones to confirm similar chromatin accessibility both between clones and also on primary human cardiac fibroblasts obtained from Cell Biologics. Library preparation and sequencing was performed by the UCSD Center for Epigenomics. ATAC-seq was performed on 50,000 nuclei per sample. Samples were permeabilized in cold

permeabilization buffer (0.2% IGEPAL-CA630 (I8896, Sigma), 1 mM DTT (D9779, Sigma), Protease inhibitor (05056489001, Roche), and 5% BSA (A7906, Sigma) in PBS (10010-23, Thermo Fisher Scientific)) for 10 minutes on a rotator at 4°C followed by centrifugation for 5 min at 500g at 4°C. The pellet was resuspended in cold tagmentation buffer (33 mM Tris-acetate (pH = 7.8) (BP-152, Thermo Fisher Scientific), 66 mM K-acetate (P5708, Sigma), 11 mM Mg-acetate (M2545, Sigma), 16% DMF (DX1730, EMD Millipore) in molecular biology grade water (46000-CM, Corning) followed by incubation with Tagmentation enzyme (FC-121-1030; Illumina) at 37°C with shaking at 500 rpm for 30 min. Tagmented DNA was purified using MinElute PCR purification kit (28004, QIAGEN). The resulting libraries were amplified using NEBNext High-Fidelity 2X PCR Master Mix (M0541, NEB) with primer extension at 72°C for 5 minutes, denaturation at 98°C for 30 s, followed by 8 cycles of denaturation at 98°C for 10s, annealing at 63°C for 30s and extension at 72°C for 60s. After purification of amplified libraries using MinElute PCR purification kit (28004, QIAGEN), double sided size selection was performed using SPRIselect beads (B23317, Beckman Coulter) with 0.55X beads and 1.5X to sample volume. Libraries were sequenced on a NextSeq500 (Illumina). Adaptor-trimmed fastq files were aligned to hg38 by Bowtie2¹⁶ using parameters “-X2000-mm-local”. After filtering via samtools¹⁷ with “-q 30 -F 1804 -f 2,” only primary and properly mated reads remained. PCR duplicates were removed by using “markduplicate” from Picard tools (<http://broadinstitute.github.io/picard/>). The remaining mapped reads were shifted +4 bp and -5 bp for “+” and “-” strand

respectively to adjust for Tn5 dimer so that the first base of each reads represents the cutting site. Then peak calling was performed by using MACS2¹⁸, all through the standard UCSD Epigenetics workflow. Peaks were called using the following settings: callpeak “-f BAMPE -g dm - -q 0.01 --nomodel --shift -100 --extsize 200 - -keep-dup all”. The output “narrowPeaks” were further filtered to remove blacklisted regions. The detailed pipeline can be accessed at https://github.com/epigen-UCSD/atac_seq_pipeline. XLS and sorted bam files were submitted to Diffbind¹⁹ in R for differential accessibility testing using an FDR cutoff of 0.01. Differentially accessible regions were submitted to GREAT ²⁰ for transcription start site distance determination and ontology annotation. Data generated in this study was deposited to NCBI under GEO GSE167368. We do not impose any restrictions on data availability.

To generate pseudobulk ATAC-seq data from patient-derived cardiomyocytes and cardiac fibroblasts for comparison with bulk ATAC-seq data from our differentiation protocol, we acquired bed files corresponding to aggregated open chromatin reads from atrial cardiomyocytes, ventricular cardiomyocytes, and cardiac fibroblasts from four cardiac chambers of four human donors (available from <http://catlas.org/humanheart> under “Bed files”) ²¹. We next used cellular barcodes to assign reads to specific donors and heart chambers based on each read’s barcode identifier. These final bed files, corresponding to either cardiomyocytes or cardiac fibroblasts from a specific donor and heart

chamber, were used as pseudobulk inputs for downstream comparative analysis. To generate genome browser tracks, we converted pseudobulk bed files to bedgraph format using BEDtools²² via the “genomecov” command with the “scale” option set to 10^6 / total number of reads in pseudobulk bed file. Bedgraph files were converted into bigwig format using the “bedGraphToBigWig” tool.

3.4 Protocol

Cardiac Progenitor Differentiation with Gsk3 inhibitor and Wnt inhibitor

Day -3

1. Culture hPSCs on Matrigel-coated 6-well plates in mTESR1 medium to 80-90% confluence. Aspirate medium and add 1 mL of room-temperature Accutase to each well. Incubate at 37 ° Celsius, 5% CO₂ for 5 minutes.
2. Add 1 mL of mTeSR1 media to each well of the 6-well plate and pool all the cells in a 15mL conical tube. Mix and count cell number on hemocytometer. Centrifuge the cells at 200g for 5 minutes at room temperature. Pipetting 3X per well with a P1000 pipette may improve count accuracy.
3. Aspirate the supernatant, resuspend the cells in mTeSR1+ 5 μ M Y27632 (ROCK inhibitor) at density of 2 million cells/mL, and plate 0.25-0.5 million cells/well in each well of a 12-well Matrigel-coated plate. Add mTeSR1 to each well for a final volume of 1mL in each well. This constitutes day -3.

1. Use 0.25 M/well for PSC lines that divide rapidly (passage every 3 days) and 0.5M/well for slower cells (passage every 4-5 days)

Day -2 and -1

4. On day -2 and -1, aspirate the medium and replace it with 2 mL of mTeSR1 per well of the 12-well plate.

Day 0

5. On day 0, prepare RPMI medium containing 6 μ M CHIR99021 (Gsk3 inhibitor). Add 4 μ L of 36 mM CHIR99021 to 24mL of RPMI basal medium. Aspirate the old medium and then add 2mL of RPMI + 6 μ M CHIR99021 medium to each well. **Record the time.**
 1. This concentration varies by PSC line, we have used 5-6 μ M.

Day 1

6. **Exactly 24 hours later (day 1)**, aspirate the medium from each well and replace it with 2mL of room-temperature RPMI basal medium.

Day 3

7. 48 hours later (day 3), prepare combined medium as follows: For each well, aspirate 1mL of conditioned media and add 1mL of freshly prepared RPMI basal medium in a 15mL conical tube (this is the combined medium). Add 1 μ L of 5mM IWP2 (final concentration is 2.5 μ M) to each conical tube.

Gently rock the plate back and forth to suspend cell debris and aspirate the remaining 1 mL of medium from each well, and then add the 2mL of combined medium + IWP2 to each well.

Day 4

8. Thaw 50 mL of Fetal Bovine Serum

Day 5

9. On day 5, aspirate the medium from each well and add 2mL of room-temperature RPMI basal medium to each well. Return to incubator. Coat a 12-well plate with 0.1% gelatin (250 uL/well) for D6, prepare RPMI20 and LaSR media (see Table 3.1).
 1. Note: **We do not recommend freezing** at CPC, but instead waiting for ProEpicardial cells to freeze. If you are not freezing now, you can usually seed 1-3 plates on D6.

Directed Differentiation of Cardiac Progenitors into Epicardial Cells

Day 6 *If freezing, prepare freezing media first* On day 6, aspirate the medium and add 1 mL of Accutase per well in a 12-well plate, and incubate the plate for 5 minutes. Prep tubes for step 10 during incubation.

10. Pipette 5-10 times with a P1000 tip to singularize the cells, and then transfer 1mL of the cell mixture to a 15mL conical tube containing 2 mL of RPMI20 medium.
11. Count the cells with a hemocytometer and centrifuge the cells at 200g for 5 minutes at room temperature, and aspirate the supernatant. **This is a potential freezing point, see freezing/thawing protocol for additional steps – these are cardiac progenitor cells.**
12. Resuspend the cell pellet in albumin-containing LaSR basal medium + 5 μ M Y27632 (Rock inhibitor) + 1% human albumin at a concentration of 100,000 cells/mL using a micropipette, and then seed onto a gelatin-coated cell culture dish (12-well) at a density of **60,000 cells/cm²** using a micropipette. Incubate overnight. FBS may be substituted for human albumin.

Days 7 and 8

13. On days 7 and 8, aspirate the medium and replace it with 1mL of room temperature LaSR basal medium + 3 μ M CHIR99021/well of the 12-well plate (this is equivalent to 1 μ L in 12mL media).

Day 9-11

14. On days 9-11, aspirate the medium and replace it with 1mL of room-temperature LaSR medium per well of the 12-well plate. On D11, make

RPMI20 and gelatin coated 12 well or 6 well plates. Secure a Mr. Frosty for D12 if freezing.

Differentiation of epicardial cells into fibroblasts

Day 12 *If freezing, prepare Epicardial Freezing media first*

15. At this point you should have epicardial cells.

1. On day 12, aspirate the medium, add 1 mL of Accutase/well of the 12-well plate, and incubate the plate for 5 minutes.
2. Pipette 5-10 times with a P1000 tip to singularize the cells, then transfer the 1mL cell mixture to a 15mL conical tube containing 2mL of RPMI20 medium.
3. Count the cells with a hemocytometer, centrifuge the cells at 200g for 5 minutes at room temperature, and aspirate the supernatant. **This is a freezing point of epicardial cells.**
4. Resuspend the epicardial cells and seed onto a gelatin-coated cell culture dish at a density of 60,000-80,000 cells/cm² in LaSR basal medium supplemented with 5 μ M Y27632 (ROCK Inhibitor). Incubate overnight to allow for cell attachment.

16. The next day and each day (days 13-32) thereafter, aspirate the medium from each well of the 12-well plate, and add 1mL per well of room-temperature LaSR basal medium with 10 ng/mL bFGF for fibroblast

differentiation (1:1000 dilution). You can also do this with 4 mL of media per well in a 6-well plate, but we suggest a slightly higher seeding density with the larger size wells.

17. On day 32, trypsinize cells (250 μ L or 125 μ L of 0.25% trypsin per well of 6-well or 12-well plate, respectively) and plate on tissue culture plastic 6-well plates at 20k cells/cm² in Promocell Fibroblast Growth Medium 3. Cells should maintain proper phenotype over 8-10 passages but not assemble matrix. For matrix assembly or other assay applications, culture cells with RPMI +10% FBS + 50uM ascorbic acid one day after passaging.

Freezing Protocol

1. After dissociation, resuspend the cardiac progenitor cells (from step 11) or proepicardial cells (from step 15) at a density of 1X10⁶ cells/mL in Cryostor for maximum viability or CPC/EpiC Freezing Medium.
2. Prepare 1mL aliquots of the cell suspension in cryovials, and freeze them in a Mr. Frosty container at -80 ° C overnight.
3. The next day, transfer the cryovials to liquid nitrogen for long term storage. Cells can be stored for at least 1 year.

Thawing Protocol

1. Incubate the vial in a 37°C water bath until almost all of the ice crystals have thawed.

2. Gently transfer the thawed cardiac progenitor cells or proepicardial cells to a 15mL conical tube containing 5mL of high glucose DMEM with 10% FBS.
3. Centrifuge the cells at 200g for 5 minutes at room temperature, and then aspirate the supernatant.
4. Gently resuspend the cells in 1 mL of LaSR basal medium + 20% FBS with 5 μ M Y27632 (ROCK Inhibitor) and transfer the mixture to a gelatin coated 12-well plate at a density of 0.5 million cells/cm². For epicardial cell thawing, addition of 0.5 μ M A83-01 to the medium will greatly increase cell attachment and viability.
5. For the next day, aspirate the medium in each well and replace with 2mL of freshly prepared room-temperature LaSR basal medium. Continue with the main protocol.

Table 3.1. Materials Checklist.

Materials required for the differentiation process from iPSC to CF, excluding materials required for iPSC maintenance.

	Item (Catalogue Number, Manufacturer)	Amount for 1 differentiation (includes 10% extra)	When Needed in the Protocol (Day)
•	6-well low evaporation plate – Matrigel coated (354277, Corning)	1	Before -3
•	Accutase (1154, Innovative Cell Technologies)	27 mL	-3,6,12
•	mTeSR1 Media (85851, Stem Cell Technologies)	63 mL	-3,-2,-1
•	Y27632 (Y-5301, LC Labs)	Depends on Cell Yield	-3, 6, 12
•	15 mL conical tubes (352095, Falcon)	~20	Several, esp. 3
•	12-well low evaporation plate – Matrigel coated (354277, 353043, Corning)	1	-3
•	RPMI 1640 Medium (11875-093, Gibco)	93 mL	0,1,3,5
•	36 mM CHIR99021 (SML1046, Sigma Aldrich)	6 µL	0,7,8
•	5mM IWP2 (S7085, Sellechem)	12 µL	3
•	RPMI20 Media (RPMI 1640 + 20% FBS) (11875, Gibco)	5 mL	6, 12
•	LaSR Basal Medium -500 mL Advanced DMEM/F12 medium (12634028, Thermo Fisher) -6.5 mL Glutamax (35050061, Gibco) -500 µL of 100mg/mL ascorbic acid solution (36237, Alfa Aesar)	230 mL	6-32
•	12-well low evaporation plate- 0.1% gelatin coated (353043, Corning, G9391, Sigma)	2	6,12
•	bFGF (233-FB, RnD Systems)	2.4 µg	13-32
•	CHIR99021 (C-6556, LC Laboratories)	Varies	0,6,7
•	Fibroblast Growth Medium 3 (C-23025, Promocell)	2mL/day	Varies
•	CPC Freezing Medium -30% FBS -10% DMSO -5µM Y27632 (Y-5301, LC Labs)	1mL/million cells	6
•	Epicardial Freezing Medium -30% FBS -10% DMSO -5µM Y27632 (Y-5301, LC Labs) -500nM A83 (019001799, Cayman Chemical)	1mL/million cells	12
•	Cryostor CS-10 (07930, Stem Cell Technologies)	1mL/million cells	12,32
•	Mr. Frosty Freezing Container (15-350-50, Fisher Scientific)	1	6,12,32
•	A83-01 (9001799, Cayman Chemical)	1uL/mL	Only when expanding Epicardial Cells

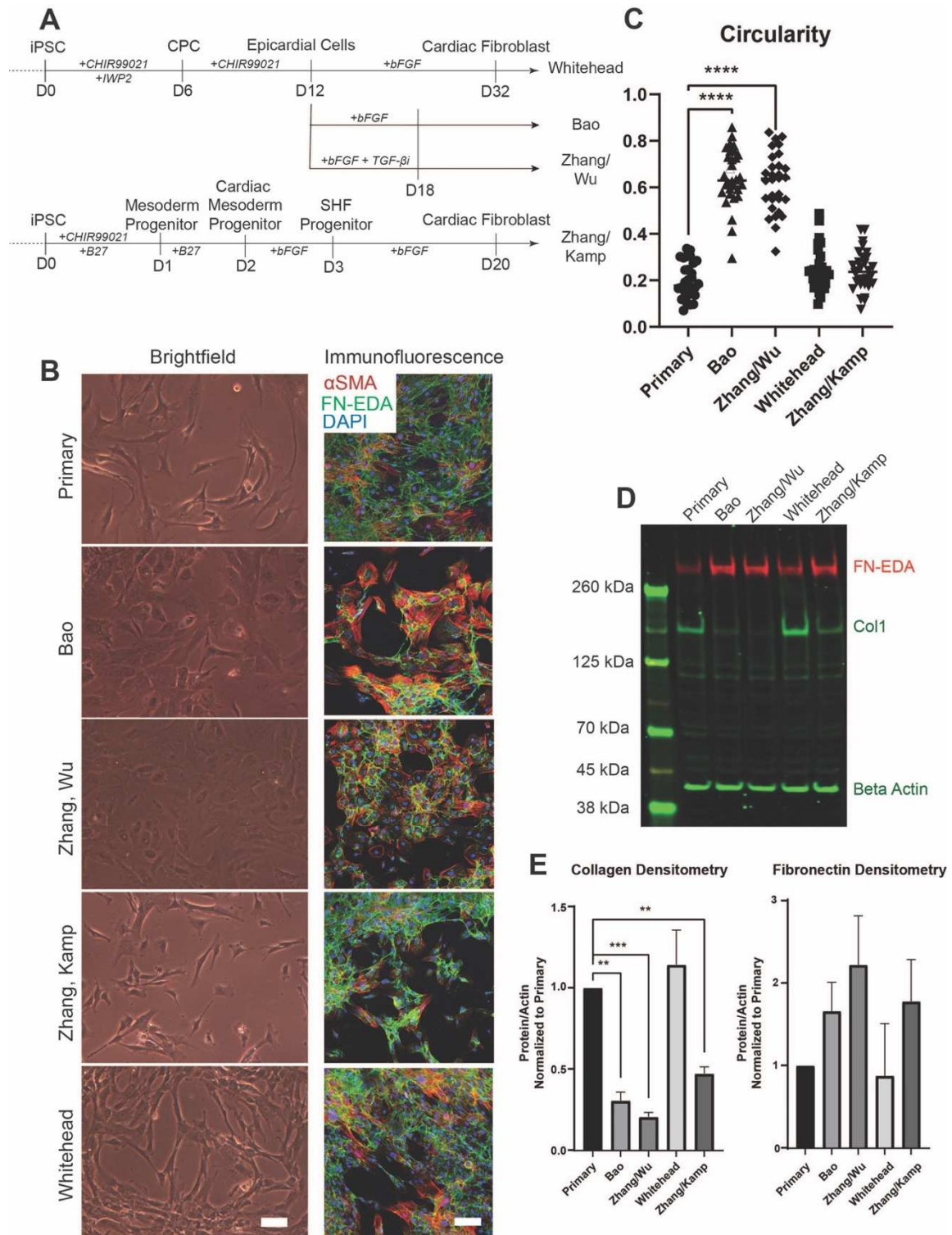
3.5 Results and Discussion

While several methods have been previously published to generate cardiac fibroblasts, we were only able to successfully reproduce the Zhang and Kamp method¹², which progresses through second heart field progenitors, and yield a cell that morphologically resembled CFs (**Fig. 3.1A-B**). We therefore sought to develop a differentiation protocol that resembles primary phenotype while progressing through the epicardial stage. We found that the Bao⁹ and Zhang/Wu¹⁰ protocols yielded cells with circular morphology (**Fig. 3.1B**, left) and poor matrix assembly (**Fig. 3.1B**, right). Quantitatively, these morphological differences were represented by large differences in circularity – canonical 2D fibroblast morphology is spindle-shaped and the existing epicardial protocols produced a more rounded shape (**Fig. 3.1C**). Analysis of soluble protein by western blot demonstrated that all protocols including our iCF method produced statistically similar amounts of Fibronectin-EDA, i.e., fibronectin containing an extra A-type domain prevalent in CFs (**Fig. 3.1D,E**). When probing for type I collagen, a key protein for modeling scar remodeling, the iCF protocol presented here had the highest type I collagen expression (**Fig. 3.1D,E**), akin to primary cells. To better understand how differences between protocols could result in morphological and matrix production differences, we dissected specific steps in select protocols. We found that the addition of TGF- β inhibitor in the Zhang/Wu¹⁰ protocol inhibited epithelial-to-mesenchymal transition (EMT), i.e., punctate nuclear WT1 staining after 6 days of treatment became diffuse in assay media (RPMI, 10% FBS and 100 mg/L Vitamin

C; **Fig. S3.1A**). In concert with this, vimentin was almost non-existent immediately after differentiation but emerged after culture in assay media, suggesting that EMT was spurred by serum and lack of TGF- β inhibition. For these reasons, we decided to compile our own modifications to the Bao protocol, better reproducing primary cell phenotype, i.e., the iCF protocol described above.

Figure 3.1. Comparison of CF differentiation protocols.

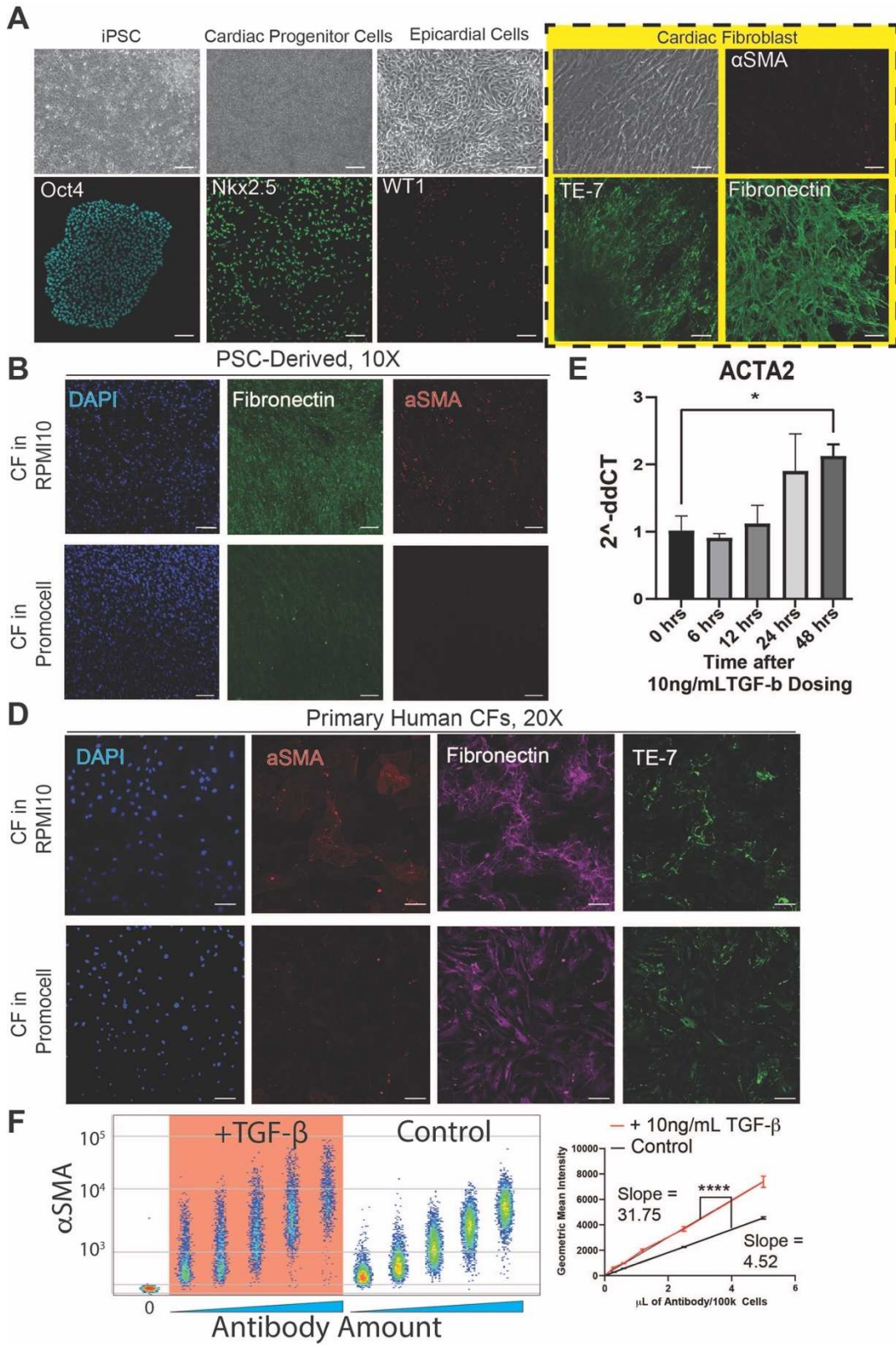
A. Schematic of various cardiac fibroblast differentiations, highlighting differences within and between developmental origins. **B.** Brightfield (left) images of Promocell primary ventricular cardiac fibroblasts and the resultant cells from each protocol after being cultured in Promocell Fibroblast Growth Medium at 25k/cm² for three days (n=3, cultured in triplicate, repeated twice). Immunofluorescent staining of CFs (25k/cm²) after 3 days of culture in assay media for fibronectin-EDA (green), α SMA (red), and DAPI (blue). **C.** Quantification of cell circularity between fibroblast differentiations. 10 cells were traced in three images for each group, p<0.05 using a one-way ANOVA. **D.** Representative western blot for type I collagen, fibronectin-EDA, and beta Actin of mRIPA soluble CF lysate (50k/cm²) cultured for 3 days in assay media (n = 3, samples differentiated in triplicate). **E.** Densitometry of western blots, bands normalized to beta actin and primary groups between blots. n=3, significance is defined as p<0.05 by one-way ANOVA.



Our modified differentiation timeline (**Fig. 3.1A**) yields cardiac progenitor, epicardial cells, and ultimately generates cardiac fibroblasts that express hallmark proteins (**Fig. 3.2A**). While many different CF markers have been reported, each has caveats in either specificity or persistence; for example, CD90 is often used as a fibroblast marker, but only marks a subset of CFs and expression decreases over several passages ²³. Fibroblast-specific protein 1 (FSP-1)—another reported CF marker—is also expressed on endothelial cells ²⁴. We found that the mesenchymal marker Fibroblast TE-7 reliably labels both primary and iPSC-derived CFs (**Fig. 3.2A**), though the specific antigen is unknown.

Figure 3.2. Differentiation and characterization of PSC-derived CFs.

A. Brightfield images (top row, black and white) of cells on days 0, 6, 12, and 32, respectively. Immunofluorescent staining of transcription factors (bottom row, left three), and CF markers (yellow box, colored images) of iPSC-derived lines. Scale bars represent 100 μ m. N=3 performed in parallel in triplicate. **B.** Immunofluorescent staining of CF markers in assay medium (top row) or growth medium (bottom row), using iPSC-derived CFs (scale bars are 200 μ m). **C.** Media comparisons using Promocell primary CFs (scale bars are 100 μ m). N=3 performed in parallel in triplicate. **D.** qPCR readout of ACTA2 after 10ng/mL of TGF- β in 1% serum-containing growth medium. **E.** Flow cytometry FSC-Area vs α SMA fluorescent intensity of untreated (control) or TGF- β (10ng/mL) after three days. Antibodies were titrated from 0.625 to 7 μ L/100k cells. Geometric mean (right) of each population and significance calculated using a regression slope test, p<0.01.



Another hallmark of this protocol is the subsequent ability to expand cells when grown in Promocell Fibroblast Medium 3. This medium was excellent at maintaining proliferation, morphology, and suppression of CF activation (i.e., α SMA positivity; **Fig. 3.2B**), but it surprisingly suppressed fibronectin assembly. When assessing CF phenotype, cells were transitioned to assay medium containing RPMI with 10% fetal bovine serum and 50 μ g/mL ascorbic acid. This permitted fibronectin assembly and production of collagen 1, though spurring α SMA activation. Culture expanded CFs, when plated at 2×10^4 cells/cm² and then switched to assay medium for 3 days (with daily media changes), produced robust extracellular matrix assembly that was easily quantifiable by immunofluorescence or western blot (**Fig. 3.2B,C, S3.1B**). In response to TGF- β stimulation, fibroblasts should upregulate α SMA as they begin to adopt a myofibroblast phenotype. We found that 10 ng/mL TGF- β was able to upregulate α SMA in our cells at the mRNA and protein levels (**Fig. 3.2D,E**). Similar to the Zhang/Wu and Zhang/Kamp findings, we observed low levels of α SMA protein expression in the absence of TGF- β stimulation, but fluorescent intensities increased drastically with dosing. We observe a strong correlation between the peak mRNA level of ACTA2 (approximately twice the level of untreated) and the geometric mean of protein fluorescence by flow cytometry (also approximately 2-fold). Zhang/Wu report a ~1.5-fold upregulation of ACTA2 following 48 hour treatment of 5ng/mL of TGF- β , and Zhang/Kamp demonstrate a 5% increase in high α SMA+ cells following two-

day treatment at 10ng/mL, suggesting both of these cell products may also be TGF- β responsive.

In vitro studies have also demonstrated that bona-fide cardiac fibroblasts require the TCF21 transcription factor, as knockout of this protein absolves the heart of any CF populations ²⁵. Since epicardial populations were derived from WT1+ cells (**Fig. 3.2A**), it is unsurprising that all derivatives also express and nuclear localize the epicardial marker TCF21 (**Fig. 3.3A**). Zhang-Kamp also report upregulation of the TCF21 mRNA toward the end of the differentiation, and we confirm these findings at the protein level. As the cells differentiate from the epicardial stage, they must undergo EMT to establish mesenchymal fate commitment. Vimentin, an intermediate filament that is indicative of EMT ²⁶, was also stained and found to be highest in Primary cells as well as the Zhang-Kamp ¹² and this protocols (**Fig. 3.3B**). Reduced vimentin expression in the Bao and Zhang-Wu protocols suggests that they have incompletely undergone the transformation. Furthermore, PDGFR α , a key protein required for CF development and survival ²⁷, was found to be highly expressed by primary, Zhang-Kamp, and Whitehead CFs, and to a lesser extent in Bao and Zhang-Wu cells (**Fig. 3.3A-C**), depending on the protein quantification technique. However when comparing these cells to other cardiac lineages, e.g., cardiomyocytes, and to their parental line, i.e., iPSCs, no cells were found to significantly express cTnT and Nanog, respectively, since none of the CFs demonstrated a significant right-shift in fluorescence histograms from flow cytometry (**Fig. S3.1C**).

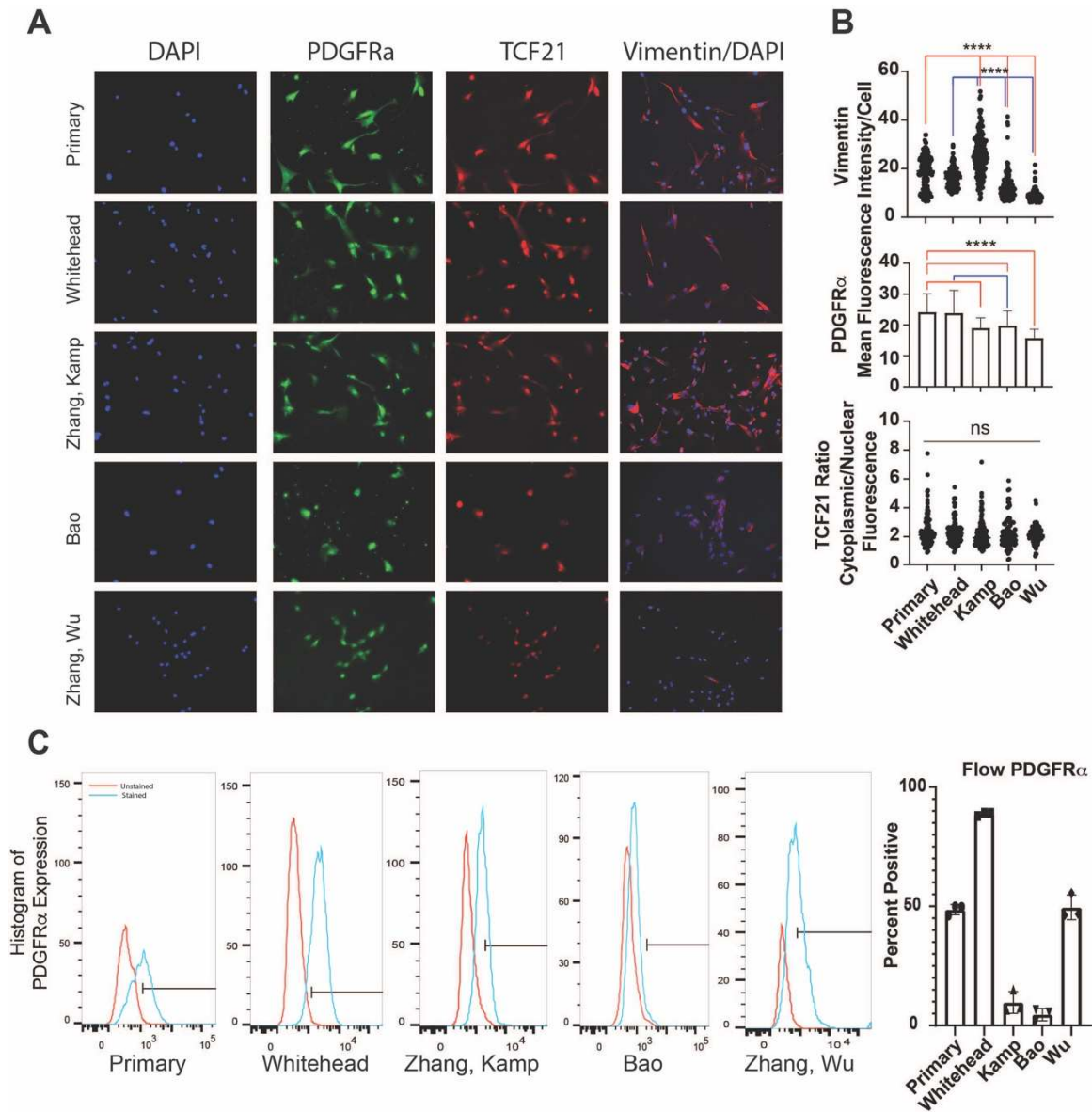
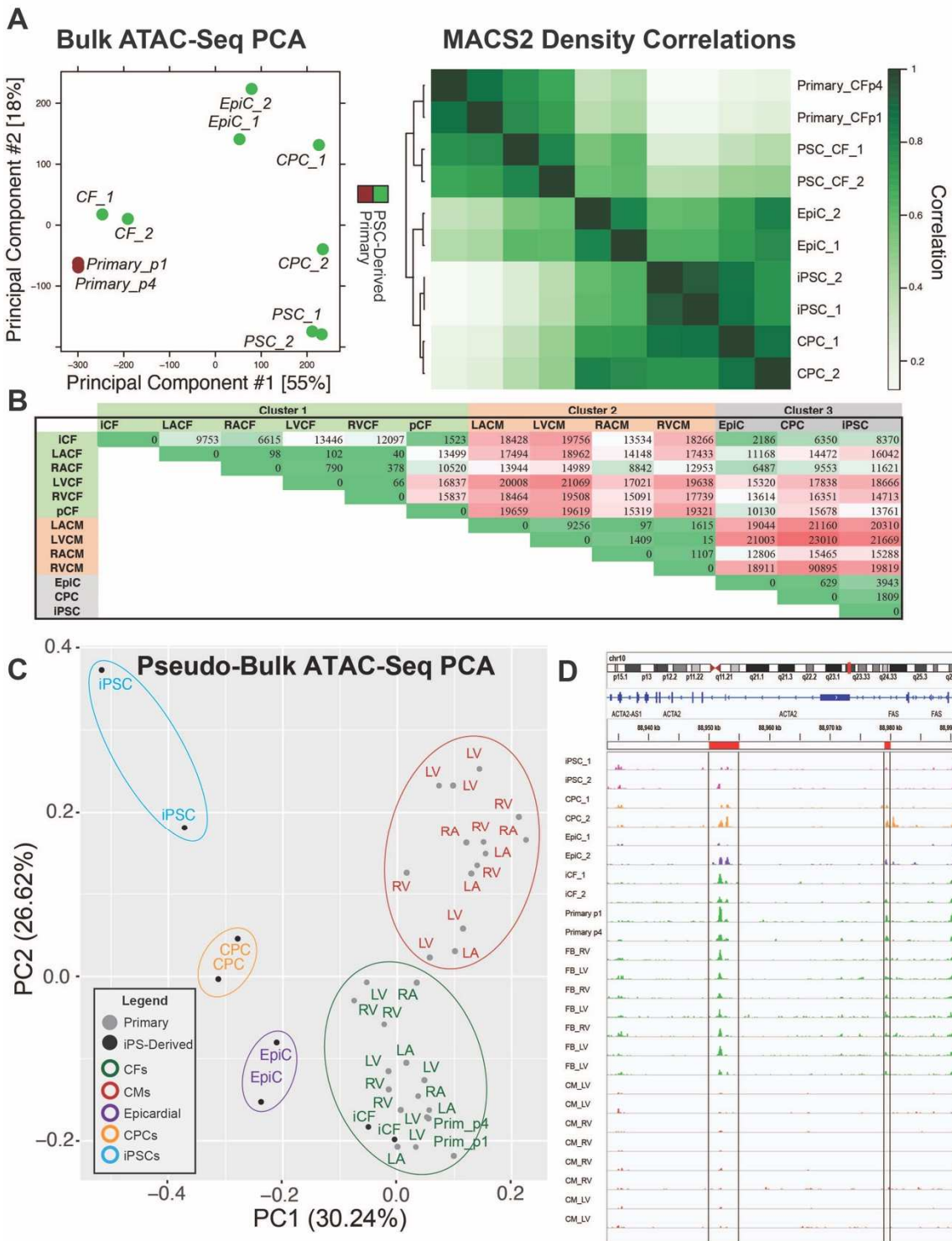


Figure 3.3. Vimentin and PDGFR α expression are Hallmarks of Differentiated CFs.

A. Immunofluorescent staining of primary and derived CFs. DAPI, PDGFR α , and TCF21 were co-stained (left) and vimentin is shown with DAPI background. **B.** Quantification of vimentin and PDGFR α intensity per cell from immunostained samples. N=3 samples, 3-4 images per sample. Testing performed using a non-parametric one-way ANOVA, $p < 0.05$. Tukey post-hoc test performed between primary (red lines) and Whitehead samples (blue lines) vs others. **C.** Flow cytometry histograms of PDGFR α fluorescence across groups demonstrating gate placement right of unstained controls. Quantification of percent PDGFR α + cells (right) over samples.

Figure 3.4. ATAC sequencing of differentiation stages.

A. Principal component analysis and correlation heatmap of iPSC-derived cells and Cell Biologics Primary CFs. Primary cells are from the same donor cultured for either 1 or 4 passages. N=2 per condition, once per iPSC clone for differentiated cells. **B.** Number of differentially accessible regions from HOMER DESEQ2 output ($q < 0.05$) when comparing sample groups (n=2 for differentiated cells and Cell Biologics samples, and N=3 for primary donor samples from Hocker et al.). There was a total of 70507 peaks in the merged peakset. **C.** ATAC sequencing principal component analysis including pseudo-bulk samples from Hocker et al. Cell types clustered together and labels were color coded based on cell identity while point color designates origin of cell, either primary or iPSC-derived. **D.** Integrative Genomics Viewer (IGV) snapshots of α SMA gene (ACTA2) peaks, including iPSC-derived (n=2 per cell type), Cell Biologics (n=2), and ventricular primary pseudo-bulk cardiomyocyte and fibroblast cells (n=3) from Hocker et al. Tracks displayed are reads per genomic content (RPGC) normalized bigwig files and color-coded by cell type.



To further validate protocol efficacy and because chromatin remodeling is an *a priori* process to the activation of transcriptional programs, we performed ATAC-seq on iPSC lines from two patient clones through each differentiation stage and found that iPSC-CFs clustered with the primary cell samples from Cell Biologics (**Fig. 3.4A**). This suggests that chromatin architectural remodeling through the differentiation closely resembles that of native CFs. As expected, each stage of the differentiation also clustered together, showing a continuous trajectory in two principal components.

Since primary cells obtained from commercial vendors expand primary cells for several passages, we compared our iCFs with primary human cardiomyocyte and cardiac fibroblast pseudobulk single nucleus ATAC sequencing profiles from Hocker et al.²¹. We found that iCFs were most similar to Promocell ventricular cardiac fibroblasts, though all fibroblast groups clustered together and were distinct from cardiomyocyte and stem/progenitor cell populations (**Fig. 3.4B-C**). Lastly, since α SMA accessibility precedes the ability of a fibroblast to become activated, we compared accessibility to this genomic region across all ventricular and iPSC-derived samples and found similar accessibility between primary, cell-line, and iCF fibroblasts (**Fig. 3.4D**).

In summary, this protocol presents an improved approach to generate CFs for modeling left ventricular fibrosis. We present methods to preserve developmental lineage accuracy via epicardial fate, deliver physiological dosing of bFGF in reduced serum conditions, and greatly improve phenotype of resulting

cells. An accurate model of matrix production is required to recapitulate native physiology in a dish, particularly cell adhesion, migration, and substrate stiffness; these cells can be used in downstream applications such as co-culture, 3D matrix assembly, and drug discovery while evading the limitations of primary cells (i.e., low Hayflick limit and varying genetic backgrounds) and murine models.

This breakthrough is particularly important as the field begins to incorporate more complex in-vitro models of disease and multicellular communication before testing in animal systems. Traditionally, mice or rats have been used to model cardiac disease, but they have several limitations: mice hearts beat at approximately 10 times the rate of humans and do not always generate human-like pharmacological responses ^{28,29}. Rats also have a significantly higher heart rate (approx. 330-480 beats per minute), and while generally better recapitulating human pathological processes, lack many of the genetic tools and strains that make mice an attractive model ^{29,30}. Though larger mammalian organisms better bridge the gap between animal and human physiology, they are often cost-prohibitive and have even fewer molecular tools than their murine counterparts. Finally, with the emerging understanding of the vast regulatory roles noncoding RNAs play in many diseases and homeostatic processes, model organism genomes often do not contain these sequences and knock-in models fail to capture clinical phenotypes ³¹⁻³⁴. Therefore, in-vitro modeling presents the opportunity narrow therapeutic targets and regenerative approaches prior to more rigorous

testing in animals - though in-vitro systems are only beginning to emerge as meaningful screens with translational promise.

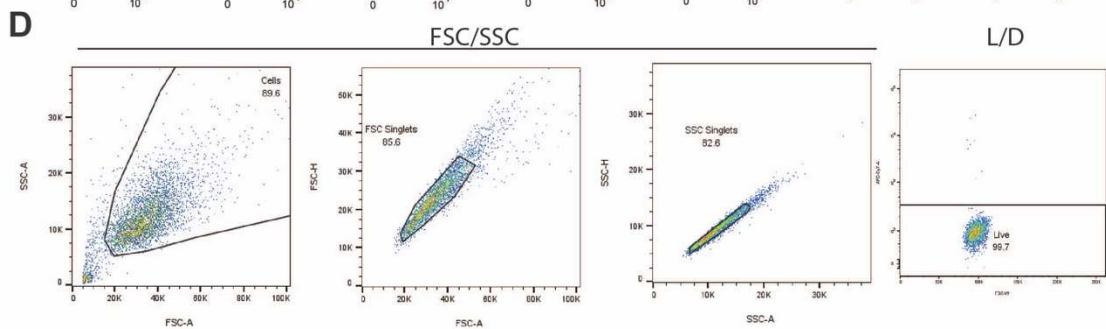
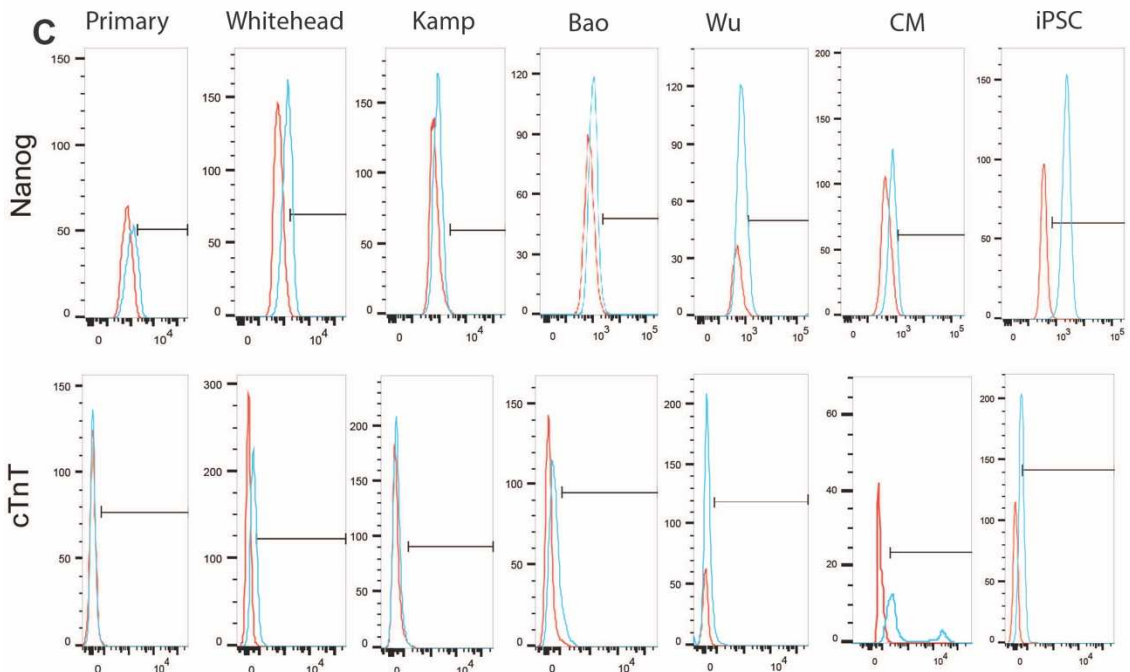
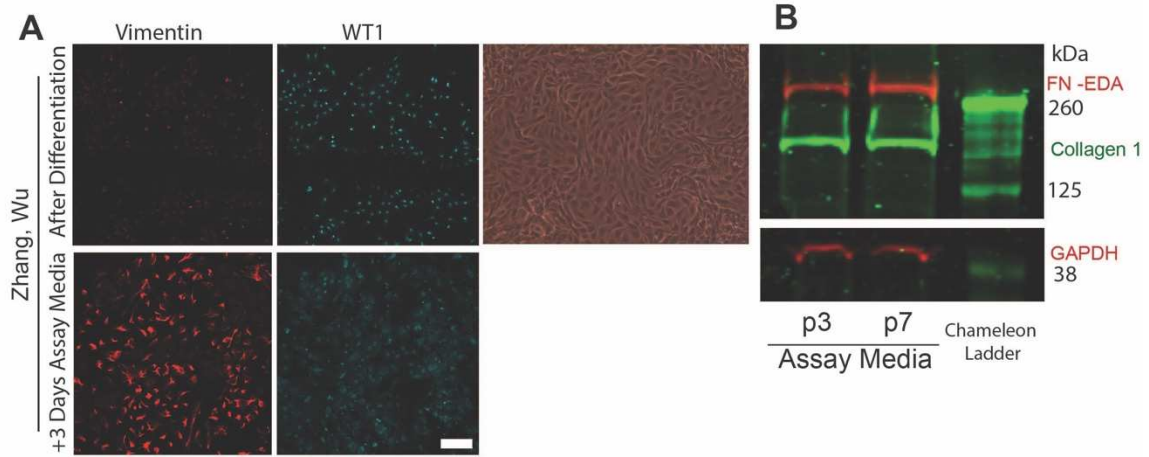
Perhaps one of the largest limitations of fibrotic disease modeling-in-a-dish is the inability of fibroblasts to assemble collagen fibrils in 2D. For this reason, many 2D systems measure collagen production by western blot, mRNA, or ELISA of soluble collagen – staining for collagen only resolves intracellular protein and does not represent the bona fide scar manufacturing capabilities of fibroblasts. To circumvent this limitation, groups have investigated using macromolecular crowding, which involves the use of high molecular weight polymers to stabilize BMP1 to cleave procollagen domains and allow for assembly ³⁵. Thus, fibrotic screens can be performed in 96-well plate formats and be read using a plate reader to quickly screen compounds. Yet even for this method, a major limitation is that different polymers yield different collagen organization and responses to pro-fibrotic agonists ³⁶. Yet another alternative, though much lower throughput, is to develop multicellular cultures or organoids. This method enables both fibril formation as well as crosstalk between multiple cell types, which may synergistically respond to physical or biological stimuli. In the context of iPSC differentiations, 3D multicellular platforms have also been shown to enhance calcium handling and maturity of cardiomyocytes, as well as their ability to recapitulate congenital heart disease ³⁷⁻³⁹. Thus, albeit more time intensive, these in-vitro approaches are more likely to provide anti-fibrotic insights that translate to human therapies than traditional 2D, macromolecular crowding, or animal models.

We hope that this differentiation protocol will enable such studies through the development of patient-specific cardiac tissues (now including fibroblasts) to interrogate human pathologies.

3.6 Supplementary Figure

Supplemental Figure 3.1. Additional marker characterization for each protocol.

A. Brightfield image (right) and immunostained (left) images of resultant Zhang/Wu cells immediately after differentiation (left) and after three days of culture in assay medium (right). WT1 and vimentin were used as pre-EMT and post-EMT markers, respectively (n = 3, performed in triplicate). **B.** Western blot of EDA isoform of fibronectin, collagen 1 and GAPDH after three days of H9 CF culture in assay medium (n=1 per condition) using passage 3 and 7 cells. **C.** Flow cytometry histograms of Nanog and cTnT staining across CF groups and positive control cells. Cardiomyocytes were iPSC-derived (day 15). **D.** Flow cytometry gating strategy for cells, singlets, and live cells.



3.7 Acknowledgements

Chapter 3, in full, a reprint of the material as it appears in the Journal of Molecular and Cellular Cardiology, 2022, Whitehead, Alexander J.; Hocker, James D.; Ren, Bing; Engler, Adam J. international Society for Heart Research. The dissertation author is the primary investigator and author of this material. Special thanks to our collaborators Jake Hocker and Bing Ren for their contributions with the ATAC-sequencing and advice when developing the analysis pipeline. The dissertation author is the primary investigator and author of this material.

iPSCs were a generous gift from Dr. Kristin Baldwin (Scripps Research). The authors acknowledge funding support from the National Institutes of Health (R01AG045428 to A.J.E.) and the National Science Foundation Graduate Research Fellowship Program (to A.J.W.). J.D.H. was supported in part by a Ruth L. Kirschstein Institutional National Research Service Award T32 GM008666 from the National Institute of General Medical Sciences. Work at the Center for Epigenomics was supported in part by the UC San Diego School of Medicine.

3.8 References

1. Wynn TA. Fibrotic disease and the TH1/TH2 paradigm. *Nature Reviews Immunology*. 2004;4(8):583–594.
2. Herum KM, Choppe J, Kumar A, Engler AJ, McCulloch AD. Mechanical regulation of cardiac fibroblast profibrotic phenotypes. *Molecular biology of the cell*. 2017;28(14):1871–1882.

3. Rayahin JE, Buhrman JS, Zhang Y, Koh TJ, Gemeinhart RA. High and Low Molecular Weight Hyaluronic Acid Differentially Influence Macrophage Activation. *ACS Biomaterials Science and Engineering*. 2015;1(7):481–493.
4. Irwin EF, Saha K, Rosenbluth M, Gamble LJ, Castner DG, Healy KE. Modulus-dependent macrophage adhesion and behavior. *Journal of Biomaterials Science, Polymer Edition*. 2008;19(10):1363–1382.
5. Landry NM, Rattan SG, Dixon IMC. An Improved Method of Maintaining Primary Murine Cardiac Fibroblasts in Two-Dimensional Cell Culture. *Scientific Reports*. 2019;9(1):1–13.
6. Witty AD, Mihic A, Tam RY, Fisher SA, Mikryukov A, Shoichet MS, Li R-KK, Kattman SJ, Keller G. Generation of the epicardial lineage from human pluripotent stem cells. *Nature Biotechnology*. 2014;32(10):1026–1037.
7. Iyer D, Gambardella L, Bernard WG, Serrano F, Mascetti VL, Pedersen RA, Talasila A, Sinha S. Robust derivation of epicardium and its differentiated smooth muscle cell progeny from human pluripotent stem cells. *Development (Cambridge)*. 2015;142(8):1528–1541.
8. Zhao J, Cao H, Tian L, Huo W, Zhai K, Wang P, Ji G, Ma Y. Efficient Differentiation of TBX18+/WT1+ Epicardial-Like Cells from Human Pluripotent Stem Cells Using Small Molecular Compounds. *Stem cells and development*. 2017;26(7):528–540.
9. Bao X, Lian X, Qian T, Bhute VJ, Han T, Palecek SP. Directed differentiation and long-term maintenance of epicardial cells derived from human pluripotent stem cells under fully defined conditions. *Nature Protocols*. 2017;12(9):1890–1900.
10. Zhang H, Tian L, Shen M, Tu C, Wu H, Gu M, Paik DT, Wu JC. Generation of quiescent cardiac fibroblasts from human induced pluripotent stem cells for in vitro modeling of cardiac fibrosis. *Circulation Research*. 2019;125(5):552–566.
11. Bao X, Lian X, Hacker TA, Schmuck EG, Qian T, Bhute VJ, Han T, Shi M, Drowley L, Plowright AT, Wang QD, Goumans MJ, Palecek SP. Long-term self-renewing human epicardial cells generated from pluripotent stem cells under defined xeno-free conditions. *Nature Biomedical Engineering*. 2017;1(1):0003.
12. Zhang J, Tao R, Campbell KF, Carvalho JL, Ruiz EC, Kim GC, Schmuck EG, Raval AN, da Rocha AM, Herron TJ, Jalife J, Thomson JA, Kamp TJ.

- Functional cardiac fibroblasts derived from human pluripotent stem cells via second heart field progenitors. *Nature Communications*. 2019;10(1):2238.
13. Zhou B, Gise A von, Ma Q, Rivera-Feliciano J, Pu WT. Nkx2-5- and Isl1-expressing cardiac progenitors contribute to proepicardium. *Biochemical and Biophysical Research Communications*. 2008;375(3):450–453.
 14. Lo Sardo V, Chubukov P, Ferguson W, Kumar A, Teng EL, Duran M, Zhang L, Cost G, Engler AJ, Urnov F, Topol EJ, Torkamani A, Baldwin KK. Unveiling the Role of the Most Impactful Cardiovascular Risk Locus through Haplotype Editing. *Cell*. 2018;175(7):1796-1810.e20.
 15. Lian X, Bao X, Al-Ahmad A, Liu J, Wu Y, Dong W, Dunn KK, Shusta E V, Palecek SP. Efficient differentiation of human pluripotent stem cells to endothelial progenitors via small-molecule activation of WNT signaling. *Stem Cell Reports*. 2014;3(5):804–816.
 16. Langmead B, Salzberg SL. Fast gapped-read alignment with Bowtie 2. *Nature Methods*. 2012;9(4):357–359.
 17. Li H, Handsaker B, Wysoker A, Fennell T, Ruan J, Homer N, Marth G, Abecasis G, Durbin R. The Sequence Alignment/Map format and SAMtools. *Bioinformatics*. 2009;25(16):2078–2079.
 18. Zhang Y, Liu T, Meyer CA, Eeckhoute J, Johnson DS, Bernstein BE, Nussbaum C, Myers RM, Brown M, Li W, Shirley XS. Model-based analysis of ChIP-Seq (MACS). *Genome Biology*. 2008;9(9):R137.
 19. Ross-Innes CS, Stark R, Teschendorff AE, Holmes KA, Ali HR, Dunning MJ, Brown GD, Gojis O, Ellis IO, Green AR, Ali S, Chin SF, Palmieri C, Caldas C, Carroll JS. Differential oestrogen receptor binding is associated with clinical outcome in breast cancer. *Nature*. 2012;481(7381):389–393.
 20. McLean CY, Bristol D, Hiller M, Clarke SL, Schaar BT, Lowe CB, Wenger AM, Bejerano G. GREAT improves functional interpretation of cis-regulatory regions. *Nature Biotechnology*. 2010;28(5):495–501.
 21. Hocker JD, Poirion OB, Zhu F, Buchanan J, Zhang K, Chiou J, Wang T-M, Zhang Q, Hou X, Li YE, Zhang Y, Farah EN, Wang A, McCulloch AD, Gaulton KJ, et al. Cardiac cell type-specific gene regulatory programs and disease risk association. *Science Advances*. 2021;7(20):eabf1444.
 22. Quinlan AR, Hall IM. BEDTools: A flexible suite of utilities for comparing genomic features. *Bioinformatics*. 2010;26(6):841–842.

23. Pinto AR, Ilinykh A, Ivey MJ, Kuwabara JT, D'antoni ML, Debuque R, Chandran A, Wang L, Arora K, Rosenthal NA, Tallquist MD. Revisiting cardiac cellular composition. *Circulation Research*. 2016;118(3):400–409.
24. Kong P, Christia P, Saxena A, Su Y, Frangogiannis NG. Lack of specificity of fibroblast-specific protein 1 in cardiac remodeling and fibrosis. *American Journal of Physiology - Heart and Circulatory Physiology*. 2013;305(9):H1363.
25. Acharya A, Baek ST, Huang G, Eskiocak B, Goetsch S, Sung CY, Banfi S, Sauer MF, Olsen GS, Duffield JS, Olson EN, Tallquist MD. The bHLH transcription factor Tcf21 is required for lineage-specific EMT of cardiac fibroblast progenitors. *Development*. 2012;139(12):2139–2149.
26. Ivaska J. Vimentin: Central hub in EMT induction? *Small GTPases*. 2011;2(1):51–53.
27. Ivey MJ, Kuwabara JT, Riggsbee KL, Tallquist MD. Platelet-derived growth factor receptor- α is essential for cardiac fibroblast survival. *American Journal of Physiology - Heart and Circulatory Physiology*. 2019;317(2):H330–H344.
28. Mitchell GF, Jeron A, Koren G. Measurement of heart rate and Q-T interval in the conscious mouse. *American Journal of Physiology - Heart and Circulatory Physiology*. 1998;274(3 43-3):747–751.
29. Camacho P, Fan H, Liu Z, He JQ. Small mammalian animal models of heart disease. *American Journal of Cardiovascular Disease*. 2016;6(3):70–80.
30. Coleman TG. Arterial baroreflex control of heart rate in the conscious rat. <https://doi.org/10.1152/ajpheart.1980.238.4.H515>. 1980;7(4):515–520.
31. Visel A, Zhu Y, May D, Afzal V, Gong E, Attanasio C, Blow MJ, Cohen JC, Rubin EM, Pennacchio LA. Targeted deletion of the 9p21 non-coding coronary artery disease risk interval in mice. *Nature*. 2010;464(7287):409–412.
32. Serocki M, Bartoszewska S, Janaszak-Jasiecka A, Ochocka RJ, Collawn JF, Bartoszewski R. miRNAs regulate the HIF switch during hypoxia: a novel therapeutic target. *Angiogenesis*. 2018;21(2):183–202.
33. van Arensbergen J, Pagie L, FitzPatrick VD, de Haas M, Baltissen MP, Comoglio F, van der Weide RH, Teunissen H, Vösa U, Franke L, de Wit E, Vermeulen M, Bussemaker HJ, van Steensel B. High-throughput identification of human SNPs affecting regulatory element activity. *Nature*

Genetics. 2019;51(7):1160–1169.

34. Lewis CM, Ravindrarajah R, Munroe PB, Stratton MR, Vukcevic D, Widden C, Simmonds MJ, Iles MM, Grozeva D, McCarthy MI, Strachan DP, Widmer B, Barrett JC, Sanderson J, Lees CW, et al. Genome-wide association study of 14,000 cases of seven common diseases and 3,000 shared controls. *Nature*. 2007;447(7145):661–678.
35. Chen CZC, Peng YX, Wang ZB, Fish P V., Kaar JL, Koepsel RR, Russell AJ, Lareu RR, Raghunath M. The Scar-in-a-Jar: Studying potential antifibrotic compounds from the epigenetic to extracellular level in a single well. *British Journal of Pharmacology*. 2009;158(5):1196–1209.
36. Puerta Cavanzo N, Bigaeva E, Boersema M, Olinga P, Bank RA. Macromolecular Crowding as a Tool to Screen Anti-fibrotic Drugs: The Scar-in-a-Jar System Revisited. *Frontiers in Medicine*. 2021;7:1092.
37. Lewis-Israeli YR, Wasserman AH, Gabalski MA, Volmert BD, Ming Y, Ball KA, Yang W, Zou J, Ni G, Pajares N, Chatzistavrou X, Li W, Zhou C, Aguirre A. Self-assembling human heart organoids for the modeling of cardiac development and congenital heart disease. *Nature Communications*. 2021;12(1):1–16.
38. Richards DJ, Li Y, Kerr CM, Yao J, Beeson GC, Coyle RC, Chen X, Jia J, Damon B, Wilson R, Starr Hazard E, Hardiman G, Menick DR, Beeson CC, Yao H, et al. Human cardiac organoids for the modelling of myocardial infarction and drug cardiotoxicity. *Nature Biomedical Engineering* 2020 4:4. 2020;4(4):446–462.
39. Ronaldson-Bouchard K, Ma SP, Yeager K, Chen T, Song LJ, Sirabella D, Morikawa K, Teles D, Yazawa M, Vunjak-Novakovic G. Advanced maturation of human cardiac tissue grown from pluripotent stem cells. *Nature*. 2018;556(7700):239–243.

**Chapter 4: Human Cardiac Fibroblast Stress Pathways and Matrix
Production are Governed by lncRNA SNPs**

4.1 Abstract

Matrix remodeling outcomes largely dictate how long patients survive after myocardial infarction, though little is understood about how human cardiac fibroblasts deposit scar tissue in response to environmental stressors. Moreover, human-restricted noncoding regulatory elements have been shown to worsen fibrosis on a clinical scale, but their mechanism of action remains elusive. Here we demonstrate that several ligands generated after infarction converge on AP-1 and NF- κ B pathways, and that long noncoding RNA (lncRNA) single nucleotide polymorphisms (SNPs) can redirect resultant stress programs. We find GATA5 to be epigenetically silenced in the presence of SNPs and stress.

4.2 Non-standard Abbreviations and Acronyms

MI – Myocardial infarction

CF- Cardiac fibroblast

ECM – Extracellular matrix

BMDM – Bone marrow-derived macrophage

NF- κ B – Nuclear Factor Kappa B

AP-1 – Activator Protein 1

DAMPs – Damage-associated molecular patterns

LMW HA – Low-molecular weight hyaluronic acid

TGF- β – Transforming growth factor beta

TLR – Toll-like receptor

ATAC-seq – Assay for transposase-accessible chromatin with sequencing

MMPs – Matrix Metalloproteases

P1/P8 – Postnatal day 1 or 8

4.3 Introduction

Heart disease is the leading cause of death worldwide, causing 18.6 million fatalities annually¹. After acute myocardial infarction (MI), a scar is formed to maintain tissue integrity and prevent cardiac rupture, however, the rigid scar impairs both mechanical and electrical coupling of the tissue, leading to worsened heart function. While fibrosis occurs in many organ systems in various states of disease², mechanisms are not always conserved, and thus need to be investigated in a context-dependent manner. Additionally, tissue-level organization can impact fibrotic models- as an extreme example, the heart lacks a commensal mucosal barrier that drives inflammation in idiopathic pulmonary fibrosis and Crohn's disease^{3,4}. Similarly, niche composition and organization differ between the heart and liver, with cells from the same developmental origin (yolk sac macrophages) driving seemingly opposite fibrotic responses^{5,6}. Therefore, tissue-restricted environmental cues can drastically alter matrix processes.

Moreover, while many molecular and genetic tools exist to study disease in mice, they lack many of the regulatory regions of the genome that exist in higher primates, and thus do not always yield the same phenotype^{4,7,8}. This is evident by the difficulty of inducing coronary artery disease in mice⁹, and why some groups

turn to other animal models. The wealth of experiments performed in mice, however, provide an excellent starting point for computational predictions, assuming they are ultimately confirmed in more accurate models. Taken together, this suggests that a human cardiac-specific model is most likely to serve as a litmus test for murine observations.

Many studies from the last few decades have identified single receptors, ligands, or biophysical stimuli that modulate fibrosis after MI. We previously sought to organize these signaling “nodes” into a network by combining several RNA-seq datasets, cell-type knockout models, and biochemical studies from existing literature, and found that many agonists have been reported to activate AP-1 and NF- κ B stress pathways. Furthermore, in regenerative models, these processes are either inhibited or are only weakly induced by models of infarction. We hypothesize that convergent signaling through these pathways ultimately determines matrix outcomes, as this would explain why single molecule/ligand/receptor inhibition only partially rescues heart fibrosis *in-vivo*.

Leaning on our recent iPSC-derived cardiac fibroblast protocol, we are also able to investigate how these stress responses and pathways may be altered in the presence of disease-causing lncRNA SNPs. Our previous work has demonstrated that lncRNA SNPs at the 9p21 locus act through JNK, a kinase upstream of AP-1, to cause gap junction decoupling in cardiomyocytes¹⁰. Recent evidence demonstrates that AP-1 family proteins cooperatively interact with these lncRNAs to promote expression in smooth muscle cells^{11,12}. We hypothesize that

this mechanism may be conserved across cardiac cellular populations, and manifest matrix differences in cardiac fibroblasts. At a population level, an estimated 25% of humans are homozygous for these SNPs that clinically present with increased arrhythmias, sudden cardiac death, and poor post-MI remodeling – maladies governed by fibroblasts.

For these reasons, we generated human cardiac-specific epicardial fibroblasts¹³ from H9 and patient-derived pluripotent stem cells to test our murine-derived computational model of sterile inflammation resulting in fibrosis¹⁴, and used haplotype-dependent differences to investigate abnormal stress responses in the context of 9p21 SNPs.

4.4 Methods

4.4.1.1 Ethical compliance and Cell lines

The authors have complied with all ethical regulations approved by UCSD (IRB #141315) for all patient-derived iPSCs, which were derived originally by the Scripps Research Institute (IRB #11-5676). Characterization of these lines has been previously reported elsewhere².

4.4.1.2 Differentiation and Cell Culture Methods

Patient-derived iPSCs and H9 ESCs were cultured using mTeSR1 and passaged using Versene (15040066, Thermo Fisher), 5 μ M rock inhibitor Y27632 (Y-5301, LC Labs) and cell scrapers prior to differentiation. Differentiations into

cardiac fibroblasts were carried out as previously described¹. Briefly, iPSCs were seeded at 250k-500k per well of 12-well tissue culture Matrigel-treated plates and converted into CPCs using 5-6 μ M CHIR (**S**ML1046, Sigma Aldrich) and 0.25 μ M IWP2 (S7085, Sellechem). Cultures were then converted into epicardial cells using 3 μ M CHIR, and into cardiac fibroblasts over 20 days with 10ng/mL bFGF (233-FB, RnD Systems). CFs were expanded and maintained in Fibroblast Growth Medium 3 (C-23025, Promocell) and passaged using Accutase for 5-10 minutes. All cells used for experiments were passage 5 or less. Any assays requiring matrix deposition were carried out in RPMI1640 + 10% FBS and 100mg/L ascorbic acid (36237, Alfa Aesar). Assays measuring protein phosphorylation were serum starved overnight using Fibroblast Growth Medium 3 basal media prior to agonist dosing. AP-1 was inhibited using 80 μ M T-5224 (22904, Cayman Chemical), added concurrently with agonists. Angiotensin II (10 nM, 1158, Tocris), low molecular weight hyaluronic acid (8-15 kDa, 30ng/mL, 40583-10MG, Millipore Sigma), TGF- β (10 ng/mL, 240-B-002, RnD Systems) were used as agonists, dosed daily for 3 days and harvested 72 hours after the first dose.

4.4.1.3 RNA-seq Mining

Sequencing files were obtained from the GEO database under accessions GSE49906¹² and GSE153481¹³. Bulk FASTQ files were aligned to the mm10 genome using STAR with the following settings: `--readFilesCommand zcat --genomeLoad LoadAndRemove --outFilterType BySJout --outFilterMultimapNmax`

10 --alignSJoverhangMin 8 --alignSJDBoverhangMin 1 --outFilterMismatchNmax 4 --alignIntronMin 20 --alignIntronMax 1000000 --alignMatesGapMax 100000¹⁴. BAM files were sorted and indexed using samtools¹⁵. Raw and transcripts per kilobase million (TPM) normalized tag directories were generated using HOMER command `makeTagDirectory` and `analyzeRepeats` scripts¹⁶. Statistical significance for Giudice et al. raw counts was determined using EdgeR¹⁷ in the `getDiffExpression` HOMER script. Counts were read in using DGEList while library sizes and normalization factors were calculated from Tag Directory sizes. Reads were counted using DGEList, with each sample constituting a treatment in the design matrix. Common dispersion was estimated at 0.05 as recommended. P-values were generated using an Exact Test and corrected using the Benjamini-Hochberg method. Only genes with an adjusted p-value of 0.05, minimum fold change of +/- 2 and minimum 32 tags in one dataset per gene were considered. Biological process and molecular function gene ontologies were generated using Metascape¹⁸. Heatmaps and PCA plots of TPM-normalized values were generated using R and ggplot and pheatmap packages¹⁹. Single cell ATAC was processed using Signac²⁰ (version 1.4.0), Seurat²¹ (Version 4.0.5), and ChromVar²² (Version 1.16.0) according to primary author's methods¹³. ECM gene signature was compiled using the `AddModuleScore` function of Seurat using `Fn1`, `Col1a1`, and `Col1a2` genes and significance was calculated using ggpubr's `stat_compare_means` function with a Kruskal-Wallis test for overall p-value generation and Wilcox signed-rank test to compare individual groups. Single-cell

accessibility of motif MA1144-1 is shown, but similar results were obtained using other AP-1 motifs such as MA0476-1.

4.4.1.4 Western Blotting

Cells were lysed using mRIPA buffer, further agitated and amassed using cell scrapers, and vortexed every 5 minutes for 30 minutes total. Samples were then centrifuged at 23,000 g for 15 minutes and the supernatant was transferred to a new tube to remove DNA. Protein concentrations were calculated using a bicinchoninic acid assay (23225, Thermo Fisher), and after denaturing at 95 ° Celsius for 5 minutes, 10 µg of protein in 30 µL of RIPA buffer was loaded per lane on a 4-12% Bis-Tris Plus Gel (for phospho-proteins, NW04122BOX, Thermo Fisher) or 25 µL in 3-8% Tris-Acetate Gel (for Fibronectin and Collagen 1, EA0375BOX, Thermo Fisher) in reducing conditions. Gels were run at 80V for 15 minutes, then 140V for 1 hour, and transferred using an iBlot nitrocellulose transfer membrane (IB301001, Thermo Fisher). Membranes were blocked using Azure Blot blocking buffer (AC2190, Azure Biosystems) for 1 hour, incubated with primary antibodies (Collagen 1, 14695-1-AP, Proteintech, 1:1000; Fibronectin-EDA, NBP1-51723, Novus Bio, 1:2500; Beta Actin, ab-8226, Abcam, 1:5000; Phospho-cJun, 9261S, Stem Cell Technologies, 1:1000; Phospho-p65, 3033S, Stem Cell Technologies, 1:1000) overnight at 4° Celsius, secondary antibodies (A11374 and A10038, Invitrogen, 1:5000) for 1 hour at room temperature, and imaged using a LI-COR Odyssey (LI-COR, Lincoln, NE). Raw intensities were calculated using LI-

COR ImageStudio Lite and significance was determined using a one-way ANOVA with a Kruskal-Wallis test.

4.4.1.5 Immunofluorescent Staining

Cells were fixed using 3.7% methanol-stabilized formaldehyde for 15 minutes and rinsed thrice with PBS. Samples were blocked in 10% donkey serum, 0.3M glycine, and 1% bovine serum albumin for 1 hour, permeabilized in blocking buffer with 0.1% Triton X-100 for 15 minutes, stained with primary antibodies (Gata5, AF2170, RnD Systems; Cx43, 71-0700, Invitrogen, both 1:100) for 2 hours or overnight at 4 degrees Celsius, and then incubated with secondary antibodies (A21202, A10042, and A21447, Invitrogen) for another two hours. Nuclei were stained with DAPI for 15 minutes at 1:10,000 dilution in DI water, and three washes were performed between each incubation for 5 minutes each. Samples were imaged using a Keyence Bz-X microscope (Osaka, JP), keeping the exposure for each channel constant between sample groups. Image intensity for each color was calculated using FIJI²³ and normalized to the number of nuclei in each image. Significance was calculated using a Dunnet's test after a one-way ANOVA. Overlays were created overexposing DAPI channels, making binary, finding edges, inverting, and then overlaying on protein channels with 30% opacity using FIJI.

4.4.1.6 ATAC-Seq

ATAC-sequencing was performed on patient-derived iPSC clones from 6 clones in triplicate. Library preparation and sequencing was performed by the UCSD Center for Epigenomics. ATAC-seq was performed on 50,000 nuclei per sample. Samples were permeabilized in cold permeabilization buffer (0.2% IGEPAL-CA630 (I8896, Sigma), 1 mM DTT (D9779, Sigma), Protease inhibitor (05056489001, Roche), and 5% BSA (A7906, Sigma) in PBS (10010-23, Thermo Fisher Scientific)) for 10 minutes on a rotator at 4°C followed by centrifugation for 5 min at 500g at 4°C. The pellet was resuspended in cold tagmentation buffer (33 mM Tris-acetate (pH = 7.8) (BP-152, Thermo Fisher Scientific), 66 mM K-acetate (P5708, Sigma), 11 mM Mg-acetate (M2545, Sigma), 16% DMF (DX1730, EMD Millipore) in molecular biology grade water (46000-CM, Corning) followed by incubation with Tagmentation enzyme (FC-121-1030; Illumina) at 37°C with shaking at 500 rpm for 30 min. Tagmented DNA was purified using MinElute PCR purification kit (28004, QIAGEN). The resulting libraries were amplified using NEBNext High-Fidelity 2X PCR Master Mix (M0541, NEB) with primer extension at 72°C for 5 minutes, denaturation at 98°C for 30 s, followed by 8 cycles of denaturation at 98°C for 10s, annealing at 63°C for 30s and extension at 72°C for 60s. After purification of amplified libraries using MinElute PCR purification kit (28004, QIAGEN), double sided size selection was performed using SPRIselect beads (B23317, Beckman Coulter) with 0.55X beads and 1.5X to sample volume. Libraries were sequenced on a NextSeq500 (Illumina).

Adaptor-trimmed fastq files were aligned to hg38 by Bowtie2²⁵ using parameters “-X2000 -local” and converted into bams and sorted using samtools¹⁵. Files were then filtered to remove improper mapped, unmapped, not primary, failing platform, and poorly mapping reads using samtools¹⁵ with the following parameters: “view -F 1804 -f 2 -q 30” and then sorted with sambamba²⁶. Mate coordinates were then filled using samtools fixmate, and then samtools filtering and sambamba sorting was repeated. Next, Picard²⁷ was used to mark and remove duplicates. Bigwig files were produced from resultant bam files using deepTools²⁸ bamCoverage with the following settings: “—binSize 10 - normalizeUsing RPGC -effectiveGenomeSize 2150570000 - ignoreForNormalization chrX -extendReads.” Bams were also sorted by name using “samtools sort -n” and then converted into bedpe using bamtools²⁹. Mitochondrial reads were then removed using grep and a Tn5 shift was reads were shifted to remove Tn5 adaptors. Peaks were then called using MACS2³⁰ using the following parameters: -q 0.01 -nomodel -nolambda -shift 100 -extsize 200 -B - keep-dup all -call-summits.

Peaks and bam files were then read into Diffbind³¹. Low read-count regions were then filtered using a cutoff sum of 15 in dba.count, normalized by sequencing depth, and then a contrast was defined by haplotype. Differential accessibility was calculated using the dba.analyze wrapper for DESEQ2³², and peaks were annotated using HOMER’s annotatepeaks.pl script. Peaks were then filtered with

a cutoff of FDR <0.01, log2 fold change of +/-2, and average concentration of >2. The top 3000 peaks that were unique to each haplotype were then fed into HOMER's findMotifsGenome.pl script using a size of 200. Following the identification of haplotype-dependent AP-1 and GATA motifs, similar motifs were merged for each transcription factor family (AP-1: Fra1, Fos, Atf3, JunB, BATF, Fra2, AP-1[from GSE21512], and GATA: Gata1-6) and DARS were annotated for each group using annotatepeaks.pl. GATA motifs were identified as being enriched in RKO AP-1 containing DARS (vs RR DARS) using a Chi-squared test ($p < 0.001$). Additional transcription factors (i.e. TEAD family proteins) were present in line pairwise comparison, but not significant when tested for haplotype-dependent enrichment using Chi-squared test. Regions containing predicted motifs for both AP-1 and GATA are provided in Supplemental Table 1.

4.5 Results

Using the pre-plated cardiac fibroblasts from day 1, 28, and 60 postnatal mice sequenced by Giudice et al.¹², we are able to see a drastic increase in inflammatory phenotype in the first four weeks of age (Fig. 4.1 A-D); This correlates with the loss of regenerative ability after the first week of life reported by Wang et al.³³, and raises the possibility of age-dependent inflammatory priming driving altered healing responses *in-vivo*. Transcriptional changes that occur between days 1 and 28 are largely stable through day 60 (Fig. 4.1A), activate many inflammatory genes (Fig. 4.1B,D) and drive most of the variance between samples

(Fig. 4.1C). Since the inflammatory pathways that are driving these changes were unclear in the bulk RNA-seq, we then employed a single-cell cardiac ATAC sequencing dataset produced by Wang et al.¹³ to discern fibroblast subpopulation changes with age and infarction. Initial clustering of fibroblasts demonstrated that infarcted non-regenerative mice (P8 d3 post-MI) largely contribute to a unique population (Fig. 4.1E, cluster 4) that is enriched in collagen 1 and fibronectin peaks (Fig. 4.1F), suggesting that these cells are responsible for matrix responses post-MI and unlikely to be nearby healthy cells (P8 d3 post-Sham clusters 2, 0, and 6). Moreover, cluster 4 was highly enriched in AP-1 family motifs (Fig. 4.1G,H) relative to the other clusters, suggesting that AP-1 differences are driving the transcriptional programs. AP-1 motifs such as MA144-1 and MA0476-1 are also uniquely enriched in nonregenerative infarcted hearts (Fig. 4.1I).

To investigate the causality of AP-1 in driving matrix responses, we employed H9 ESC-derived cardiac fibroblasts and challenged them with agonists predicted to generate large matrix responses in adult hearts³. TGF- β , angiotensin II, and low-molecular weight hyaluronic acid were found to induce an upregulation of the cellular isoform of fibronectin (as measured by antibodies specific to the EDA domain), but not collagen after 3 days of treatment (Fig. 4.2A). Since 2D matrices do not support BMP-1 cleavage of pro-collagen 1 and thus prevent collagen fibril assembly in shorter timeframes (<2 weeks)^{34–36}, and artificially inducing BMP stabilization through crowding agents yields varied matrix responses^{37,38}, we instead decided to assay fibronectin. Fibronectin is generally expressed in

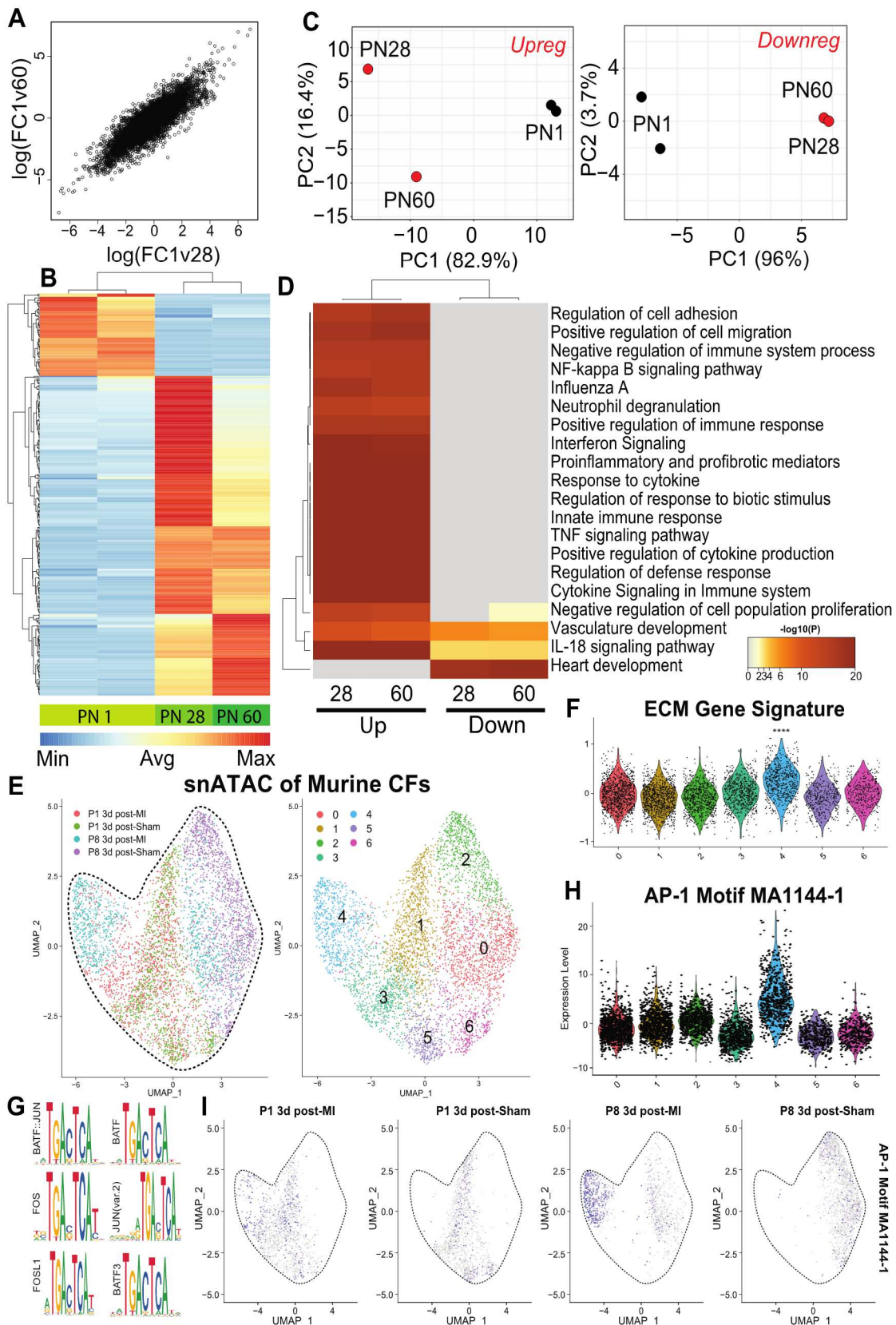
response to the same agonists and in the same timeframes as type 1 and 3 fibrillar collagens³, and the protein can be used in downstream functional assays (whereas secreted collagen would be limited to conditioned media ELISAs).

Next, we measured phosphorylation of the stress pathways we previously predicted to drive matrix formation: AP-1 (via cJun) and NF- κ B (via p65). We found that all three agonists drove a peak in phosphorylation of cJun and p65 after 30 and 60 minutes, respectively by western blot (Fig. 4.2B). The experiment was repeated, and cells were fixed 30 and 60 minutes after dosing and stained for their respective phospho-proteins, again demonstrating an upregulation in these pathways by each agonist (Fig. 4.2C). To validate that AP-1 drives the observed matrix responses, we used T-5224 to pharmacologically inhibit binding of AP-1 complexes to cognate DNA binding sites. We found that blocking AP-1 variably impacted matrix responses; hyaluronic acid's upregulation was entirely rescued, angiotensin II's was partially downregulated, and inhibition had no impact on TGF- β treated cells (Fig. 4.2D).

Since AP-1 at least partially coordinates fibroblast responses to catastrophic physiological events like myocardial infarction, we wanted to

Figure 4.1: Inflammatory signatures drive differences in regenerative (non-scarring) and adult (scarring) hearts.

(A) Scatter plot showing strong correlation between genes up/down-regulated after 28 days and 60 days. **(B)** Heatmap of top 500 differentially expressed genes. **(C)** Principal component analysis (PCA) of differentially expressed genes. Age drives the majority of variance in the dataset. **(D)** Metascape gene ontologies of differentially expressed genes. **(E)** Clustering of cardiac fibroblasts colored by sample (left) and non-biased cluster (right). **(F)** Score of collagen and fibronectin accessibility using the `add_score_module` function of Signac. **(G)** Top motif results from ChromVar when contrasting cluster 4 with 1. Similar results were obtained when comparing against each other cluster. **(H)** Violin plot of AP-1 motif enrichment in accessible regions for each cluster. **(I)** Feature plot of the AP-1 motif, split by sample origin.

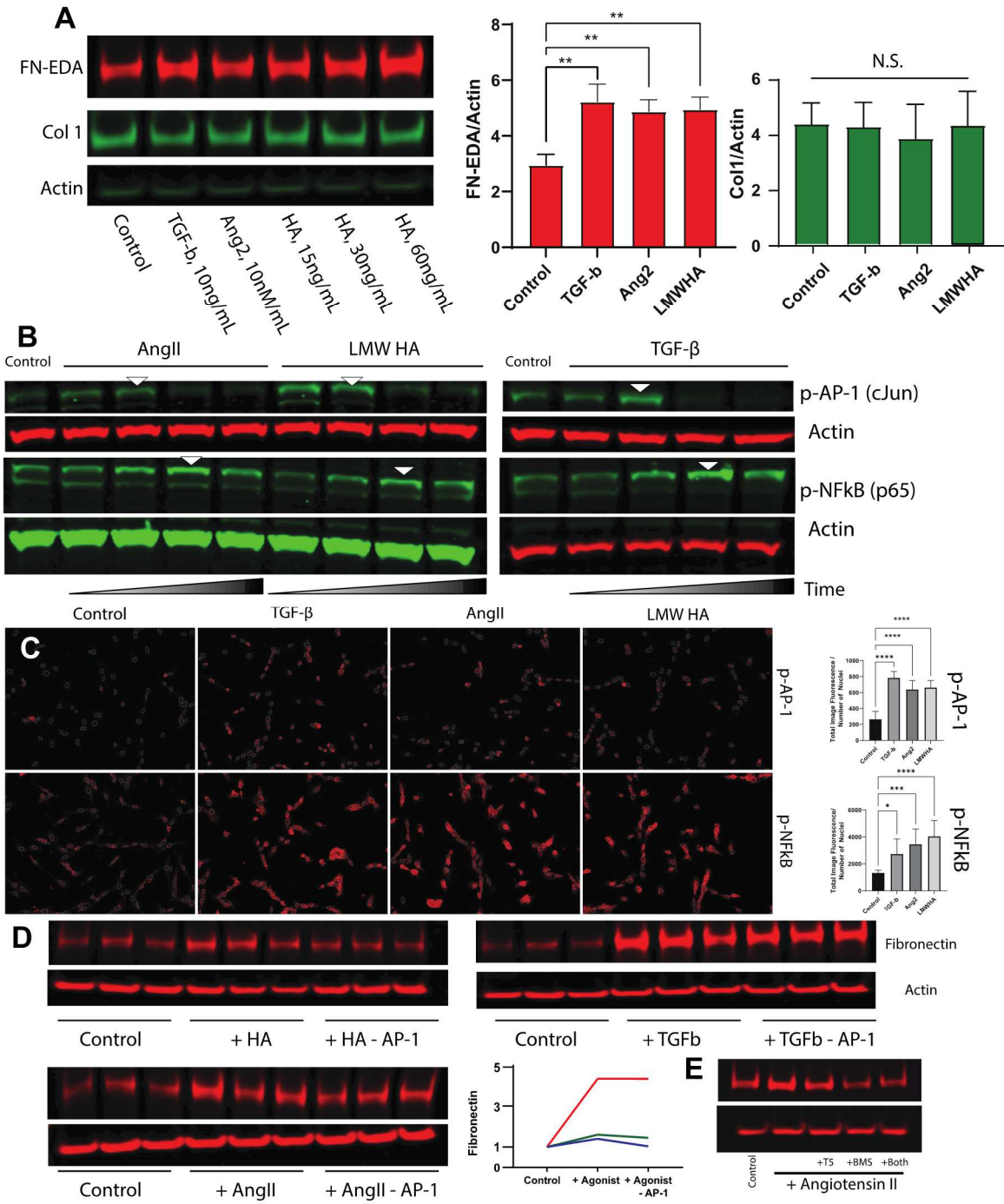


investigate how AP-1 may interact with regions of the genome associated with cardiovascular disease, specifically at the 9p21 locus. This non-coding region of the genome contains 61 SNPs in high linkage disequilibrium and a Mendelian distribution across the global population; is it also correlated with high clinical incidence of recurrent MI, arrhythmias, and sudden cardiac death, pathologies associated with matrix remodeling^{2,10,39-41}.

Our group has previously demonstrated that presence of these SNPs alters cardiomyocyte responses to stiffness, resulting in differences in gap junction assembly and suggesting that the non-coding RNA (ANRIL) may be stress induced. HOMER motif finding predicted two AP-1 binding sites at the promoter region of ANRIL, a region in which ENCODE UCSC genome browser tracks highlight as a probable super enhancer (Fig. 4.3A). In an effort to understand how AP-1 works in conjunction with ANRIL SNPs to dictate stress responses, we performed ATAC-sequencing on 6 lines of iCFs in triplicate, spanning two patients. For each risk line, a TALEN knockout of the SNP-containing region was performed, generating three isogenic clonal comparisons (Fig. 4.3B). After excluding lowly accessible regions (concentration < 3 in Diffbind), 3,569 sites were found to be differentially accessible (log₂ fold change +/- 2, FDR < 0.01) between risk and knockout lines (Fig. 4.3C). HOMER motif finding identified enrichment in AP-1 binding motifs in both risk and knockout lines, but only knockout lines contained GATA motifs (Fig. 4.3D).

Figure 4.2: Computationally predicted post-MI agonists upregulate matrix and phosphorylate AP-1 and NF- κ B and AP-1 inhibition only partially rescues matrix production.

(A) Western blot of cellular fibronectin and collagen with actin as loading control. Expression differences were defined by one-way ANOVA with Kruskal-Wallis test, $p < 0.05$, $n = 3$. **(B)** Western blots of phosphorylated proteins following agonist dosing. From left to right, times are 0, 15, 30, 60, and 120 minutes, $n = 1$. **(C)** Immunofluorescent staining of phospho-cJun (30 minutes post-dosing), and phospho-p65 (60 minutes post-dosing). Statistical significance was determined by one-way ANOVA with Dunnett test comparison to control, $p < 0.05$, $n = 3$. **(D)** Western blots of fibronectin expression with actin as a loading control. Points on the graph were generated based on the sum of fibronectin intensities from each group. **(E)** Western blots of Fibronectin and actin in the presence of T-5224 (AP-1 inhibitor) and BMS-345541 (NF- κ B inhibitor) after 3 days of culture.



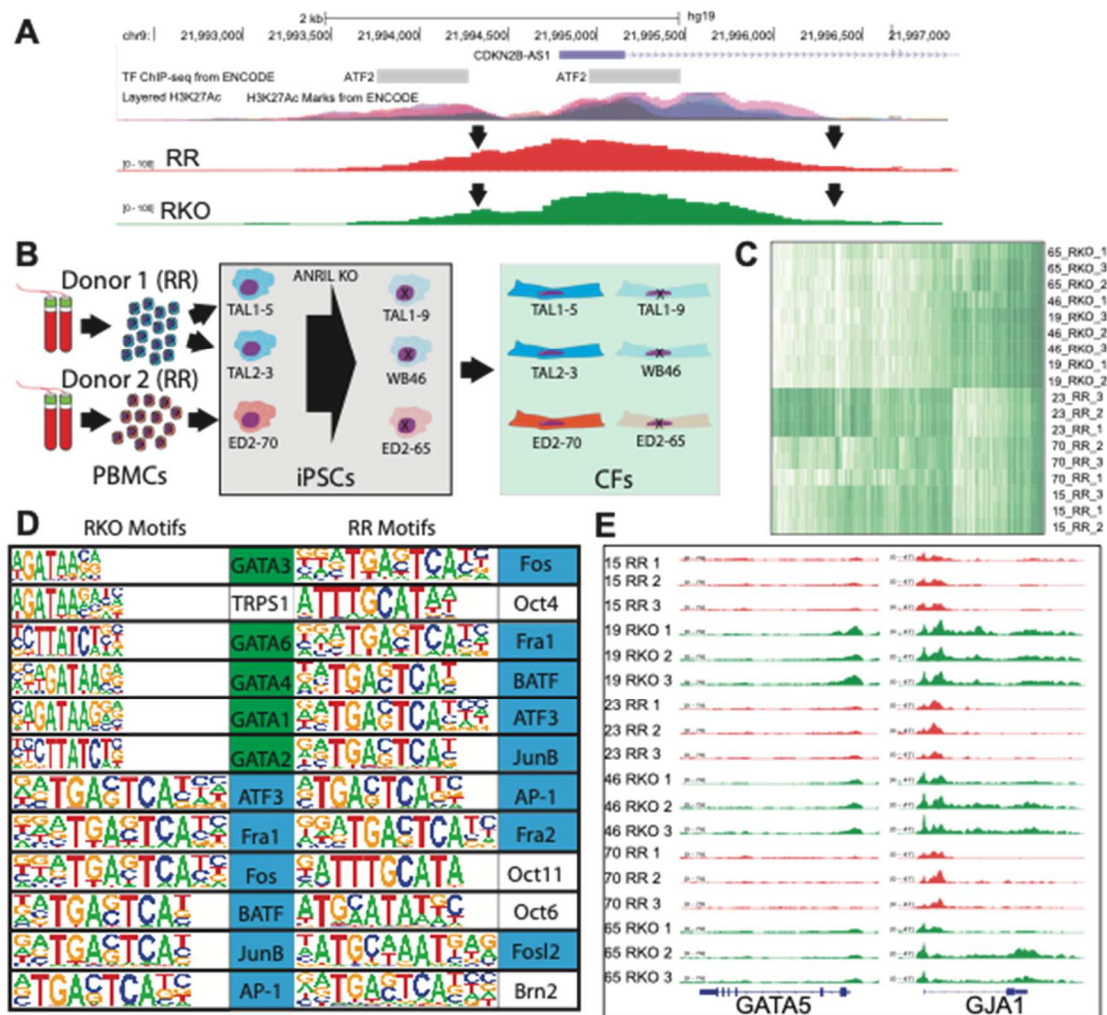


Figure 4.3. ANRIL SNPs alters AP-1 accessibility and silence GATA5 and Connexin 43.

(A) UCSC Genome track with ENCODE tracks labelling H3K27Ac (top) and representative IGV track demonstrating open chromatin at promoter region. (B) Schematic of lines used. (C) Heatmap of differentially accessible regions between haplotypes. (D) Top 12 motifs, in order, for regions unique to risk and risk knockout haplotypes, respectively. AP-1 family motifs are colored blue and GATA family motifs are colored green. (E) IGV screenshots of all 18 lines, colored by haplotype (red: risk, green: knockout).

The promoter region of GATA5 was found to be inaccessible in risk lines, suggesting that ANRIL SNPs silence GATA5 epigenetically. The ANRIL promoter region was found to be equally accessible between genotypes, further suggesting

that the presence of the SNPs, and not ANRIL transcription differences, are driving CF differences. After annotating the differentially accessible regions based on AP-1 and GATA motif presence, the regions were intersected, generating a list of regions are thought to contain both GATA and AP-1 motifs (Supplementary Table 4.1). Interestingly, connexin 43 (gene GJA1) is thought to bind both transcription factors and has significant differences in chromatin accessibility (Fig. 4.3E).

4.6 Discussion

In our previous work, we mined several RNA-seq datasets to identify ligands and pathways that lead to a fibrotic phenotype after MI and found a wealth of evidence suggesting AP-1 and NF- κ B's involvement¹⁴. In the time following publication, we continued to use improved computational tools and additional datasets to refine these hypotheses. When reanalyzing the Giudice¹⁵ dataset with the enhanced version of Metascape, NF- κ B signaling was highlighted as being upregulated in adult CFs along with TNF signaling, which is an acute activator of NF- κ B (Fig. 4.1D). Therefore, some process during the first few weeks of life, perhaps the establishment of pulmonary circulation, initiates the activation of NF- κ B at steady state.

To investigate how CFs change after infarction (in addition to aging), we mined the single-cell companion dataset¹⁶ to the previously used bulk neonatal MI data. The uniquely accessible chromatin regions of adult CFs three days after infarction were epigenetically distinct and demonstrated marked AP-1 activation

(Fig. 4.1H). These cells also contained the most unique regions associated with extracellular matrix genes (Fig. 4.1F), building the case for AP-1 regulation of matrix processes. While both pathways predicted by our initial model seemed to gain additional evidence, we still lacked an understanding of their interplay and relative contributions to matrix turnover, despite advancements in analytics and additional datasets.

Using our iCFs, we found that several common post-MI ligands could activate both AP-1 (after 30 minutes) and NF- κ B (after 60 minutes). AP-1 inhibition had little effect on inhibiting angiotensin II induced fibronectin upregulation, while NF- κ B inhibition drastically reduced fibronectin production. Similar levels of inhibition were observed when both pathways were inhibited. Other groups have reported that genetic deletions of Ikk1 and Ikk2 (kinases that are required for p65 activation) in murine fibroblasts⁴⁴, inhibited elk-1 production, which in turn is necessary for AP-1 family transcription. In T cells, NF- κ B is required to open the chromatin at the promoters of Fos and Jun⁴⁵ and initiate activation. It is possible, therefore, that AP-1 is dependent on NF- κ B activity, but AP-1 alone is not responsible for fibronectin production. The activation of fibroblast NF- κ B in the first week of life could enable AP-1 activation for the first time, and thus lead to the motif-finding results we observe.

We also detected AP-1 accessibility differences in 9p21 isogenic iCFs, this time suggesting that lncRNA SNPs alter the ability of GATA family factors to cooperate with AP-1 during stress responses. The regions predicted to occupy

both AP-1 and GATA binding sites were primarily attributed to cadherin and connexin genes, suggesting that while NF- κ B drives matrix responses, AP-1 is involved in intercellular connection and communication. In the context of cardiac wound healing, both pathways and their corresponding processes are critical to patching the wound and ensuring that migrating and proliferating cells functionally integrate with the surrounding tissue.

4.7 Conclusions

We demonstrated that iCFs can be used to model post-MI inflammation, and that AP-1 and NF- κ B can mediate matrix-responses to stress. While the authors do not suggest inhibiting either pathway directly in a clinically context (due to the transcription factors' necessary functions at steady state), AP-1 and p65 phosphorylation (or lack thereof) could be used as a surrogate measure of pharmacological success. We also demonstrate that SNPs in ANRIL produce a silencing effect on GATA5, a critical transcription factor for cardiac development^{46–48}, and now, also after morphogenesis.

4.8 Acknowledgements

Chapter 4, in full, is currently being prepared as a manuscript for submission and publication of the material. Whitehead, Alexander J.; Hocker, James D.; Ren, Bing; Engler, Adam J. I would again like to thank Jake and Bing for their

sequencing contributions. The dissertation author is the primary investigator and author of this material.

The authors would like to thank Dr. Tatiana Kisseleva for helpful discussions.

4.9 Sources of Funding

Research reported in this publication was supported by NIH Grant R01AG045428 (to A.J.E.), the National Science Foundation Graduate Research Fellowship Program (to A.J.W.), and the ARCS Foundation (to A.J.W.).

4.10 Disclosures

None.

4.11 References

1. Heart Association A. 2021 Heart Disease and Stroke Statistics Update Fact Sheet At-a-Glance.
2. Wynn TA. Fibrotic disease and the TH1/TH2 paradigm. *Nature Reviews Immunology*. 2004;4(8):583–594.
3. Glass DS, Grossfeld D, Renna HA, Agarwala P, Spiegler P, Kasselmann LJ, Glass AD, DeLeon J, Reiss AB. Idiopathic pulmonary fibrosis: Molecular mechanisms and potential treatment approaches. *Respiratory Investigation*. 2020;58(5):320–335.
4. Stange EF, Schroeder BO. Microbiota and mucosal defense in IBD: an update. *Expert Review of Gastroenterology and Hepatology*. 2019;13(10):963–976.
5. Bennett H, Troutman TD, Sakai M, Glass CK. Epigenetic Regulation of Kupffer Cell Function in Health and Disease. *Frontiers in Immunology*. 2021;11:3600.

6. Dick SA, Macklin JA, Nejat S, Momen A, Clemente-Casares X, Althagafi MG, Chen J, Kantores C, Hosseinzadeh S, Aronoff L, Wong A, Zaman R, Barbu I, Besla R, Lavine KJ, et al. Self-renewing resident cardiac macrophages limit adverse remodeling following myocardial infarction. *Nature Immunology*. 2019;20(1):29–39.
7. Visel A, Zhu Y, May D, Afzal V, Gong E, Attanasio C, Blow MJ, Cohen JC, Rubin EM, Pennacchio LA. Targeted deletion of the 9p21 non-coding coronary artery disease risk interval in mice. *Nature*. 2010;464(7287):409–412.
8. Jarinova O, Stewart AFR, Roberts R, Wells G, Lau P, Naing T, Buerki C, McLean BW, Cook RC, Parker JS, McPherson R. Functional analysis of the chromosome 9p21.3 coronary artery disease risk locus. *Arteriosclerosis, Thrombosis, and Vascular Biology*. 2009;29(10):1671–1677.
9. Liu G, Liao J, Huang W. Animal models of coronary heart disease. *The Journal of Biomedical Research*. 2017;31(1):3–10.
10. Kumar A, Thomas SK, Wong KC, Io Sardo V, Cheah DS, Hou Y-HH, Placone JK, Tenerelli KP, Ferguson WC, Torkamani A, Topol EJ, Baldwin KK, Engler AJ. Mechanical activation of noncoding-RNA-mediated regulation of disease-associated phenotypes in human cardiomyocytes. *Nature Biomedical Engineering*. 2019;3(2):137–146.
11. Io Sardo V, Chubukov P, Ferguson W, Kumar A, Teng EL, Duran M, Zhang L, Cost G, Engler AJ, Urnov F, Topol EJ, Torkamani A, Baldwin KK. Unveiling the Role of the Most Impactful Cardiovascular Risk Locus through Haplotype Editing. *Cell*. 2018;175(7):1796-1810.e20.
12. Zhao Q, Wirka R, Nguyen T, Nagao M, Cheng P, Miller CL, Kim JB, Pjanic M, Quertermous T. TCF21 and AP-1 interact through epigenetic modifications to regulate coronary artery disease gene expression. *Genome Medicine*. 2019;11(1):23.
13. Whitehead AJ, Hocker JD, Ren B, Engler AJ. Improved epicardial cardiac fibroblast generation from iPSCs. *Journal of molecular and cellular cardiology*. 2021;164:58–68.
14. Whitehead AJ, Engler AJ. Regenerative cross talk between cardiac cells and macrophages. *American Journal of Physiology - Heart and Circulatory Physiology*. 2021;320(6):H2211–H2221.
15. Giudice J, Xia Z, Wang ET, Scavuzzo MA, Ward AJ, Kalsotra A, Wang W, Wehrens XHT, Burge CB, Li W, Cooper TA. Alternative splicing regulates vesicular

trafficking genes in cardiomyocytes during postnatal heart development. *Nature Communications*. 2014;5.

16. Wang Z, Cui M, Shah AM, Tan W, Liu N, Bassel-Duby R, Olson EN. Cell-Type-Specific Gene Regulatory Networks Underlying Murine Neonatal Heart Regeneration at Single-Cell Resolution. *Cell Reports*. 2020;33(10):108472.

17. Dobin A, Davis CA, Schlesinger F, Drenkow J, Zaleski C, Jha S, Batut P, Chaisson M, Gingeras TR. STAR: Ultrafast universal RNA-seq aligner. *Bioinformatics*. 2013;29(1):15–21.

18. Li H, Handsaker B, Wysoker A, Fennell T, Ruan J, Homer N, Marth G, Abecasis G, Durbin R. The Sequence Alignment/Map format and SAMtools. *Bioinformatics*. 2009;25(16):2078–2079.

19. Heinz S, Benner C, Spann N, Bertolino E, Lin YC, Laslo P, Cheng JX, Murre C, Singh H, Glass CK. Simple Combinations of Lineage-Determining Transcription Factors Prime cis-Regulatory Elements Required for Macrophage and B Cell Identities. *Molecular Cell*. 2010;38(4):576–589.

20. Robinson MD, McCarthy DJ, Smyth GK. edgeR: A Bioconductor package for differential expression analysis of digital gene expression data. *Bioinformatics*. 2009;26(1):139–140.

21. Zhou Y, Zhou B, Pache L, Chang M, Khodabakhshi AH, Tanaseichuk O, Benner C, Chanda SK. Metascape provides a biologist-oriented resource for the analysis of systems-level datasets. *Nature communications*. 2019;10(1).

22. Wickham H. ggplot2. *ggplot2*. 2009.

23. Stuart T, Srivastava A, Madad S, Lareau CA, Satija R. Single-cell chromatin state analysis with Signac.

24. Stuart T, Butler A, Hoffman P, Hafemeister C, Papalexi E, Mauck WM, Hao Y, Stoeckius M, Smibert P, Satija R. Comprehensive Integration of Single-Cell Data. *Cell*. 2019;177(7):1888-1902.e21.

25. Schep AN, Wu B, Buenrostro JD, Greenleaf WJ. chromVAR: inferring transcription-factor-associated accessibility from single-cell epigenomic data. *Nature Methods* 2017 14:10. 2017;14(10):975–978.

26. Schindelin J, Arganda-Carreras I, Frise E, Kaynig V, Longair M, Pietzsch T, Preibisch S, Rueden C, Saalfeld S, Schmid B, Tinevez JY, White DJ, Hartenstein V, Eliceiri K, Tomancak P, et al. Fiji: an open-source platform for biological-image analysis. *Nature Methods* 2012 9:7. 2012;9(7):676–682.

27. Langmead B, Salzberg SL. Fast gapped-read alignment with Bowtie 2. *Nature Methods*. 2012;9(4):357–359.
28. Tarasov A, Vilella AJ, Cuppen E, Nijman IJ, Prins P. Sambamba: fast processing of NGS alignment formats. *Bioinformatics*. 2015;31(12):2032–2034.
29. Broad Institute. Picard:A set of command line tools (in Java) for manipulating high-throughput sequencing (HTS) data and formats such as SAM/BAM/CRAM and VCF. [Http://Broadinstitute.Github.io/Picard/](http://Broadinstitute.Github.io/Picard/). 2016.
30. Ramírez F, Ryan DP, Grüning B, Bhardwaj V, Kilpert F, Richter AS, Heyne S, Dünder F, Manke T. deepTools2: a next generation web server for deep-sequencing data analysis. *Nucleic Acids Research*. 2016;44(W1):W160–W165.
31. Barnett DW, Garrison EK, Quinlan AR, Stürmborg MP, Marth GT. BamTools. *Bioinformatics*. 2011;27(12):1691–1692.
32. Zhang Y, Liu T, Meyer CA, Eeckhoute J, Johnson DS, Bernstein BE, Nussbaum C, Myers RM, Brown M, Li W, Shirley XS. Model-based analysis of ChIP-Seq (MACS). *Genome Biology*. 2008;9(9):1–9.
33. Ross-Innes CS, Stark R, Teschendorff AE, Holmes KA, Ali HR, Dunning MJ, Brown GD, Gojis O, Ellis IO, Green AR, Ali S, Chin SF, Palmieri C, Caldas C, Carroll JS. Differential oestrogen receptor binding is associated with clinical outcome in breast cancer. *Nature*. 2012;481(7381):389–393.
34. Love MI, Huber W, Anders S. Moderated estimation of fold change and dispersion for RNA-seq data with DESeq2. *Genome Biology*. 2014;15(12):550.
35. Wang Z, Cui M, Shah AM, Ye W, Tan W, Min YL, Botten GA, Shelton JM, Liu N, Bassel-Duby R, Olson EN. Mechanistic basis of neonatal heart regeneration revealed by transcriptome and histone modification profiling. *Proceedings of the National Academy of Sciences of the United States of America*. 2019;116(37):18455–18465.
36. Puerta Cavanzo N, Bigaeva E, Boersema M, Olinga P, Bank RA. Macromolecular Crowding as a Tool to Screen Anti-fibrotic Drugs: The Scar-in-a-Jar System Revisited. *Frontiers in Medicine*. 2021;7:1092.
37. Lareu RR, Subramhanya KH, Peng Y, Benny P, Chen C, Wang Z, Rajagopalan R, Raghunath M. Collagen matrix deposition is dramatically enhanced in vitro when crowded with charged macromolecules: The biological relevance of the excluded volume effect. *FEBS Letters*. 2007;581(14):2709–2714.

38. Chen D, Burdick JA. Versican/Collagen Interactions in Tissue Structure and Mechanics. *ProQuest Dissertations and Theses*. 2021.
39. Chen CZC, Peng YX, Wang ZB, Fish P v., Kaar JL, Koepsel RR, Russell AJ, Lareu RR, Raghunath M. The Scar-in-a-Jar: Studying potential antifibrotic compounds from the epigenetic to extracellular level in a single well. *British Journal of Pharmacology*. 2009;158(5):1196–1209.
40. Rønnow SR, Dabbagh RQ, Genovese F, Nanthakumar CB, Barrett VJ, Good RB, Brockbank S, Cruwys S, Jessen H, Sorensen GL, Karsdal MA, Leeming DJ, Sand JMB. Prolonged Scar-in-a-Jar: An in vitro screening tool for anti-fibrotic therapies using biomarkers of extracellular matrix synthesis. *Respiratory Research*. 2020;21(1):1–14.
41. Helgadóttir A, Thorleifsson G, Manolescu A, Gretarsdóttir S, Blondal T, Jonasdóttir A, Jonasdóttir A, Sigurdsson A, Baker A, Palsson A, Masson G, Gudbjartsson DF, Magnusson KP, Andersen K, Levey AI, et al. A common variant on chromosome 9p21 affects the risk of myocardial infarction. *Science*. 2007;316(5830):1491–1493.
42. Newton-Cheh C, Cook NR, Vandenburg M, Rimm EB, Ridker PM, Albert CM. Common variants at 9p21 are associated with sudden and arrhythmic cardiac death. *Circulation*. 2009;120(21):2062–2068.
43. Yamagishi K, Folsom AR, Rosamond WD, Boerwinkle E. A genetic variant on chromosome 9p21 and incident heart failure in the ARIC study. *European Heart Journal*. 2009;30(10):1222–1228.
44. Fujioka S, Niu J, Schmidt C, Sclabas GM, Peng B, Uwagawa T, Li Z, Evans DB, Abbruzzese JL, Chiao PJ. NF- κ B and AP-1 Connection: Mechanism of NF- κ B-Dependent Regulation of AP-1 Activity. *Molecular and Cellular Biology*. 2004;24(17):7806.
45. Lupino E, Ramondetti C, Piccinini M. I κ B Kinase β Is Required for Activation of NF- κ B and AP-1 in CD3/CD28-Stimulated Primary CD4⁺ T Cells. *The Journal of Immunology*. 2012;188(6):2545–2555.
46. Bonachea EM, Chang S-W, Zender G, LaHaye S, Fitzgerald-Butt S, McBride KL, Garg V. Rare GATA5 sequence variants identified in individuals with bicuspid aortic valve. 2014.
47. Reiter JF, Alexander J, Rodaway A, Yelon D, Patient R, Holder N, Stainier DYR. Gata5 is required for the development of the heart and endoderm in zebrafish. *Genes & Development*. 1999;13(22):2983.

48. Singh MK, Li Y, Li S, Cobb RM, Zhou D, Lu MM, Epstein JA, Morrissey EE, Gruber PJ. Gata4 and Gata5 Cooperatively Regulate Cardiac Myocyte Proliferation in Mice. *Journal of Biological Chemistry*. 2010;285(3):1765–1772.

4.12 Supplemental Table

Supplemental Table 4.1. Regions with predicted to have both AP-1 and GATA binding sites.

Chr	Start	End	Annotation	Distance to TSS	Nearest PromoterID	Nearest Refseq	Gene Name	Gene Type
chr2	4683501	4683899	Intergenic	-27478	NR_034134	NR_034134	LINC01249	ncRNA
chr11	24198486	24198884	Intergenic	-298368	NM_001009909	NM_001009909	LUZP2	protein-coding
chr7	102973165	102973563	promoter-TSS (NM_001085386)	-66	NM_001085386	NM_001085386	NFE4	protein-coding
chr6	121459679	121460077	Intergenic	24232	NM_000165	NM_000165	GJA1	protein-coding
chr8	23049879	23050277	intron (NM_147187, intron 1 of 9)	-18151	NR_038873	NR_038873	LOC286059	pseudo
chr6	2124324	2124722	intron (NM_001253846, intron 2 of 10)	51468	NM_001253846	NM_001500	GMDS	protein-coding
chr14	77738530	77738928	intron (NM_001318844, intron 5 of 12)	-22039	NR_161324	NM_174943	C14orf178	ncRNA
chr8	11168732	11169130	intron (NR_138154, intron 1 of 2)	32435	NR_138153	NM_173683	XKR6	protein-coding
chr12	69442885	69443283	Intergenic	-27304	NM_001278351	NM_006654	FRS2	protein-coding
chr12	63382890	63383288	Intergenic	-230279	NM_000706	NM_000706	AVPR1A	protein-coding
chr9	12133397	12133795	Intergenic	-559789	NM_000550	NM_000550	TYRP1	protein-coding
chr4	187333167	187333565	intron (NR_038931, intron 1 of 4)	-37282	NR_149103	NR_149103	LINC02514	ncRNA
chr9	30301466	30301864	Intergenic	106789	NR_046204	NR_046204	LINC01242	ncRNA
chr18	35462989	35463387	Intergenic	34420	NM_001308064	NM_194281	INO80C	protein-coding
chr3	118200277	118200675	Intergenic	-441292	NR_135573	NR_135573	LOC101926968	ncRNA
chr11	95977576	95977974	3' UTR (NM_032427, exon 5 of 5)	-53568	NM_016156	NM_016156	MTMR2	protein-coding
chr8	40643143	40643541	intron (NM_001135731, intron 4 of 5)	254484	NM_001135731	NM_024645	ZMAT4	protein-coding
chr16	64180647	64181045	Intergenic	941217	NM_001797	NM_001797	CDH11	protein-coding
chrX	131258005	131258403	Intergenic	30857	NM_001170963	NM_001555	IGSF1	protein-coding
chr13	114004848	114005246	intron (NM_001320821, intron 20 of 25).2	-30971	NM_001365455	NM_001365455	C13orf46	protein-coding
chr5	173854460	173854858	Intergenic	-33690	NM_001308189	NM_030627	CPEB4	protein-coding
chr6	152171055	152171453	intron (NM_182961, intron 130 of 145)	-2967	NM_001347702	NM_015293	SYNE1	protein-coding
chrY	4035790	4036188	Intergenic	456904	NM_139214	NM_139214	TGIF2LY	protein-coding
chr2	123455867	123456265	Intergenic	-382585	NR_147208	NR_147208	LINC01826	ncRNA
chr2	122056881	122057279	Intergenic	301429	NM_004622	NM_004622	TSN	protein-coding
chrX	56833613	56834011	Intergenic	-96228	NR_002308	NR_002308	UQCRBP1	pseudo

chr6	84752223	84752621	intron (NM_001080508, intron 4 of 7)	12176	NM_001080508	NM_001080508	TBX18	protein-coding
chr12	11746086	11746484	intron (NM_001987, intron 1 of 7)	96431	NM_001987	NM_001987	ETV6	protein-coding
chr6	115830904	115831302	Intergenic	-187268	NR_134602	NR_134602	LINC02534	ncRNA
chr16	64826363	64826761	Intergenic	295501	NM_001797	NM_001797	CDH11	protein-coding
chr11	11672755	11673153	Intergenic	-16232	NR_036184	NR_036184	MIR4299	ncRNA
chr5	106940976	106941374	intron (NR_104671, intron 2 of 3)	69839	NR_104671	NR_104671	LINC01950	ncRNA
chr9	133269245	133269643	intron (NM_020469, intron 1 of 6)	5757	NM_020469	NM_020469	ABO	protein-coding

Chapter 5: Concluding Remarks

5.1 Project Summary

In this thesis, I modeled cardiac fibrosis using computational and in-vitro strategies. Employing four publicly available sequencing datasets, and two that were generated in-house, I identified critical ligands and pathways that govern fibrosis. To test computationally derived hypotheses, I generated my own cardiac fibroblast differentiation protocol that outperformed existing methods and recapitulates primary cell phenotypes. Cell culture media conditions, densities, timeframes, additive concentrations, and assay techniques were optimized and now provide a platform for further in-vitro study of fibrotic mechanisms. While angiotensin II and TGF- β have been previously described as pro-fibrotic molecules, I was able to demonstrate that they, along with low molecular weight hyaluronic acid, converge to activate AP-1 and NF- κ B. Lastly, I was able to identify how AP-1 alters stress response in the presence or absence of mutations that manifest disease in a large portion of the global population.

5.2 Computational Modeling

While several agonists are included in the signaling diagram from the second chapter, many facets of post-MI healing were omitted for clarity. Additional factors such as glycosylation differences, metabolic adaptation, calcium handling, lipid biology, and drug interactions can all alter the wound microenvironment and result in varying outcomes. Our study focused on more prominent ligands and receptors which not only appeared in the sequencing datasets but were also

documented in additional biochemical/biomolecular studies to support their function. It is worth noting that since both HA and angiotensin II are able to act on extracellular TLR agonists, we hope to encompass some of the many DAMPs that are produced after infarction; here we are primarily concerned with TLRs 2 and 4, but acknowledge that additional signaling through TLRs 1, 5, and 6 may occur either through conserved MyD88 pathways or others.

5.3 iCF Culture and Limitations

The need for human cardiac fibroblasts in culture systems is met by our protocol. During the development of the protocol, we realized that regardless of the quality of our cellular product, we would trigger a Catch-22 scenario: either iCFs accurately resemble primary cells which means they fail to maintain phenotype during culture and are severely limited by passage number, or they behave similarly to a cell line which is more stable but less biologically relevant. We found that we could expand the iCFs at least through passage 16, but after passage 5 they became insensitive to the stimuli used in chapter 4. This presents an opportunity for innovation in the culture systems used for CFs. Naturally, an approachable 3-dimensional culture system with high dissociation yield would be ideal, but most research groups predominantly depend on 2-dimensional systems due to their convenience and cost-efficiency. We found Fibroblast Growth Medium 3 to suppress CF activation in both primary cells and iCFs, but it still relies on serum and high bFGF supplementation. After several passages, the fibroblasts

hypertrophy, the growth rate slows, and the cells become more inert. These changes are likely accompanied by metabolic changes and mTOR signaling activation, though we have not investigated these changes. Engineering better supplement formulations would present a great opportunity to support research of stromal cells that are often overlooked. Moreover, we discovered the X-VIVO15 could be used as a serum-free media formulation, as it allows for matrix assembly and supports co-culture systems with immune cells. We have established the fibroblast building block for future multicellular systems and hope that this will lead to additional discoveries in fibrotic signaling.

5.4 9p21 Etiologies and Stress Response

Cardiac cell types can be divided into initiators and responders of acute myocardial infarction; smooth muscle, endothelial, and foam cells initiate atherosclerosis that ultimately builds the occlusion, while cardiomyocytes, fibroblasts, resident leukocytes, and recruited cells are responders. When dissecting the pathogenic mechanism of ANRIL's problematic SNPs, it seems that haplotype differences are present in most cell types, including both initiators and responders, thus convoluting the problem. Dysregulation in each cell type alone could cause disease, but disease is more likely an emergent property of collective systemic dysregulation, since risk individuals still live long enough to reproduce and risk alleles are Mendelian at the population level. For this reason, generating

additive models (i.e. cocultures, micro-vessels, organoids, etc.) are more likely to provide better insight to therapeutic windows for intervention.

To credit the reductionist single cell-type studies (which should be characterized before building summative systems), JNK was previously identified as being a driver of cardiomyocyte asynchrony after mechanical stress, and now we have discovered AP-1 (immediately downstream of JNK) as responsible for altered fibroblast matrix production, raising the possibility of a cardiac conserved pathological mechanism. Global redirection of AP-1 stress responses could generate cell-type specific responses springing from a single genetic cause. However, since these mutations are incredibly permeant at the population level, they could be beneficial in some other contexts (perhaps in host pathogen defense) where increased inflammation resulting in greater fibrosis could be helpful. Building better organ-system based tools to answer these questions and reduce off-target effects could avoid many of safety pitfalls for therapeutic approaches.

This is further suggested by the observation that GATA5 silencing in risk individuals is emergent at the epicardial cell stage; preliminary results (n=1 per stage and haplotype) show similar GATA5 accessibility through cardiac progenitor cells but diverge thereafter. Therefore, it is likely that GATA5 is silenced in smooth muscle cells and the epicardial progenitor pool that is activated upon injury. Mouse studies from the late 1990's demonstrated the necessity of GATA5 in heart formation, and we hypothesize that it remains important after development as well.

The remodeling proteins that lead to these epigenetic changes remain elusive, and identifying them could provide a therapeutic angle for risk haplotype individuals immediately post-MI. We observe that GATA5 can be reactivated upon removal of stress conditions, suggesting that damaged-induced epigenetic changes may be rescuable *in-vivo*.

5.5 Influence on Future Therapies

The agonists and pathways discussed in this thesis offer insight to possible avenues for therapeutic intervention. In the case of angiotensin II, the standard of care already addresses ligand generation through ACE inhibitors, which is preferable to individually blocking each cognate receptor. In the case of TGF- β and DAMPs, some signaling occurs in neonates, suggesting that reduction and not complete abrogation of signaling would be beneficial *in-vivo*. This could be achieved using decoy TLRs or an acute and targeted inhibition of the receptors *in-situ*. Moreover, targeting macrophages from definitive hematopoiesis could be achieved by prolonged administration of CXCL12 (which anchors pre-monocytes in the bone marrow stroma), or hijacking the Slit2/Robo axis to repel recruited macrophages. A combinatorial therapy incorporating these interventions may not initiate complete regeneration but avoids cardiac puncture and is likely to significantly improve outcomes.

APPENDIX

I was also a co-author on the following two papers and book chapter and my contributions are given below.

1. NJ Kirkland, **AJ Whitehead**, JD Hocker, P Beri, G Vogler, B Hum, B Ren, R Bodmer, AJ Engler. “Age-dependent Lamin remodeling induces cardiac dysfunction via dysregulation of cardiac transcriptional programs.” (in review)

For this research article, I developed the ATAC-sequencing pipeline and helped analyze the data, comparing accessible regions of the genome in aging and lamin knockout flies with their transcriptomes.

2. S Ruoss, ST Ball, SN Dorn, JN Parekh, **AJ Whitehead**, AJ Engler, S Ward. “Acetabular bone marrow aspiration during total hip arthroplasty” *Journal of the American Academy of Orthopedic Surgeons*. 2021

For this research article, I cultured the bone marrow and fat after harvest and tracked population doubling times.

3. **AJ Whitehead**, N Kirkland, AJ Engler. “Atomic Force Microscopy for Live-Cell and Hydrogel Measurement” in *Myofibroblasts: Fundamentals, Laboratory Methods and Anti-Fibrotic Drug Discovery*, Series: Methods. Mol. Biol., Hinz, B. and Lagares, D., Editors. 2021, Springer Nature. Vol: 2299, pg. 217-226.

For this book chapter, Dr. Kirkland and I (contributing equally) outlined several methods to measure material properties of live cells and hydrogels using an atomic force microscope and mathematical models of biological elasticity.